

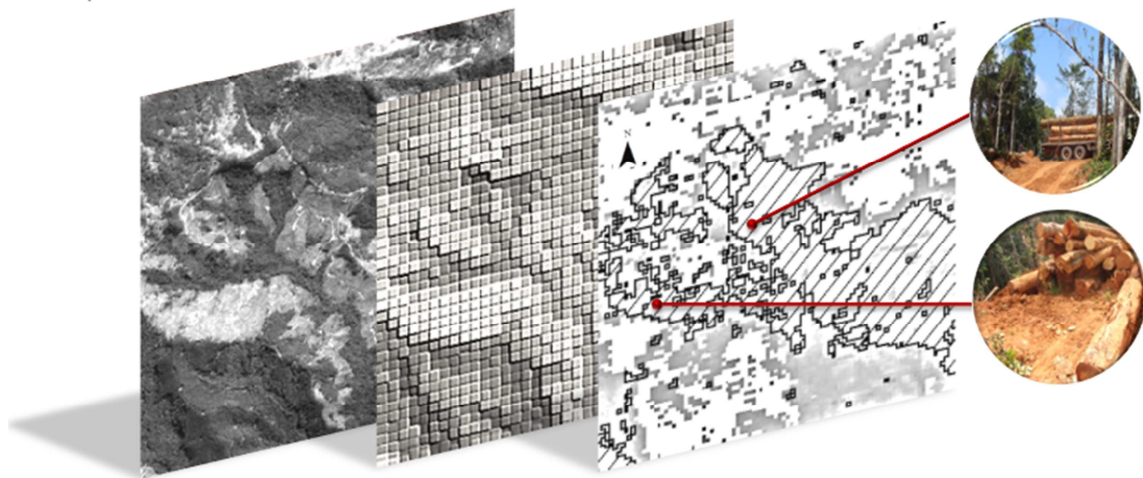
Centre for Geo-Information

Thesis Report GIRS-2013-22

---

# OPTICAL TIME SERIES ANALYSIS FOR MONITORING LAND-COVER CHANGES IN FIJI

Anika Paschalidou



October 2013



WAGENINGEN UNIVERSITY

WAGENINGEN UR



# **Optical time series analysis for monitoring land-cover changes in Fiji**

Anika Paschalidou

Registration number 851127642040

## Supervisors

Johannes Reiche

prof. dr. Martin Herold

dr. ir. Jan Verbesselt

A thesis submitted in partial fulfillment of the degree of Master of Science  
at Wageningen University and Research Centre,  
The Netherlands.

October 2013  
Wageningen, The Netherlands

Thesis code number: GRS-80436

Thesis Report: GIRS-2013-22

Wageningen University and Research Centre

Laboratory of Geo-Information Science and Remote Sensing



## **ACKNOWLEDGEMENTS**

The present master thesis was performed in the Laboratory of Geo-Information Science and Remote Sensing of Wageningen University and Research Centre. With this note I would like to express my sincere gratitude to my supervisors, Johannes Reiche, Martin Herold and Jan Verbesselt, for their excellent guidance, support and patience all these months. Without their supervision and constant help this thesis would not have been possible. In addition, I would like to thank Ben DeVries and Johannes Reiche for permission to use prior to publication R functions for my data analysis (soon available as R package). Moreover, many thanks go to all the members of the Department and to the other MSc students with whom I've shared both my excitement and worries.

Finally, I would like to give my thankfulness to my family and friends for their priceless support.



## ABSTRACT

Monitoring forest cover dynamics is crucial for any initiative to combat tropical deforestation. Remote sensing approaches have the potential to determine forest cover dynamics, providing valuable information for monitoring mechanisms, such as REDD+.

This MSc research assessed the potential of optical time series analysis to capture forest cover changes related to harvest operations. Landsat 7 derived NDVI and NDFI time series (2000 - 2012) were analysed by BFASTmonitor algorithm to retrieve temporal changes in forest cover of a study area. We validated the change detection ability and estimation accuracy of BFASTmonitor based on cross-comparison with a generated reference dataset and further, we assessed the performance of the examined spectral indices as change indicators. In addition, we examined factors potentially influencing the accuracy of the proposed method (e.g. magnitude of change, cloud contamination).

Our results showed that, forest cover changes in the study area, were depicted similarly by BFASTmonitor analysis in NDVI and NDFI time series. The overall accuracy of break-time estimation was 61% and 64% for NDVI and NDFI, respectively and mapping accuracy (mean) was 45% for both indices over the monitoring years 2007 - 2010. Though, we observed variations in BFASTmonitor performance among the monitoring years. For 2007 and 2008, the results were depicted higher rates of accuracy (mean mapping accuracy above 52%, 24% and 36%, mean commission and omission error, respectively), while significant lower rates were observed for 2009 and 2010 (mean mapping accuracy about 35%, 60% and 55% omission and commission error for 2009 and 2010, respectively).

Further, we estimated the magnitude of change corresponded to an actual forest cover change. High rates of agreement between the estimated breaks and the generated reference dataset (above 80% and 60%, overall and mean mapping accuracy, respectively for both indices) were obtained by applying a magnitude threshold of -0.15 to -0.20. We suggested that for a *P.caribea* plantation, a drop on NDVI and NDFI values with magnitude between -0.15 to -0.20 was likely related to deforestation. BFASTmonitor analysis in NDFI time series was demonstrated slightly better ability to correctly estimate the time of actual forest cover changes compared to NDVI (overall accuracy 78% and 82%, for NDVI and NDFI, respectively).

Moreover, cloud contamination in time series was affected the accuracy of BFASTmonitor analysis. High rates of commission for 2010 were mainly induced by remaining clouds. Our results were indicated enhancement of BFASTmonitor break-estimation ability after the removal of cloud contaminated scenes. We conclude that BFASTmonitor analysis in optical satellite time series has the potential to capture changes in forest cover, associated with deforestation, with sufficient spatiotemporal accuracy.

## KEY WORDS

Remote sensing, Time series analysis, Land-cover changes, NDVI, NDFI, BFASTmonitor algorithm, REDD+.

## Contents

<b>1. INTRODUCTION: CONTEXT AND BACKGROUND</b> .....	1
1.1 Land-cover changes and REDD+ policy.....	1
1.2 Importance of forest changes monitoring in Fiji .....	2
<b>2. THEORETICAL CONSIDERATIONS</b> .....	4
2.1 Vegetation Spectral Indices.....	4
2.1.1 Normalized Difference Vegetation Index (NDVI) .....	4
2.1.2 Normalized Fraction Vegetation Index (NDFI) .....	4
2.1.3 Disturbance Index (DI) .....	5
2.2 Change detection algorithms.....	6
2.2.1 Breaks For Additive Seasonal Trend (BFAST) algorithm.....	6
2.2.2 BFASTmonitor algorithm .....	6
<b>3. RESEARCH NEEDS, OBJECTIVES AND QUESTIONS</b> .....	7
3.1 Problem statement .....	7
3.2 Research objectives and questions.....	8
<b>4. MATERIALS</b> .....	9
4.1 Available data .....	9
4.2 Software and script-programing requirements.....	10
<b>5. METHODOLOGY</b> .....	11
5.1 Pre-processing .....	11
5.2 Time series analysis.....	12
5.2.1 Pixel-level time series analysis.....	12
5.2.2 Area-level time series analysis.....	13
5.3 Reference data generation .....	15
5.4 Accuracy assessment .....	16
5.5 Improving the accuracy of the analysis.....	17
5.5.1 Magnitude thresholds .....	17
5.5.2 Cloud contaminated scene removal .....	17
<b>6. RESULTS</b> .....	18
6.1 Pixel-level analysis.....	18
6.1.1 Spectral indices sensitivity differences towards seasonal variations .....	18
6.1.2 Temporal dynamics of Fiji pine.....	20
6.2 Area-level analysis.....	24
6.2.1 Detection and characteristics of land cover changes .....	24
6.2.2 Accuracy assessment (static magnitude threshold).....	28
6.2.3 Accuracy assessment over varying magnitude thresholds.....	29
6.2.4 Improving the accuracy .....	34

<b>7. DISCUSSION</b> .....	38
7.1 Pixel – level analysis .....	38
7.1.1 Spectral indices sensitivity differences towards seasonal variations .....	38
7.1.2 Temporal dynamics of Fiji pine .....	39
7.2 Area analysis.....	39
7.2.1 Detection and characteristics of land cover changes .....	39
7.2.2 Accuracy assessment based on reference data.....	42
7.2.3 Improving break-time estimation accuracy.....	44
7.2.4 Methodological considerations .....	46
<b>8. CONCLUSIONS</b> .....	48
<b>9. RECOMMENDATIONS</b> .....	50
<b>REFERENCES</b> .....	52
<b>APPENDIXES</b> .....	56
I.Appendix – Available Landsat scenes. ....	56
II.Appendix - Location of selected pixels for pixel- level analysis. ....	59
a.Mangrove forest pixels .....	59
b.Intact hardwood forest pixels .....	60
c.Sugarcane pixels .....	61
III.Appendix – Net break calculation flow chart. ....	62
IV. Appendix –Reference dataset generation.....	63
V.Appendix - Accuracy assessment flow chart for monitoring years 2007 - 2010 and stable pine forest.....	70
VI. Appendix – Confusion matrices and error matrix metrics for NDVI time series. ....	71
VII.Appendix – Confusion matrices and error matrix metrics for NDFI time series.....	73
VIII.Appendix - Length of time series and available Landsat images after the scene removal. ....	75
Available Landsat images after the scene removal .....	75
IX.Appendix – Confusion matrices and error matrix metrics for NDVI time series after scene removal. ....	78
X.Appendix – Confusion matrices and error matrix metrics for NDFI time series after scene removal. ....	80

## List of figures

<b>Figure 1.</b> Study area location map. ....	3
<b>Figure 2.</b> Landsat 7 ETM+ imagery coverage of the study area (path/row 75/72, WRS-2).....	9
<b>Figure 3.</b> Spatiotemporal availability of KOMPSAT-2 images (2007 - 2012) for Viti Levu. ....	10
<b>Figure 4.</b> Land-use classification map (2007) of Viti Levu Island, Fiji. ....	12
<b>Figure 5.</b> Example of BFASTmonitor time series analysis outcome.....	14
<b>Figure 6.</b> Spatiotemporal patterns of major forest changes in the study area from 2007 – 2010 and stable pine area.....	15
<b>Figure 7.</b> Indicative example of BFASTmonitor algorithm analysis for NDFI time series of a mangrove forest pixel. ....	18
<b>Figure 8.</b> Example of BFASTmonitor algorithm outcome for NDVI (a) and NDFI (b) time series analysis of a sugarcane pixel (path/row 1730/849). ....	19
<b>Figure 9.</b> NDFI time series (Yt) 2000 – 2012 of a sugarcane pixel.....	20
<b>Figure 10.</b> BFASTmonitor analysis in NDVI (a), NDFI (b) and DI (c) time series for a <i>P.caribea</i> pixel.....	21
<b>Figure 11.</b> Trend changes in NDVI time series (2000 – 2012) for a <i>P.caribea</i> pixel.....	22
<b>Figure 12.</b> Decomposition of Landsat NDVI (a) and NDFI (b) time series (Yt) for a single <i>P.caribea</i> pixel .....	23
<b>Figure 13.</b> Spatial distribution of land cover changes with negative magnitude and detected breaks by BFASTmonitor analysis in NDVI time series for the monitoring periods 2005 - 2010. ....	25
<b>Figure 14.</b> Spatial distribution of land cover changes with negative magnitude and detected breaks by BFASTmonitor analysis in NDFI time series for the monitoring periods 2005 - 2010. ....	26
<b>Figure 15.</b> Map illustrating the spatial distribution of net break detection by BFASTmonitor analysis in (a) NDVI and (b) NDFI time series for the monitoring years 2005 – 2010. ....	27
<b>Figure 16.</b> Mapping accuracy (%) for the individual monitoring years (2007 – 2010, stable pine) and mean mapping accuracy of breaks by BFASTmonitor analysis in NDVI and NDFI time series.....	28
<b>Figure 17.</b> Error of omission (%) in NDVI and NDFI time series based on the generated reference dataset for detected breaks during 2007 – 2010 and stable pine. ....	28
<b>Figure 18.</b> Error of commission (%) in NDVI and NDFI time series based on the generated reference data for detected changes during 2007 – 2010 and stable pine. ....	29
<b>Figure 19.</b> Overall accuracy (%) of BFASTmonitor break-time detection in NDVI and NDFI over varying magnitude thresholds. ....	29
<b>Figure 20.</b> Mapping accuracy (%) for the individual monitoring years (2007 – 2010, stable pine) and mean mapping accuracy (mean MA) of breaks by BFASTmonitor analysis in NDVI time series over the implemented magnitude thresholds.....	30
<b>Figure 21.</b> Omission error (%) of estimated break-time by BFASTmonitor analysis in NDVI time series over the varying magnitude thresholds.....	30
<b>Figure 22.</b> Commission error (%) of estimated break-time by BFASTmonitor analysis in NDVI time series over the varying magnitude thresholds.....	31
<b>Figure 23.</b> True-positive predictions and overall accuracy of BFASTmonitor analysis in NDVI time series (as % of total breaks recorded in reference dataset for each monitoring year and stable pine) over varying magnitude thresholds.....	31
<b>Figure 24.</b> Mapping accuracy (%) for the individual monitoring years (2007 – 2010, stable pine) and mean mapping accuracy (mean MA) of breaks by BFASTmonitor analysis in NDFI time series over the implemented magnitude thresholds.....	32

<b>Figure 25.</b> Omission error (%) of estimated break-time by BFASTmonitor analysis in NDFI time series over the varying magnitude thresholds.....	32
<b>Figure 26.</b> Commission error (%) of estimated break-time by BFASTmonitor analysis in NDFI time series over the varying magnitude thresholds.....	33
<b>Figure 27.</b> True-positive predictions and overall accuracy of BFASTmonitor analysis in NDFI time series over varying magnitude thresholds. ....	33
<b>Figure 28.</b> Overall accuracy (%) of break-time detection by BFAST monitor analysis in NDVI and NDFI before (NDVI, NDFI) and after (NDVI', NDFI') the removal of cloud contaminated scenes over the implemented magnitude thresholds. ....	34
<b>Figure 29.</b> Mapping accuracy (%) for the individual monitoring years (2007 – 2010, stable pine) and mean mapping accuracy (after the removal: mean MA' and before: mean MA) of breaks by BFASTmonitor analysis in NDVI time series over the implemented magnitude thresholds after the scene removal. ....	34
<b>Figure 30.</b> Omission error (%) of estimated break-time by BFASTmonitor analysis in NDVI time series over the varying magnitude thresholds after the removal of cloud contaminated Landsat scenes.....	35
<b>Figure 31.</b> Commission error (%) of estimated break-time by BFASTmonitor analysis in NDVI time series over the varying magnitude thresholds after the removal of cloud contaminated Landsat scenes.....	35
<b>Figure 32.</b> True-positive predictions and overall accuracy of BFASTmonitor analysis in NDVI time series over varying magnitude thresholds after scene removal. ....	36
<b>Figure 33.</b> Mapping accuracy (%) for the individual monitoring years (2007 – 2010, stable pine) and mean mapping accuracy (after the removal: mean MA' and before: mean MA) of breaks by BFASTmonitor analysis in NDFI time series over the implemented magnitude thresholds after the scene removal. ....	36
<b>Figure 34.</b> Omission error (%) of estimated break-time by BFASTmonitor analysis in NDFI time series over the varying magnitude thresholds after the removal of cloud contaminated Landsat scenes.....	36
<b>Figure 35.</b> Commission error (%) of estimated break-time by BFASTmonitor analysis in NDFI time series over the varying magnitude thresholds after the removal of cloud contaminated Landsat scenes.....	37
<b>Figure 36.</b> True-positive predictions and overall accuracy of BFASTmonitor analysis in NDFI time series over varying magnitude thresholds after scene removal. ....	37
<b>Figure 37.</b> Sensitivity differences to changes with low magnitude between (a) NDVI time series and (b) NDFI time series for the monitoring years 2005 and 2006. ....	40
<b>Figure 38.</b> Detected breaks for 2008 and 2009 by BFASTmonitor analysis in (a) NDVI time series and (b) NDFI time series. ....	41
<b>Figure 39.</b> Areas where breaks and changes were detected for 2007 and 2010 by BFASTmonitor analysis in (a) NDVI time series and (b) NDFI time series. ....	42
<b>Figure 40.</b> True-positive and false predictions of 2010 by BFASTmonitor for NDVI time series and pixel-level analysis.....	43
<b>Appendix Figure 1.</b> Net break detection calculation flowchart for NDVI and NDFI time series. ....	62
<b>Appendix Figure 2.</b> Accuracy assessment flowchart .....	70
<b>Appendix Figure 3.</b> Accuracy assessment flowchart .....	70
<b>Appendix Figure 4.</b> Annual length of Landsat time series before (dark blue) and after (green) the removal of cloud-contaminated scenes. ....	75

## List of tables

<b>Table 1.</b> Years of change detection and their corresponding monitoring and historic periods.....	13
<b>Table 2.</b> Example of the generated confusion matrix.. .....	16
<b>Table 3.</b> Magnitude thresholds and their corresponding range that were applied in the detected breaks.....	17
<b>Table 4.</b> Descriptive statistics for NDVI, NDFI and DI time series analysis (2000 – 2012) of mangrove forest, intact hardwood forest and sugarcane plantation (40 pixels per class).....	18
<b>Table 5.</b> Spatial extend of detected breaks and areas where changes with negative magnitude were depicted by BFASTmonitor analysis in NDVI and NDFI time series from 2005 – 2011. ...	24

## List of acronyms

ADEOS	ADvanced Earth Observing Satellite
AVNIR	Advanced Visible and Near Infrared Radiometer
B	Brightness (B) index (Derived from Tasseled-Cap standard transformation)
BFAST	Breaks For Additive Seasonal Trend algorithm
DI	Disturbance Index
ETM+	Enhanced Thematic Mapper (Landsat 7 sensor)
FAO	Food and Agriculture Organization of United Nations
G	Greenness (G) index (Derived from Tasseled-Cap standard transformation)
GV	Green Vegetation (Derived from Tasseled-Cap standard transformation)
IPCC	Intergovernmental Panel on Climate Change
JAXA	Japan Aerospace Exploration Agency
MRV	Monitoring, reporting and verification
NDFI	Normalized Fraction Vegetation Index
NDVI	Normalized Difference Vegetation Index
NIR	NIR is the spectral response in the near-infrared
NPV	Non-photosynthetic vegetation (Derived from Tasseled-Cap standard transformation)
REDD+	Reduce carbon Emissions from Deforestation, forest Degradation and enhancement of forest carbon stocks
SMA	Spectral Mixture Analysis
SOPAC	Applied Geoscience and Technology Division of Secretariat of the Pacific Community, SPC
UNFCC	United Nations Framework Convention in Climate Change
W	Wetness (W) index (Derived from Tasseled-Cap standard transformation)



# **1. INTRODUCTION: CONTEXT AND BACKGROUND**

## **1.1 Land-cover changes and REDD+ policy**

Tropical forests cover about 15% of the world's land surface (FAO, 2006). They are considered as major carbon pools (IPCC, 2000), containing about 25% of the carbon in the terrestrial biosphere (Bonan, 2008).

Land-cover changes are one of the major processes of global change (Foley et al., 2005). Among the drivers of land-cover change, deforestation has received increasing attention (Gasparri et al., 2011). Though, tropical regions have been undergoing rapid changes in forest cover since the 1980s (Achard et al., 2002; Hansen et al., 2008; DeFries et al., 2002) leading to forest degradation (Asner et al., 2009), and further resulting in emissions of heat-trapping carbon dioxide (CO<sub>2</sub>) to the atmosphere (Parker et al., 2009). Arcidiacono-Bársony et al. (2011) were reported that carbon emissions from tropical deforestation account for 12% of global anthropogenic CO<sub>2</sub> emissions, ranking carbon emissions from deforestation and forest degradation as the second largest source of anthropogenic carbon emissions after the energy sector (IPCC, 2007). Tropical forests play an important role to the global carbon cycle (Houghton et al., 2001) and hence their conservation should be prioritized in any initiative to combat climate change (Parker et al., 2009).

The United Nations Framework Convention in Climate Change (UNFCCC) has developed a mechanism to Reduce carbon Emissions from Deforestation, forest Degradation and enhancement of forest carbon stocks (REDD+) in developing countries (UNFCCC, 2009). For monitoring, reporting and verification (MRV) of REDD+ activities countries need to set up a robust and transparent national forest monitoring system which is appropriate for their national circumstances (UNFCCC, 2010). According to the Intergovernmental Panel on Climate Change guidelines (IPCC, 2006) two inputs are necessary to calculate greenhouse gas emissions: activity data in forest areas and emissions factors. Activity data refer to the location and spatial extent of forest cover loss or degradation. Emissions factors describe the emissions of greenhouse gases per unit area of forest cover loss of a specific type (e.g. tons of carbon per hectare of cover loss of a specific forest type).

Remote sensing technologies are able to provide objective, practical and cost-effective solutions for developing and maintaining REDD+ monitoring systems (De Sy et al., 2012). Hence, remote sensing has the potential to contribute to reach the eventual goal of forest carbon assessment under REDD+: continuous annual national assessments forming a global REDD+ monitoring system (Baker et al., 2010).

## 1.2 Importance of forest changes monitoring in Fiji

Fiji forested area covers approximately 960000 ha, consisting mainly from indigenous forest, softwood plantations (mostly *Pinus caribea*) and hardwood plantations covering 89%, 6% and 5% of the total forested area, respectively (Ministry of Forest, 2006:9). Over the last decades deforestation threatens forest conservation in Fiji. According to Weaver et al. (2009) all forest types in Fiji are under particular pressure for human intervention and deforestation or degradation. Among the anthropogenic forces, forest clearance, largely attributed to agriculture, is mainly affecting the tropical forests of Fiji (Fijian Department of Environment, 2010).

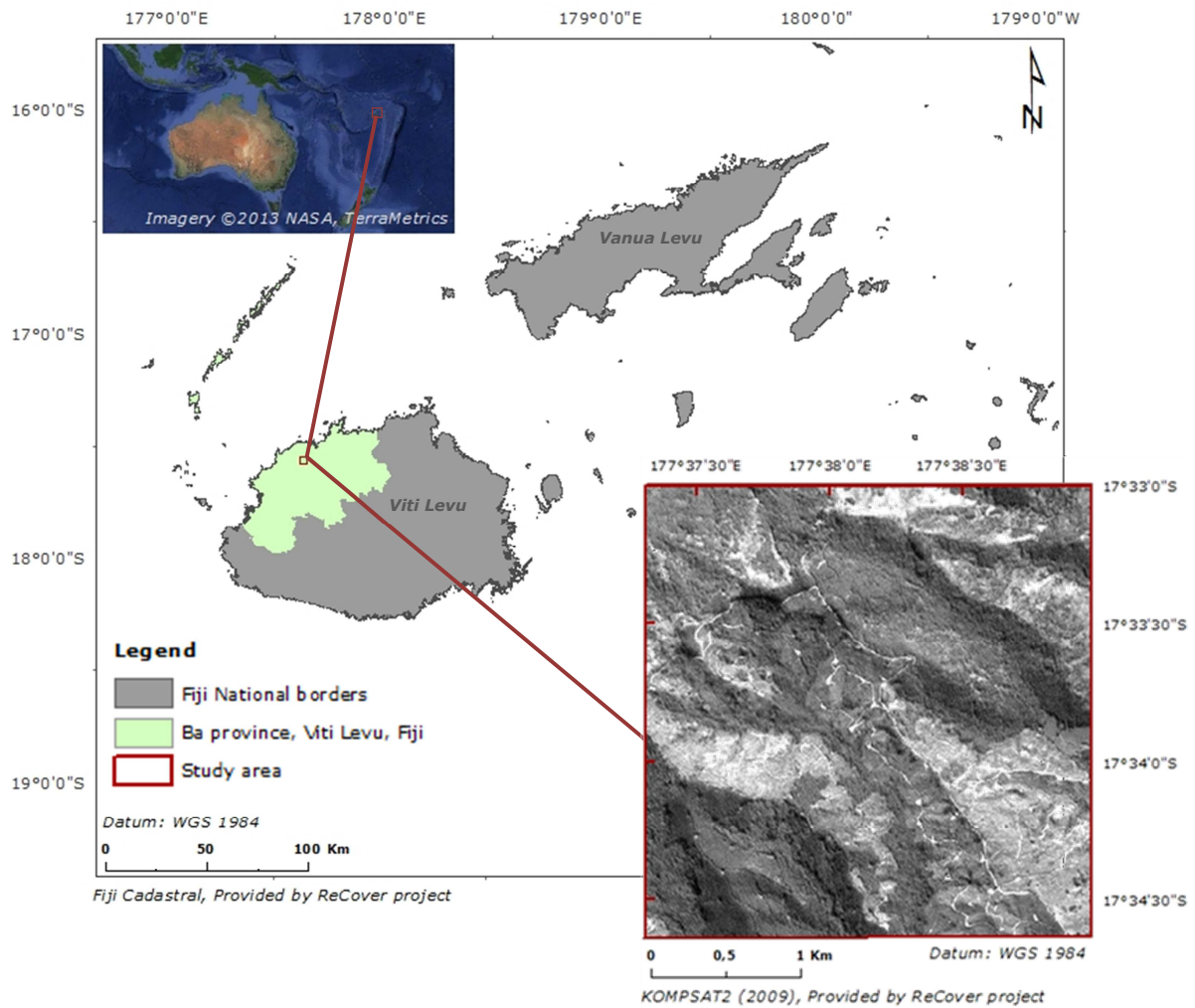
Fiji government acknowledging the threats and recognising the importance of forest conservation has approved in 2010 the Fiji National REDD+ Policy, setting the framework for the development of REDD+ activities in Fiji (Fiji REDD+ policy, 2011). The policy aimed to have Fiji achieved national REDD – readiness by 2012.

The development of MRV systems is fundamental for the accomplishment of a national scale REDD+ readiness. Though, a fully operational monitoring system for forest cover dynamics, in accordance with the objectives of REDD+ has not developed in Fiji yet. This study is focusing in optical time series analysis for monitoring forest cover changes, related to deforestation in Fiji and is intended to contribute towards to the development of a monitoring tool for REDD+ activities.

### ***The study area***

For the purposes of the present research, we selected a forested area located at Ba province, in North West part of Viti Levu Island, Fiji. The specific study area is a small part (900 ha) of a monoculture Caribbean pine (*Pinus caribea*) plantation. Figure 1, shows the location map of the selected study area.

Logging operations for timber extraction, mainly between 2007 and 2010, have fragmented a large part of the forest cover. Aside from partial clearing, forested locations remained intact (full grown stable pine) within the study area. The heterogeneous spatial patterns of forest cover have made the location suitable to assess the accuracy of the proposed methodology for change detection within the disturbed area and further, to validate the performance in stable pine. Our aim was to test the suggested methodology in a small scale (100 x 100 pixels), with the prospect that later on could be implemented in a larger spatial extend.



## 2. THEORETICAL CONSIDERATIONS

### 2.1 Vegetation Spectral Indices

Vegetation indices are commonly employed for characterisation of plant cover (Govaerts et al., 1999) and monitoring land-cover changes (Hayes and Sader, 2001). By combining different spectral bands, they aim to enhance the information of the spectral reflectance data and hence are able to depict the variability due to vegetation characteristics (Viña et al., 2011). The relationship between remotely-sensed vegetation indices and canopy attributes have been extensively studied (see Verstrate et al. (1996), Glenn et al., 2008 for a review). For the purposes of this study the Normalized Difference Vegetation Index (NDVI), the Normalized Fraction Vegetation Index (NDFI) and the Disturbance Index (DI) were selected to explore their potentials for monitoring forest cover changes related to deforestation in Fiji.

#### 2.1.1 Normalized Difference Vegetation Index (NDVI)

The Normalized Difference Vegetation Index (NDVI) (Rouse et al. 1974) is widely used for monitoring, analysing, and mapping temporal and spatial distributions of physiological and biophysical characteristics of vegetation (Gitelson, 2004). It is calculated by:

$$NDVI = \frac{NIR-RED}{NIR+RED} \quad (1)$$

Where NIR is the spectral response in the near-infrared (Landsat ETM+ band 4) and RED (Landsat ETM+ band 3) is the spectral response in the red range of the spectrum.

Healthy green vegetation absorbs strongly in the red range of the spectrum whereas, near-infrared (NIR) radiation is strongly reflected (Glenn et al., 2008). NDVI involves this distinctive contrast in spectral behaviour of vegetation to account for temporal and spatial variations in vegetation structure and density (Gitelson, 2004).

#### 2.1.2 Normalized Fraction Vegetation Index (NDFI)

The Normalized Fraction Vegetation Index (NDFI) was developed by Souza et al. (2005a). NDFI computation requires the decomposition of Landsat ETM+ reflectance data of each pixel into fraction images of Green Vegetation (GV), Non-photosynthetic vegetation (NPV), Soil and Shade through a spectral mixture analysis (SMA) model (Adams et al., 1993). Next, the index is computed as follows:

$$\text{NDFI} = \frac{\text{GVshade} - (\text{NPV} + \text{Soil})}{\text{GVshade} + \text{NPV} + \text{Soil}} \quad (2)$$

Where  $\text{GV}_{\text{shade}}$  is the shade-normalised GV fraction given by:

$$\text{GVshade} = \frac{\text{GV}}{100 - \text{Shade}} \quad (3)$$

The GV, NPV, Soil and Shade image spectra are probably expected in degraded forest environments (Souza et al., 2005a). Selectively logged forests have lower proportion of GV and a higher proportion of NPV, Soil and Shade relative to intact forest (Souza et al., 2003, Souza et al., 2005b). The NDFI has the advantage of combining in one synthetic band, all the information that has been shown to be likely relevant for identifying and mapping degraded forests (Souza et al., 2005a).

### **2.1.3 Disturbance Index (DI)**

The Disturbance Index (DI) (Healey et al., 2005) is potentially a change detection metric suitable for forest environments (Masek et al., 2008). The DI is a transformation of the Landsat Tasseled-Cap data space (Huang et al., 2002) designed to provide sensitivity to forest disturbances (Healey et al., 2005). The Tasseled-Cap brightness (B), greenness (G) and wetness (W) indices are results of a standard transformation of the original Landsat spectral bands. According to Masek et al. (2008) B, G, and W can effectively capture the three major axes of spectral variation across the solar reflective spectrum. The DI is calculated by:

$$\text{DI} = \text{B} - (\text{G} + \text{W}) \quad (4)$$

Unlike simple visible and near-infrared ratio indices (e.g. NDVI), the incorporation of the Tasseled-Cap wetness index in DI, provides further shortwave infrared information, which according to Cohen and Goward (2004) has the potential to detect changes in the forest structure.

## 2.2 Change detection algorithms

Several change detection techniques have been proposed for use in satellite image time series (see Coppin et al., 2004; Lu et al., 2004). Kennedy et al. (2007) were developed a trajectory-based change detection algorithm and Huang et al. (2010) were used thresholds of consecutive high and low forest probability observations. Despite the advantages of their approaches (see Broich et al., 2011), change detection techniques must allow for change detection across complete long-term datasets and further, they need to be independent of the data type, change trajectories or thresholds. Additionally, should be able to detect changes in non-gap-filled time series (Verbesselt et al., 2010a). To overcome these limitations Verbesselt et al. were proposed two algorithms for disturbance detection in satellite image time series; BFAST (Verbesselt et al., 2010a and 2010b) and BFASTmonitor (Verbesselt et al., 2011) algorithms.

### 2.2.1 Breaks For Additive Seasonal Trend (BFAST) algorithm

BFAST algorithm (Verbesselt et al., 2010a) is a change detection method in time series. The algorithm implements an additive decomposition model that iteratively fits a piecewise linear trend and seasonal model. Decomposed time series are the sum of trend ( $T_t$ ), seasonal ( $S_t$ ), and remainder ( $e_t$ ) components. As an improvement of the method Verbesselt et al. (2010b) were proposed the implementation of a harmonic seasonal model for break detection within the seasonal component of the time series.

### 2.2.2 BFASTmonitor algorithm

BFASTmonitor (Verbesselt et al., 2011) is a multi-purpose change detection algorithm for near real-time disturbance detection in time series. Unlike other proposed change detection algorithms BFASTmonitor does not require specific thresholds and is able to deal with missing data (Verbesselt et al., 2011). The algorithm is modelling the seasonal-trend variation in time series for a certain period (stable history) based on disturbances (breaks) can be detected within newly acquired data (monitoring period). To account for seasonal and trend changes BFASTmonitor algorithm implements an additive season and harmonic model, similar to BFAST algorithm (see Verbesselt et al., 2011, for details).

## **3. RESEARCH NEEDS, OBJECTIVES AND QUESTIONS**

### **3.1 Problem statement**

In 2010 the Fiji Government was approved the Fiji National REDD+ Policy (Fiji REDD+ policy, 2011) setting the framework for the development of REDD+ activities in Fiji (Fiji REDD+ policy, 2011). However, a fully operational monitoring system for forest cover dynamics, in accordance with REDD+ objectives, has not established in Fiji yet.

Forests are naturally dynamic ecosystems in continuous change (Gómez et al. 2011). Changes in ecosystems can be seasonal, gradual or abrupt, with the latest referring to disturbances (e.g. deforestation, fires, and floods) (Verbesselt et al., 2010a). Disturbance and post-disturbance recovery are key processes in the development of forest ecosystems (Peterken, 2001; Huang et al., 2010) and main drivers of spatiotemporal heterogeneity (Turner 2010). Abiotic and biotic ecosystem disturbances raise CO<sub>2</sub> levels in the atmosphere due to the emission of CO<sub>2</sub> from terrestrial biomass loss (Potter et al., 2003). Thus, understanding of spatial and temporal extend of these processes is important for forest management and carbon cycle modelling (Hirsch et al., 2004; Law et al., 2004; Zhu et al., 2012). Furthermore, forest cover dynamics assessment is contributing to REDD+ monitoring activities (UNFCCC, 2005).

Remote sensing approaches are suitable for monitoring forest cover changes, accurately and consistently (Broich et al, 2011). Further, in combination with ground measurements are able to determine loss of forest cover (DeFries et al., 2007), caused both from natural and anthropogenic disturbances (Jin & Sader, 2005). For monitoring forest canopy changes the use of dense time series is essential since the spatial signature of most logging activities can be obscured by regrowing vegetation within a year or two (Stone and Lefebvre, 1998; Souza et al., 2005a). Additionally, reduces the risk of confounding seasonal variability with change (de Beurs and Henebry, 2005). Landsat images due to their spatiotemporal characteristics (30m spatial resolution, 16 days temporal resolution, and 185km × 185km area extent) have been the data source of choice for many tropical forest monitoring efforts (Broich et al., 2011; Killeen et al., 2007).

However, change estimation from remotely sensed data series can be complicated. Time series contain a combination of changes (seasonal, gradual and abrupt) occurring in parallel, in addition to noise that originates from the sensing environment (e.g. atmospheric scatter, cloud effects) (de Beurs and Henebry, 2005; Roy et al., 2002). Particularly in tropical forests, optical remote sensing is challenging because of the complex and variable forest structure (Lu, 2005; Steininger, 2000) and furthermore, due to persistent cloud-cover (Asner, 2001). Cloud cover in the tropics is affecting the

availability and quality of optical image data (Siren and Brondizio, 2009), therefore potentially can influence the accuracy of time series analysis.

Different change detection methods have been proposed for use in Landsat and other satellite data (see Lu et al., 2004). In the present research the potentials of BFASTmonitor algorithm in forest change detection will be further investigated. Until recently, BFAST and BFASTmonitor algorithms have been used mainly for Normalized Difference Vegetation Index (NDVI) time series analysis, aiming to monitor forest changes in temperate climate (Verbesselt et al., 2010a; Verbesselt et al., 2010b; Verbesselt et al., 2011; de Jong et al., 2012, Lambert et al., 2011). In these studies, BFAST was successfully detected spatial and temporal changes in time series with different noise levels and seasonal amplitudes. In tropical regions the effectiveness of BFASTmonitor to detect and characterise land-cover changes was assessed by Tanago-Meñaca (2012) for a tropical forest in Vietnam. Hence, is necessary to evaluate BFASTmonitor break detection ability in different ecosystems, types of change events, and moreover to assess the behaviour and responses in forest canopy changes for additional spectral indices time series.

### **3.2 Research objectives and questions**

This research aims to propose a remote sensing method in accordance with the REDD+ guidelines for monitoring forest dynamics in tropical regions. It is intended to explore the potential of long-term time series analysis for capturing changes related to deforestation in tropical forest. For the purposes of this research, a plantation of *Pinus caribea* was selected in Viti Levu Island, Fiji. The specific objectives of this research are:

- To evaluate the performance of different candidate indices as temporal change indicators in tropical forests.
- To assess the potential of BFASTmonitor time series analysis algorithm for deforestation detection and further to assess the accuracy of break-time estimation in a *P.caribea* plantation.
- To specify the magnitude of change characterising an actual deforestation event in the selected study area.

The following research questions will be investigated:

- i. What is the potential of dense and long-term Landsat derived indices for detecting deforestation?
- ii. How accurate BFASTmonitor can estimate the time of change in indices time series?
- iii. What is the magnitude threshold that characterises an actual deforestation event in the study area?

## 4. MATERIALS

### 4.1 Available data

Long and dense time-series were required for monitoring changes in tropical forests. Landsat image data have proven essential for quantification of tropical deforestation rates (Williams et al., 2006), due their temporal (revisit cycle every 16 days) and spatial resolution (30m). In the present study data were acquired from the Enhanced Thematic Mapper Plus (ETM+) sensor onboard of Landsat 7. ETM+ is an eight-band multispectral scanning radiometer (spatial resolution: 30 m (60m – thermal, 15m - pan)) capable of providing medium resolution imaging information of the Earth's surface (NASA, ETM+ technical specifications). The data were obtained in Level 1 Product Generation System (LPGS) level L1T (full Terrain Correction) from the US Geological Survey's Earth Resources Observation and Science (EROS) (data were freely downloaded from USGS Global Visualization Viewer at <http://glovis.usgs.gov/>, on Dec. 2012). Landsat images covered the period from May 2000 to November 2012 (see Appendix I). We selected the path/row 75/72 (WRS-2) for the study area (Figure 2).

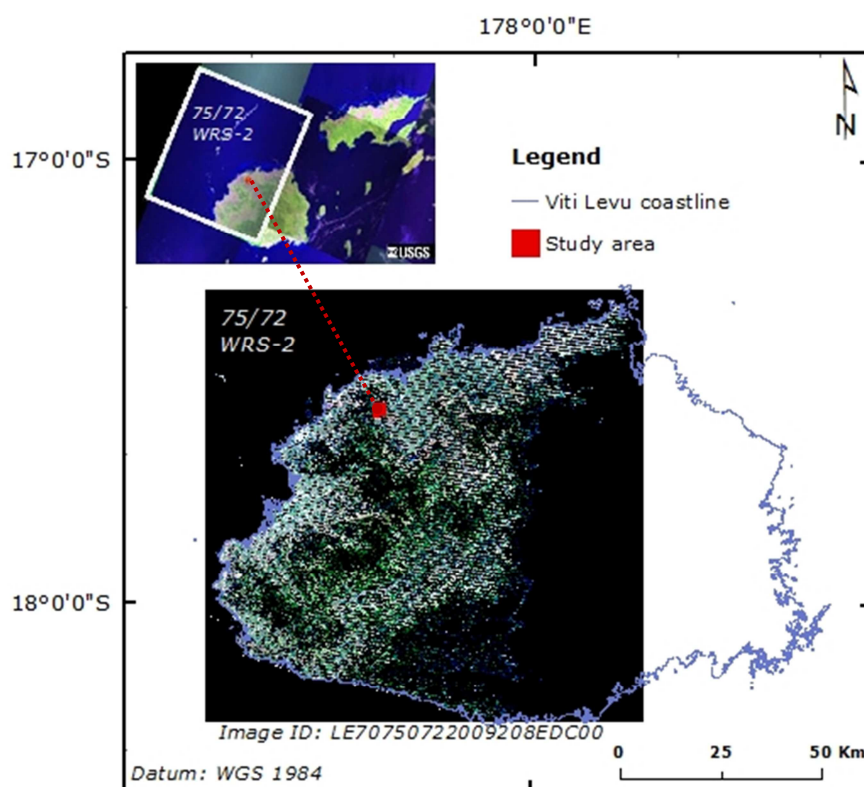


**Figure 2. Landsat 7 ETM+ imagery coverage of the study area (path/row 75/72, WRS-2).**

*Data source: Fiji Cadastral provided by ReCover project (EU-funded Framework 7), Landsat image were downloaded by US Geological Survey's Earth Resources Observation and Science (acquired on Dec. 2012), USGS Global Visualization Viewer (Earth Resources Observation and Science Center, EROS).*

In addition, a land use map for 2007 (Advanced Visible and Near Infrared Radiometer (AVNIR) on-board the ADvanced Earth Observing Satellite (ADEOS), Japan Aerospace

Exploration Agency (JAXA)), was provided by SOPAC (Applied Geoscience and Technology Division of Secretariat of the Pacific Community, SPC). The land use map was used to provide spatial information about the land-cover classes of Fiji. Further, KOMPSAT-2 data were used (Korea Multi-Purpose Satellite, Multi-Spectral Camera sensor with spatial resolution 1m panchromatic and 4m multispectral) for specific locations of the study area in conjunction with other data sources (Figure 3). The data were acquired between 2007 and 2012 but their spatiotemporal density was limited and varied among the years (2007, 2010 and 2012 single image, 2008, 2009 and 2011 multiple acquisitions).

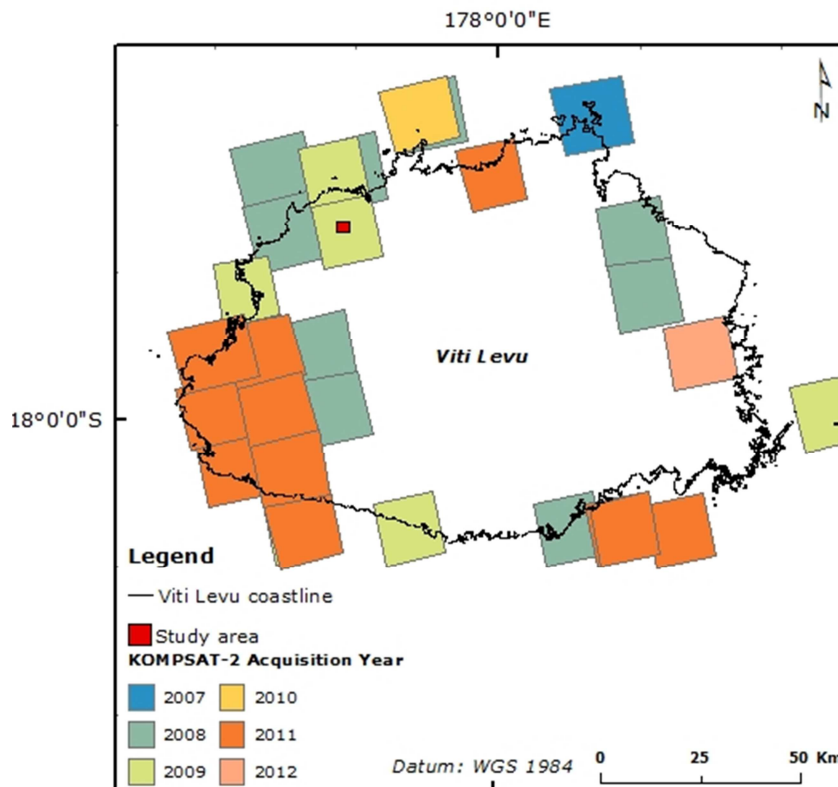


**Figure 3. Spatiotemporal availability of KOMPSAT-2 images (2007 - 2012) for Viti Levu.**

*Data Source: Fiji cadastral and KOMPSAT-2 spot catalogue provided by ReCover project (EU-funded Framework 7).*

Fiji cadastral data were also available. KOMPSAT-2 and Fiji cadastral data were all provided by the EU-funded Framework 7 (Theme Space program of the European Commission) ReCover project for the purposes of the present research.

## 4.2 Software and script-programing requirements

The remote sensing data pre-processing and analysis was performed mainly in open source R environment (R Development Core Team 2010), version 2.15.1. Specific pre-processing operations such as Fmask (Zhu and Woodcock, 2012) were performed in Matlab (version R2012a). The application of change detection algorithms was conducted in R and further GIS analysis was performed in ArcGIS 10.1 and IDL-ENVI 4.8. The statistical analysis was performed partially in R and Excel.

## 5. METHODOLOGY

### 5.1 Pre-processing

We performed radiometric calibration on Landsat 7 ETM+ scenes to remove the effects of changes in sun elevation angle and illumination conditions as well as atmospheric decontamination (NASA 2011). The acquired images were calibrated to transform digital numbers (DN) values into top of the atmosphere (TOA) reflectance and further to remove clouds and cloud shadows. DN values were converted to TOA reflectances with the Landsat Ecosystem Disturbance Adaptive Processing System (LEDAPS) atmosphere correction tool (Masek et al., 2006). The LEDAPS approach was performed in R environment by implementing the modified R package "PreFAST" (developed by Detroix, DeVries and Reiche).

In addition, we removed cloud and cloud-shadows from the time series. Cloud contamination of images could reduce significantly the derived spectral indices values. Change detection algorithms while accounting for abrupt changes related to deforestation could misclassify these indices drops as forest cover changes. Thus, the Fmask algorithm (Zhu and Woodcock, 2012) was implemented to remove clouds and cloud-shadow contamination of Landsat scenes. Fmask algorithm was provided an automated method for screening clouds and their shadows from Landsat images. The algorithm first was implemented rules based on cloud physical properties and a series of spectral tests to produce a layer of potential cloud pixels (PCPs). Next, the darkening effect of the cloud shadows in the near infrared (Landsat ETM+ band 4) was used to generate a potential cloud-shadow layer. Finally, a 3D object-based cloud and cloud shadow matching was performed based on their geometric relationship and illumination conditions, leading to the production of the final cloud and cloud shadow mask. The Fmask analysis was conducted in Matlab. The algorithm was successfully detected and removed most of the medium and big size clouds and cloud-shadows. However, clouds and cloud-shadows were still present in the images after the pre-processing.

Thereafter, the images were re-projected to the UTM WGS 84 60S projection system. The pre-processed image time-series were used as inputs for the indices calculations (NDVI, NDFI and DI). NDVI and DI computations were performed in R environment, based on computation equations (1) and (4) (see Chapter 2.1). To retrieve the NDFI the *ImgTools* were implemented. *ImgTools* were used to perform the Spectral Mixture Analysis and the NDFI calculation from the Landsat band stack (bands 1,2,3,4,5 and 7, path/row 75/72 Landsat image). All the derived indices were scaled in order to represent the same range of values. Then, indices layer stacking was performed by a script in R environment. The pre-processing steps and indices computations were performed by Reiche J. and were provided prior to the analysis.

## 5.2 Time series analysis

We assessed the change detection capacity of BFASTmonitor algorithm by analysing indices time series from 2000 - 2012. Prior to attempting any deforestation detection in the selected study area, it was necessary to explore the indices responses in a pixel-level approach.

### 5.2.1 Pixel-level time series analysis

A series of pixel-level tests were performed in Viti Levu Island to evaluate the indices properties. Sensitivity differences towards seasonal variations of different land-cover classes and the typical temporal patterns of Fiji pine dynamics were assessed in a pixel-level time series analysis.

#### *Sensitivity differences towards seasonal variations*

Three land cover classes, mangrove forest, stable hardwood forest (mature and undisturbed) and sugarcane plantations were analysed due to their expected distinctive temporal characteristics. Figure 4, illustrates the location of the examined land cover classes in Viti Levu Island.

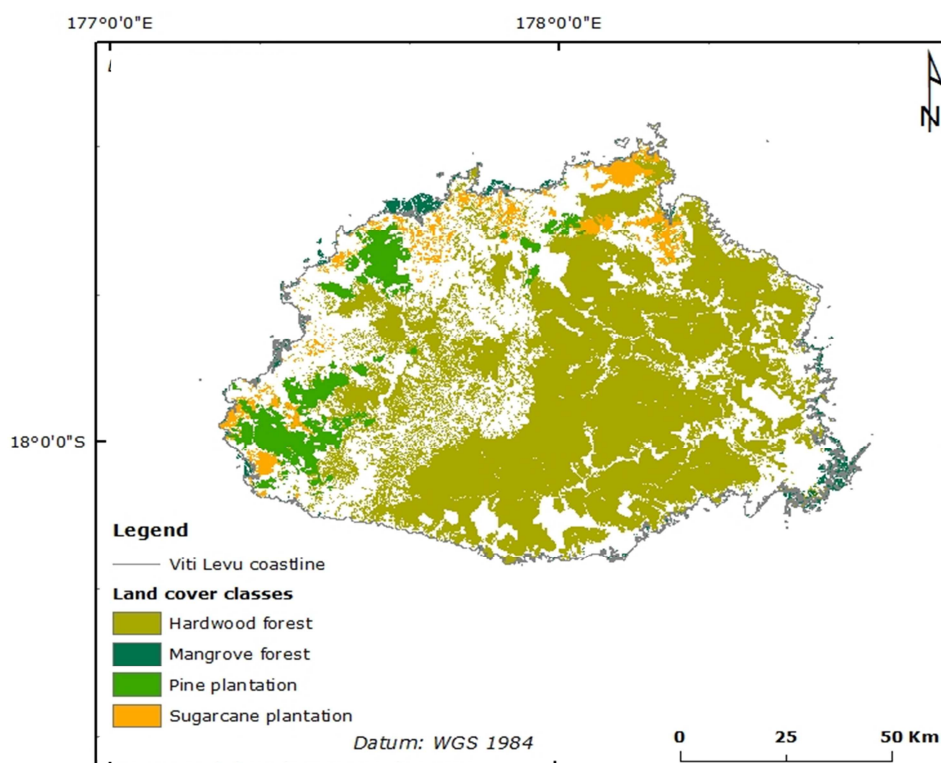


**Figure 4. Land-use classification map (2007) of Viti Levu Island, Fiji.**

Data source: Land-use classification map provided by SOPAC and Fiji cadastral by the ReCover project (EU-funded Framework 7).

Forty (40) representative cloud-free pixel time series were selected for each land-cover class based on the land-use map of 2007 and visual interpretation of Landsat time series and KOMPSAT-2 images (see Appendix II for pixel location). Thereafter, descriptive statistics (mean values, variance, and standard deviation) were calculated in R for the indices time series (NDVI, NDFI and DI) over the period 2000 - 2012.

### ***Temporal patterns of Fiji pine dynamics***

We retrieved the temporal patterns of undisturbed, deforested and reforested Fiji pine from pixel-level time series analysis. Undisturbed (fully grown) pine pixels were selected based on visual interpretation of the time series. Descriptive statistics of indices time series (2000 - 2012) were computed in R, to assess the indices fluctuations among the years. Additionally, we performed BFAST and BFASTmonitor analysis in undisturbed pine pixel time series. Further, deforested pine pixels with visible regrowth patterns were selected to assess the deforestation and regrowth typical patterns of pines. BFAST algorithm was implemented to depict the temporal dynamics of deforestation (forest clearance) and regrowth in indices time series.

### **5.2.2 Area-level time series analysis**

We validated the change detection ability of BFASTmonitor algorithm by analysing NDVI and NDFI time series (2000 - 2012) for a test area of 100 x 100 pixels (900ha). BFASTmonitor algorithm enables the detection of near real-time disturbances in time series. Based on a model for stable historical behaviour, abnormal changes within newly acquired data can be detected. A regression model with harmonic component of first order was used for modelling the historical behaviour, due to low rates of pine seasonality that were depicted in Landsat time series. The change detection was limited from 2005 to 2011, in order to have sufficient number of observations while modelling the historical behaviour. Table 1, describes the implemented monitoring years and their corresponding historic periods.

**Table 1. Years of change detection and their corresponding monitoring and historic periods.**

<b>Year of change detection</b>	<b>Duration of monitoring period</b>	<b>Start of historic period</b>	<b>End of historic period</b>
2005	Jan 2005 – Jan 2006	2000	2004
2006	Jan 2006 – Jan 2007	2000	2005
2007	Jan 2007 – Jan 2008	2000	2006
2008	Jan 2008 – Jan 2009	2000	2007
2009	Jan 2009 – Jan 2010	2000	2008
2010	Jan 2010 – Jan 2011	2000	2009
2011	Jan 2011 – Jan 2012	2000	2010

The main outcomes of BFASTmonitor time series analysis were three matrices (Figure 5), depicting (i) spatiotemporal information of detected breaks in the monitoring period, (ii) spatial distribution and magnitude (m) of changes in the monitoring period (without classifying them as breaks) and (iii) the length of historic (modelling) period.

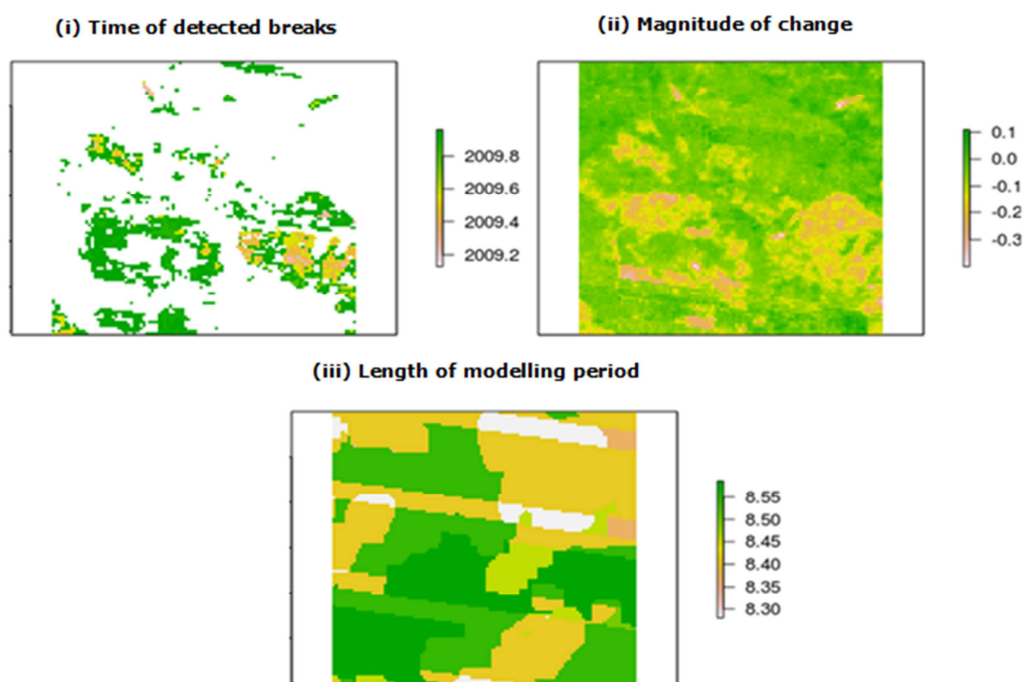


**Figure 5. Example of BFASTmonitor time series analysis outcome.**

To retrieve information about potential deforestation patterns in the study area, we limited the analysis to BFASTmonitor break estimations with negative magnitude of change ( $m < -0.01$ ). Area level BFASTmonitor analysis in NDVI and NDFI time series was performed in R environment, using R functions developed by DeVries and Reiche. We repeated the procedure for every monitoring year.

BFASTmonitor analysis was performed in successive monitoring years. Thus, detected breaks of prior years were likely present within the results of a following year. To assess the break detection rates for a specific year (without considering previously detected breaks) we calculated for every monitoring year the “net” break detection. For each year we performed mosaicking and removal of prior detected breaks. Net break calculations from 2005 – 2011 were conducted in ArcGIS 10.1. Appendix III, describes the detailed work flow for net break detection calculation. Thereafter, break estimations by BFASTmonitor were compared to the generated reference dataset.

### 5.3 Reference data generation

We validated BFASTmonitor break estimation accuracy based on comparison with a generated reference dataset. Reference dataset was contained the major forest cover changes of the study area. We visually interpreted the available Landsat image time series and clear canopy changes were delineated on a shapefile in ArcGIS. Additionally, we defined the stable pine area (full grown pine trees) in the plantation.

The observed forest cover changes and intact pine area were further evaluated manually. Pixel-level analysis was performed to ensure the integrity of the reference dataset and further to limited as possible human bias. Due to the spatial resolution of Landsat images (30m) the delineation was eliminated to major visible forest clearances in the study area. Thus, minor forest cover changes were excluded from the analysis. Appendix IV, describes the generation of the reference dataset and examples of pixel-level analysis. Figure 6, shows the generated reference dataset for the study area.

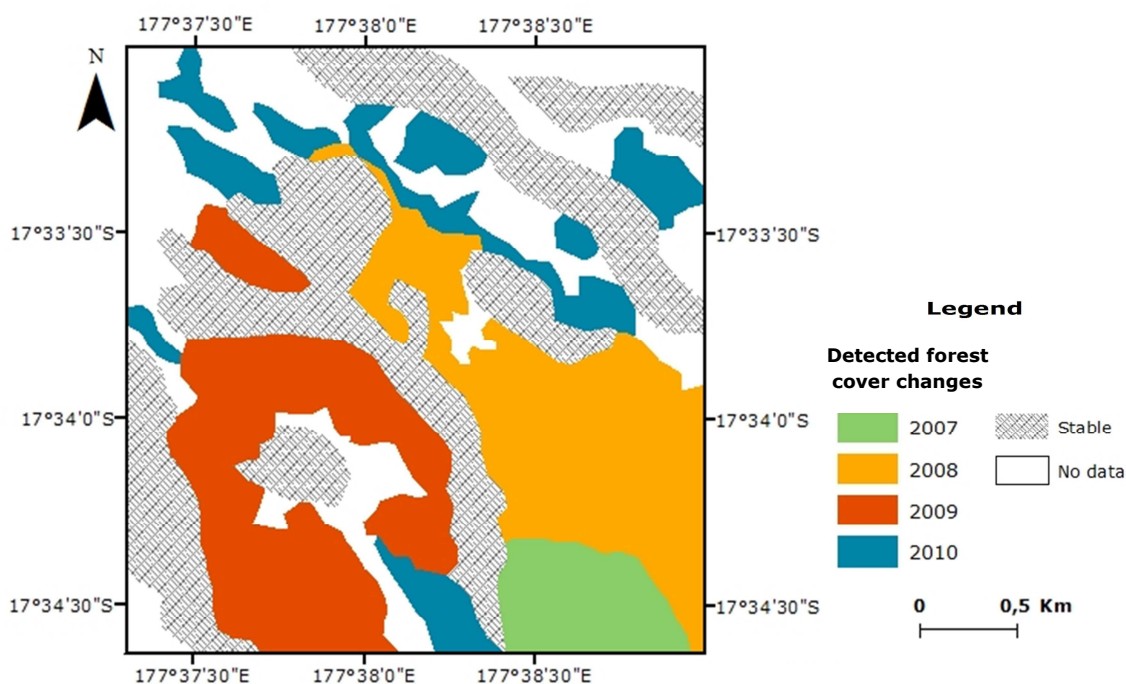


**Figure 6. Spatiotemporal patterns of major forest changes in the study area from 2007 – 2010 and stable pine area.**

## 5.4 Accuracy assessment

We cross-compared the detected breaks for the individual monitoring years with the generated reference dataset, to evaluate the accuracy of the BFASTmonitor estimations. From the accuracy assessment we excluded break predictions for 2005, 2006 and 2011 due to lack of changes in the reference dataset. Appendix V, describes the implemented methodological flowchart for the accuracy quantification of change detection from 2007 to 2010 (Appendix Figure 2) and additionally for stable pine (Appendix Figure 3). Thereafter, confusion matrices were calculated. Table 2, describes a confusion matrix.

**Table 2. Example of the generated confusion matrix.**

Rows represent the break-time prediction by BFASTmonitor and columns the ground truth. Diagonal elements show the correct prediction per monitoring year (true positive (tp) in bold). Off-diagonal values along a row indicate the false negative (fn), while off-diagonal values below a column heading indicate the false positive (fp) predictions per year.

Predicted year of change (BFASTmonitor results)	Actual year of change (Reference dataset)				
	2007	2008	2009	2010	Stable
2007	<b>tp<sub>(2007)</sub></b>	fn <sub>(2007)</sub>	fn <sub>(2007)</sub>	fn <sub>(2007)</sub>	fn <sub>(2007)</sub>
2008	fp <sub>(2007)</sub>	<b>tp<sub>(2008)</sub></b>			
2009	fp <sub>(2007)</sub>		<b>tp<sub>(2009)</sub></b>		
2010	fp <sub>(2007)</sub>			<b>tp<sub>(2010)</sub></b>	
Stable Pine	fp <sub>(2007)</sub>				<b>tp<sub>(Stable)</sub></b>

We calculated confusion matrix metrics (Congalton, 1991) to assess the accuracy of break-time detection of the individual monitoring years. Producer's / user's accuracy, commission /omission error and mapping accuracy, were computed for the detected changes of 2007 – 2010 and for stable pine. Producer's accuracy is the ratio between the true-positive predictions of a year and the sum of true and false positives of the specific year. Further, omission error was calculated based on the equation:

$$\text{Omission error} = 1 - \text{producer's accuracy} \quad (5)$$

User's accuracy is the ratio between the true positives predictions of a year and the sum of true and negative positives within the year. It's indicative of the probability that a pixel classification actually represents that category on the ground (Story and Congalton, 1986). Commission error was computed by:

$$\text{Commission error} = 1 - \text{user's accuracy} \quad (6)$$

Finally, we assessed the mapping accuracy for the individual monitoring years. For each year, mapping accuracy (MA) was calculated as the ratio of true-positive predictions for a certain year divided by the sum of correctly identified pixels for a year plus the pixels representing errors of commission (i.e. for X year, all other years in the X row) and omission (i.e. for X year, all other years in the X column) associated with that year.

## 5.5 Improving the accuracy of the analysis

To improve the accuracy of BFASTmonitor break detection we estimated the magnitude of change that was corresponded to an actual clearance event and further, we excluded remaining cloud contaminated layers after the image pre-processing that could potentially lead to false break detection.

### 5.5.1 Magnitude thresholds

Magnitude thresholds were implemented to the analysis to eliminate indices variations unrelated to actual clearance events in the study area. The thresholds were gradually divided the magnitude of change from low magnitude changes ( $m < -0.01$ ) to high magnitude changes ( $m < -0.30$ ). The highest threshold was set to  $-0.30$  due to limited occurrence of areas with higher magnitude of change. Table 3, presents the magnitude thresholds that were applied in the study. We repeated the BFASTmonitor analysis for NDVI and NDFI time series over the varying thresholds. The analysis was performed in R.

**Table 3. Magnitude thresholds and their corresponding range that were applied in the detected breaks.**

Threshold	Magnitude of change range (m)
-0.01 (low)	$m < -0.01$
-0.05	$m < -0.05$
-0.10	$m < -0.10$
-0.15	$m < -0.15$
-0.20	$m < -0.20$
-0.25	$m < -0.25$
-0.30 (high)	$m < -0.30$

### 5.5.2 Cloud contaminated scene removal

Remaining clouds in the time series after the image pre-processing, were dropped significantly the derived indices values. Hence, change detection algorithms could potentially misclassify remaining clouds as changes. We performed selection and removal of remaining cloud contaminated scenes, to reduce the false break detection by BFASTmonitor. Visual interpretation of Landsat image time series and pixel-level analysis was performed to select scenes with high rates of remaining clouds in the study area. Appendix VIII, describes the initial and final length of the time series. Next, indices time series were analysed anew by BFASTmonitor algorithm. We performed the analysis over the varying magnitude thresholds for the same monitoring years (2005 - 2011). The results were cross-compared to the reference shapefile. We recalculated the overall accuracy and confusion matrix metrics for the detected breaks based on the initially implemented methodology (see Appendices III and IV). Finally, we estimated the remaining cloud effect on BFASTmonitor performance and break-time detection accuracy by comparing the obtained results before and after the image removal.

## 6. RESULTS

### 6.1 Pixel-level analysis

#### 6.1.1 Spectral indices sensitivity differences towards seasonal variations

Descriptive statistics were calculated for selected pixels of mangrove forest, intact hardwood forest and sugarcane plantations (Table 4).

**Table 4. Descriptive statistics for NDVI, NDFI and DI time series analysis (2000 – 2012) of mangrove forest, intact hardwood forest and sugarcane plantation (40 pixels per class).**

Land cover class		Indices time series		
		NDVI	NDFI	DI
Mangrove forest	Mean	0,92	0,76	0,91
	SD	0,02	0,01	0,02
	SD (% of mean)	2,6%	1,3%	2,4%
Intact hardwood forest	Mean	0,94	0,74	0,86
	SD	0,01	0,01	0,02
	SD (% of mean)	1,5%	2,1%	2,8%
Sugarcane plantation	Mean	0,83	0,58	0,73
	SD	0,08	0,11	0,09
	SD (% of mean)	9,5%	19,6%	12,6%

Mangrove forest pixels and intact hardwood forest pixels were demonstrated similar temporal patterns. Consistently high indices values and low rates of seasonality (SD < 3% of mean values) were depicted in Landsat time series. Figure 7, illustrates an indicative example of BFASTmonitor algorithm analysis for NDFI time series (2000 – 2012) of a mangrove forest pixel.

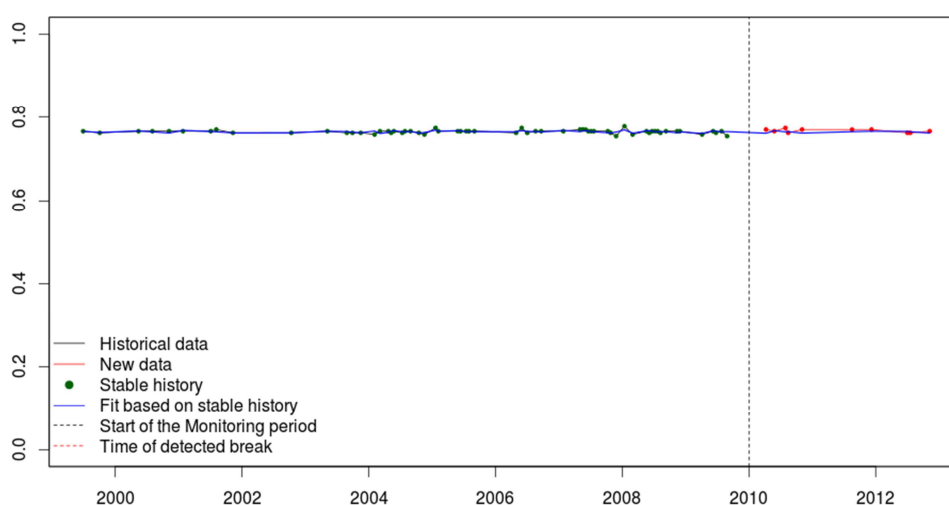


**Figure 7. Indicative example of BFASTmonitor algorithm analysis for NDFI time series of a mangrove forest pixel.**

Unlike the two previous land-cover classes, sugarcane pixel analysis was depicted lower indices values and higher standard deviation. Remarkable difference was observed between the standard deviation values for NDVI and NDFI. The standard deviation of NDFI (20%) was considerably higher relative to NDVI (10%). Figure 8, shows the results of NDVI and NDFI time series analysis for the same sugarcane pixel.

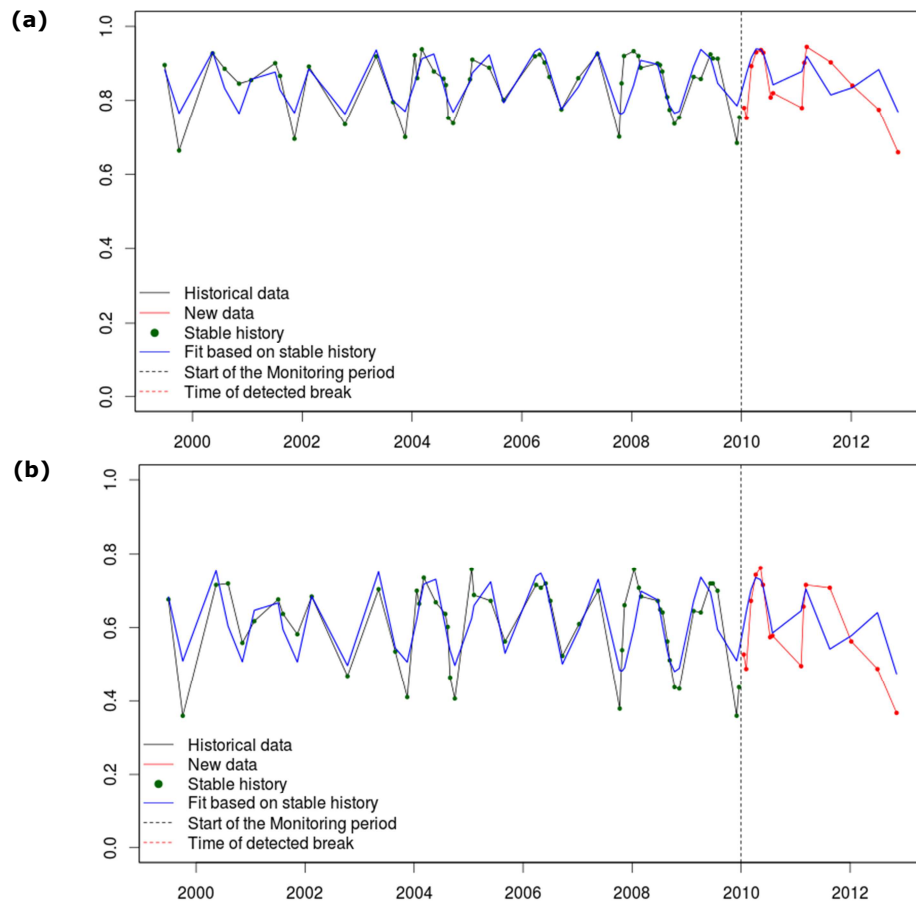


**Figure 8. Example of BFASTmonitor algorithm outcome for NDVI (a) and NDFI (b) time series analysis of a sugarcane pixel (path/row 1730/849).**

Further, we retrieved the typical temporal profile of a sugarcane pixel. Two discrete phases in sequence were depicted within the temporal profile of sugarcane; the growth phase and the change phase. The growth stages of sugarcanes (10-12 months) were characterised by a gradual increase of indices values. At the mature point of the plant was observed a peak on indices rates. Thereafter, the change phase was followed, where a gradual decrease trend was depicted in indices values, reaching eventually the lowest point. Beyond that point the growth cycle was repeated.

BFAST algorithm analysis was performed in NDVI, NDFI and DI the time series, where the algorithm was likely able to capture the seasonality of sugarcane without detecting breaks. Figure 9, illustrates how BFAST was decomposed NDFI time series (seasonal ( $S_t$ ), trend ( $T_t$ ) and remainder ( $e_t$ ) components) for a sugarcane pixel.

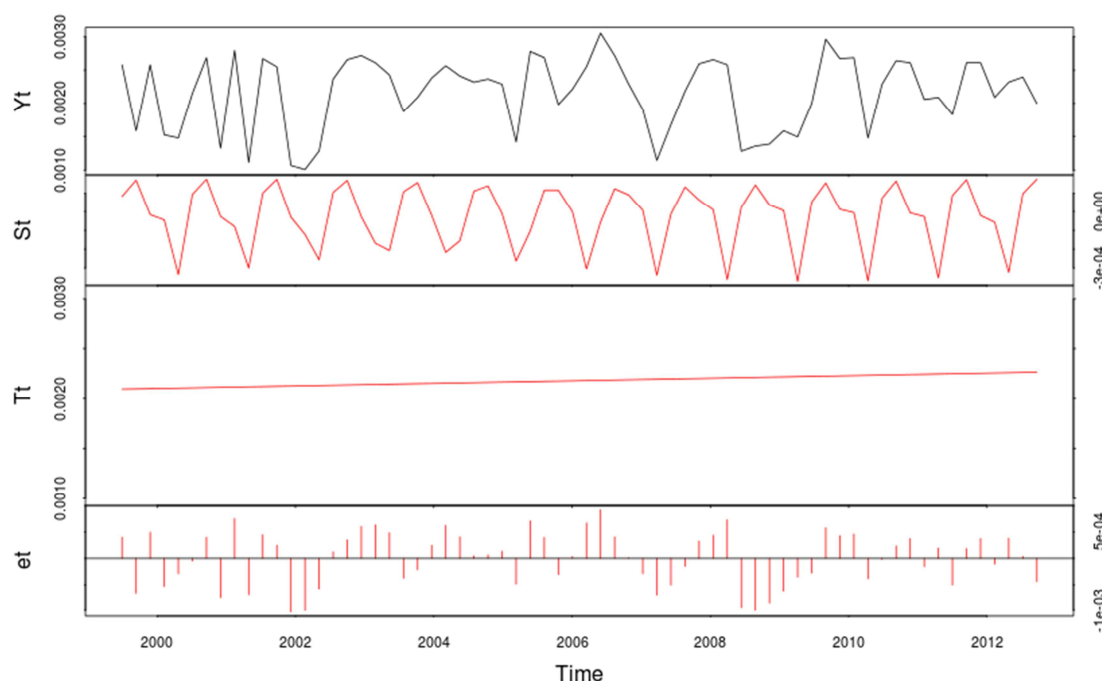


**Figure 9. NDFI time series ( $Y_t$ ) 2000 – 2012 of a sugarcane pixel (path/row 1746/869). The estimated seasonal ( $S_t$ ), trend ( $T_t$ ) and remainder ( $e_t$ ) components are illustrated in red. BFAST did not detect breaks within the trend component of the time series.**

### 6.1.2 Temporal dynamics of Fiji pine

#### ***Intact P.caribea***

High indices values and low seasonality without significant seasonal variations were depicted on Landsat time series for intact *P.caribea*. Mean values were 0.94, 0.75 and 0.88 for NDVI, NDFI and DI, respectively. Standard deviation was below 4% of mean values for all indices. However, NDFI and DI results were illustrated slightly lower values of standard deviation compared to NDVI.

Figure 10, shows a representative example of BFASTmonitor single-pixel analysis in NDVI, NDFI and DI time series on intact pine. The lower standard deviation rates of NDFI and DI time series compared to NDVI for intact pines were further visible at BFASTmonitor analysis output. Intact pine NDFI and DI time series were demonstrated lower seasonal fluctuations compared to NDVI results.

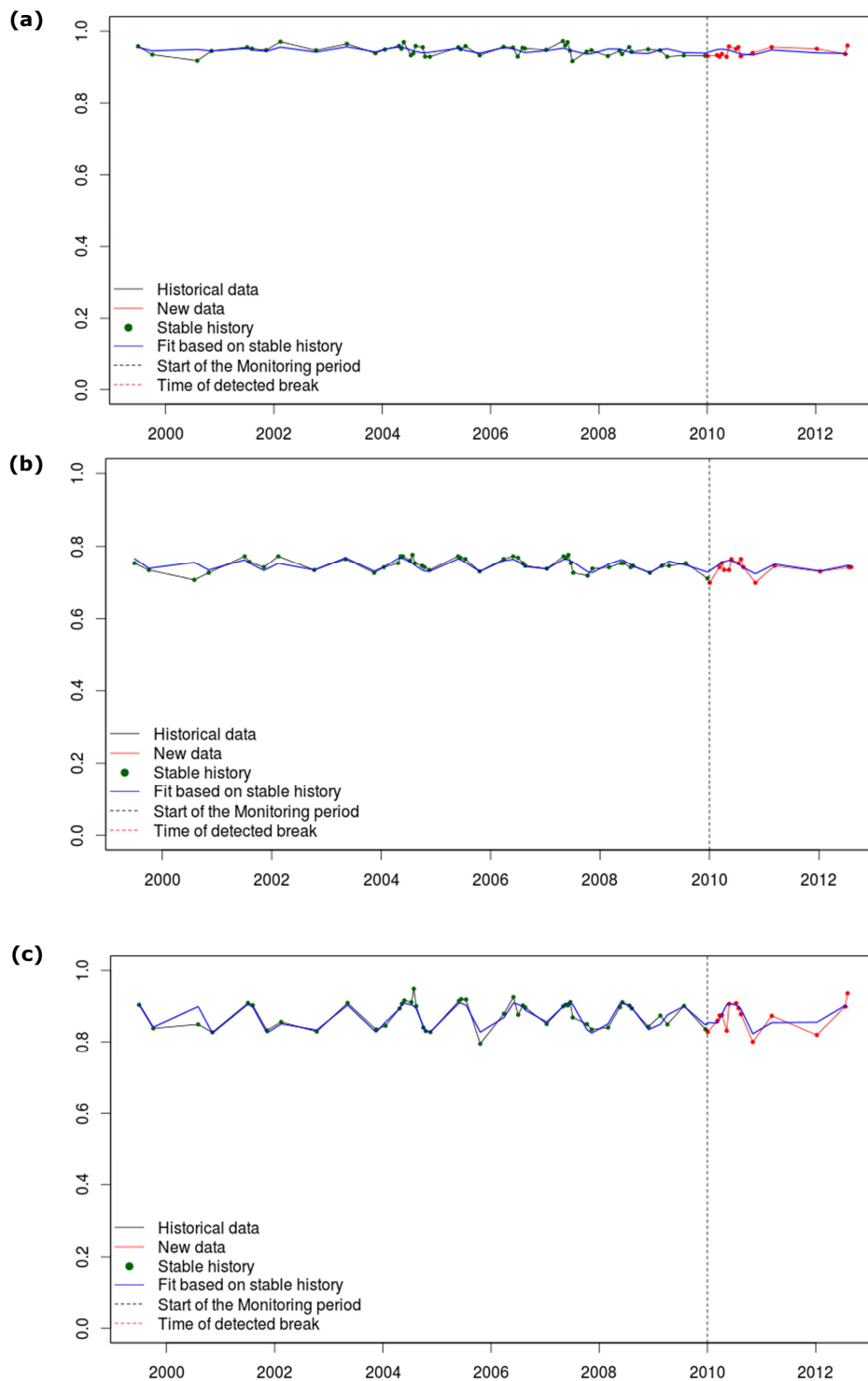


**Figure 10. BFASTmonitor analysis in DI (a), NDFI (b) and NDVI (c) time series for a *P.caribea* pixel (path/row 1011/1203). The defined historical period is from 2000 -2009 and the monitoring period starts on 2010.**

### ***Deforestation and regrowth temporal patterns of P.caribea***

We performed single pixel analysis for *P.caribea* with documented harvest operations and a visible regrowth, to retrieve the deforestation and recovery temporal patterns. Based on the obtained results, the harvest cycle of pines was composed by the pre-harvesting period, breakpoint (harvest event) and a following recovery phase. Figure 11, illustrates the retrieved deforestation and regrowth patterns for a pine pixel, where a harvest operation occurred in 2006 and a regrowth period was followed.

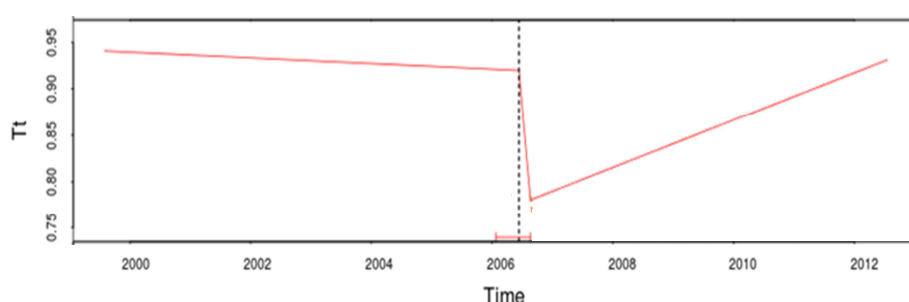


**Figure 11. Trend changes in NDVI time series (2000 – 2012) for a *P.caribea* pixel (path/row 395/492). The fitted trend component (Tt) shows the pre-harvest period (2000 - 2006), the detected breakpoint (2006) and the following gradual recovery phase (2006 - 2012).**

The pre-harvesting period was demonstrated low seasonal variations and high values for all indices. At the breakpoint, an abrupt decrease of indices values was observed with negative slope. Next, the recovery period was followed, demonstrating a successive positive slope and a gradual increase on indices rates.

Figures 12, illustrates the decomposition and change detection by BFAST algorithm analysis in NDVI and NDFI time series of the same *P.caribea* pixel with a harvest operation in 2006. The main difference between the indices performance was the depicted length of the regrowth phase of pines. A series of tests were demonstrated generally longer regrowth period in NDFI time series, with a more gradual recovery trend relative to NDVI and DI. NDVI and DI time series about four years after the clearance event were reached high values representative of healthy *P.caribea* (above 0.9). Six years after the detected change the indices were demonstrated the pre-harvest period values.

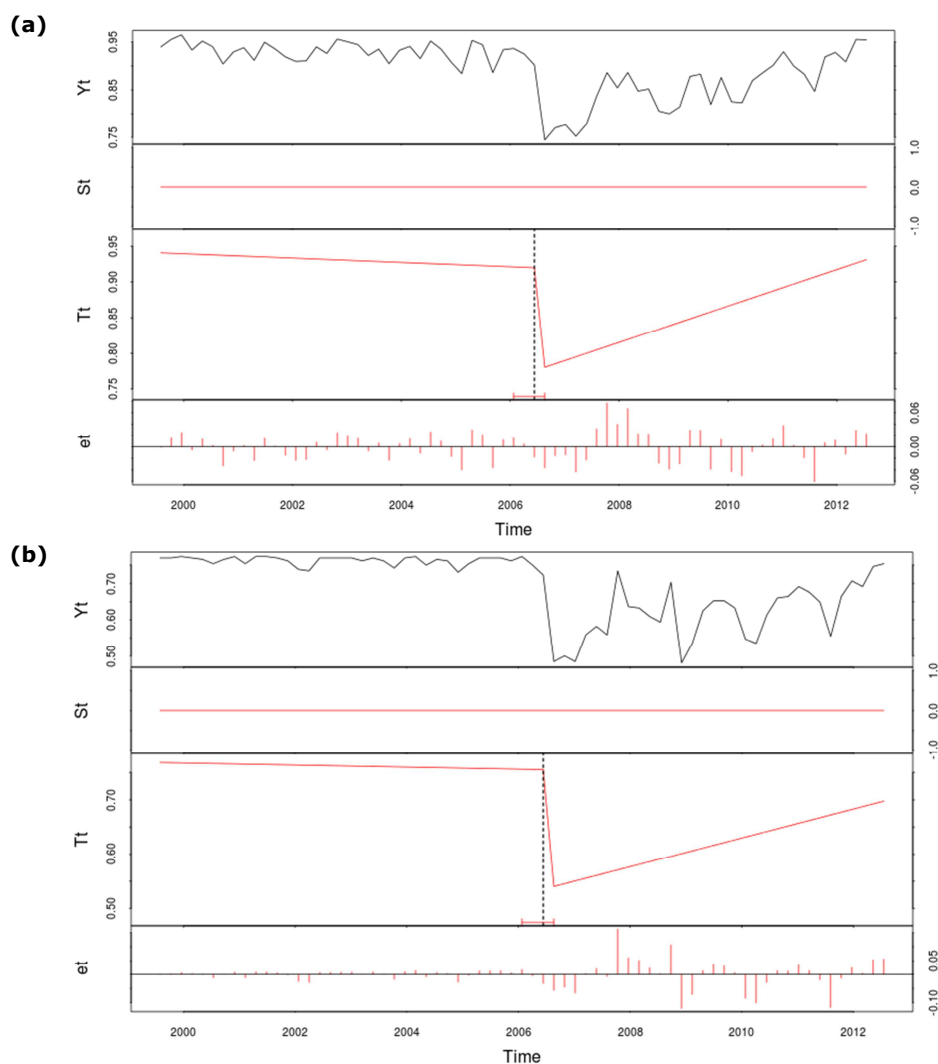


**Figure 12. Decomposition of Landsat NDVI (a) and NDFI (b) time series ( $Y_t$ ) for a single *P.caribea* pixel (Path/Row 395/2492). The time of the detected change and its confidence interval are shown in red.**

In contrast, in NDFI time series we observed a more gradual increase of indices values at the recovery phase. Unlike NDVI and DI, four years after the detected break, NDFI values were still low and six years after the harvest event the index did not reach the initial values.

In the next section, are presented the area-level BFASTmonitor results for a pine plantation. Previously obtained results have depicted high similarities between the performances of NDVI and DI time series. DI time series were considered as insignificant for comparison purposes. Hence, DI validation was limited to pixel-level exploratory analysis.

## 6.2 Area-level analysis

We analysed Landsat derived NDVI and NDFI time series (2000 – 2012) to detect forest cover changes (breaks) related to clearance operations in a *P.caribea* plantation. Initially, we applied a static threshold for the magnitude (m) of change, including all detected breaks with negative magnitude ( $m < -0.01$ ).

### 6.2.1 Detection and characteristics of land cover changes

Table 5, presents the spatial extend of detected breaks and the areas where changes with negative magnitude were depicted (without necessarily a break) by BFASTmonitor analysis in NDVI and NDFI time series over the monitoring periods 2005 – 2011.

**Table 5. Spatial extend of detected breaks and areas where changes with negative magnitude were depicted by BFASTmonitor analysis in NDVI and NDFI time series from 2005 – 2011.**

Monitoring Year	NDVI time series				NDFI time series			
	Negative change		Net break detection		Negative change		Net break detection	
	Hectares (ha)	% of study area	Hectares (ha)	% of study area	Hectares (ha)	% of study area	Hectares (ha)	% of study area
<b>2005</b>	335	37%	4	1%	208	23%	10	5%
<b>2006</b>	427	47%	3	0,7%	253	28%	8	3%
<b>2007</b>	522	58%	65	12%	496	55%	86	17%
<b>2008</b>	662	74%	217	33%	581	65%	263	45%
<b>2009</b>	759	84%	79	10%	627	70%	116	18%
<b>2010</b>	799	89%	168	21%	703	78%	145	21%
<b>2011</b>	102	11%	0	0	0	0	0	0

BFASTmonitor analysis was depicted minor changes for 2005 and 2006 (spatial extend less than 5% of the study area) in both indices time series, while major changes were observed between 2007 and 2010. The highest rates of breaks were detected at 2008 in both time series (33% and 45% of the study area for NDVI and NDFI, respectively). In general, BFASTmonitor analysis in NDVI time series was revealed higher rates of areas where changes with negative magnitude were occurred, while NDFI time series analysis was depicted higher rates of breaks.

Figure 13, shows the spatial distribution of land cover changes with negative magnitude and detected breaks by BFASTmonitor analysis in NDVI time series for the monitoring periods 2005 - 2010.

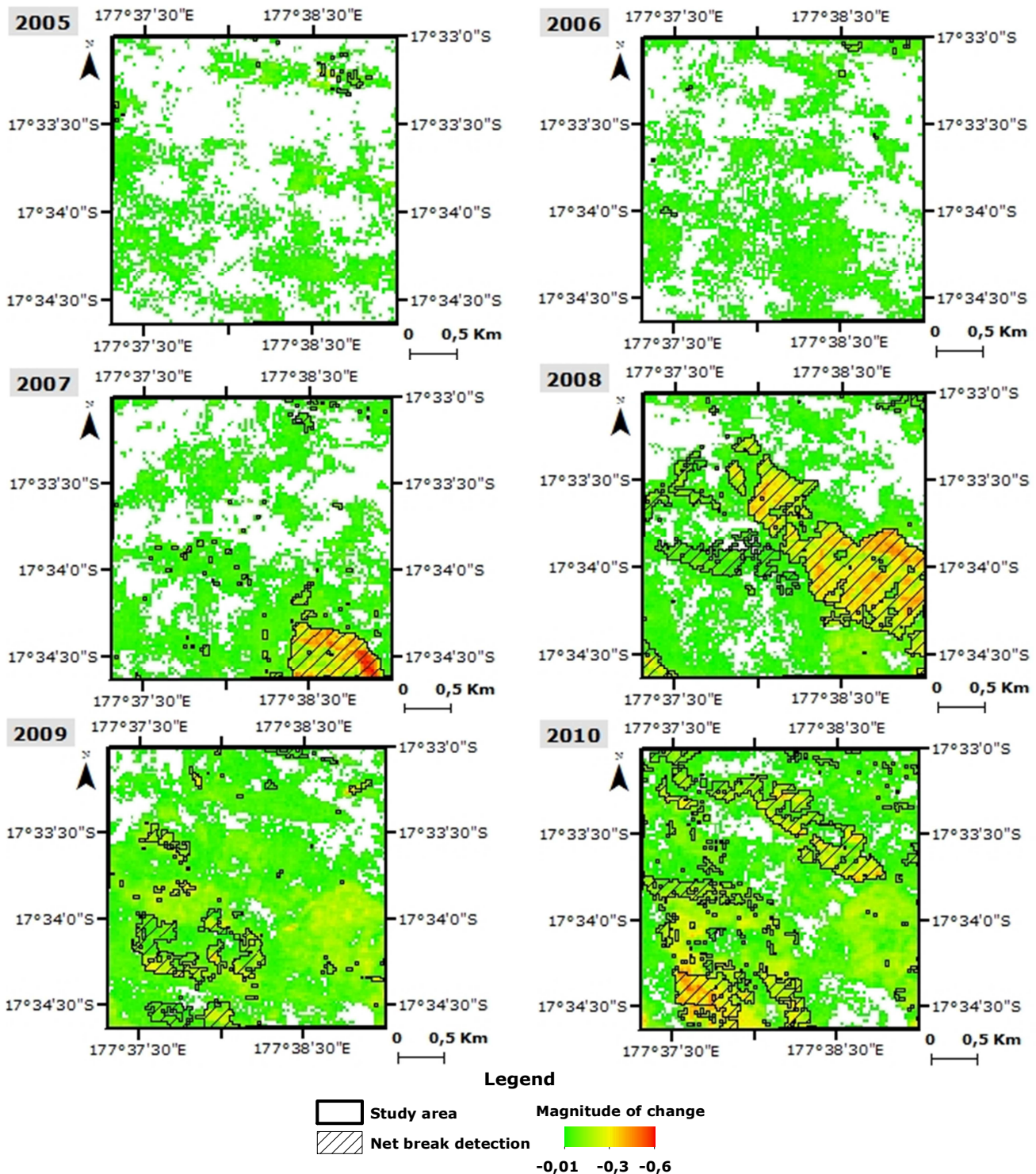


**Figure 13. Spatial distribution of land cover changes with negative magnitude and detected breaks by BFASTmonitor analysis in NDVI time series for the monitoring periods 2005 - 2010.**

The detected breaks were appeared mainly in clusters, where high magnitude of change ( $m < -0.15$ ) was depicted. However, breaks were also detected in areas with lower magnitude of change ( $m < -0.05$ ). Very few isolated pixels were depicted as breaks in NDVI time series. Figure 14, presents the spatial distribution of land cover change with negative magnitude and the net break detection by BFASTmonitor in NDFI time series from 2005 to 2010.

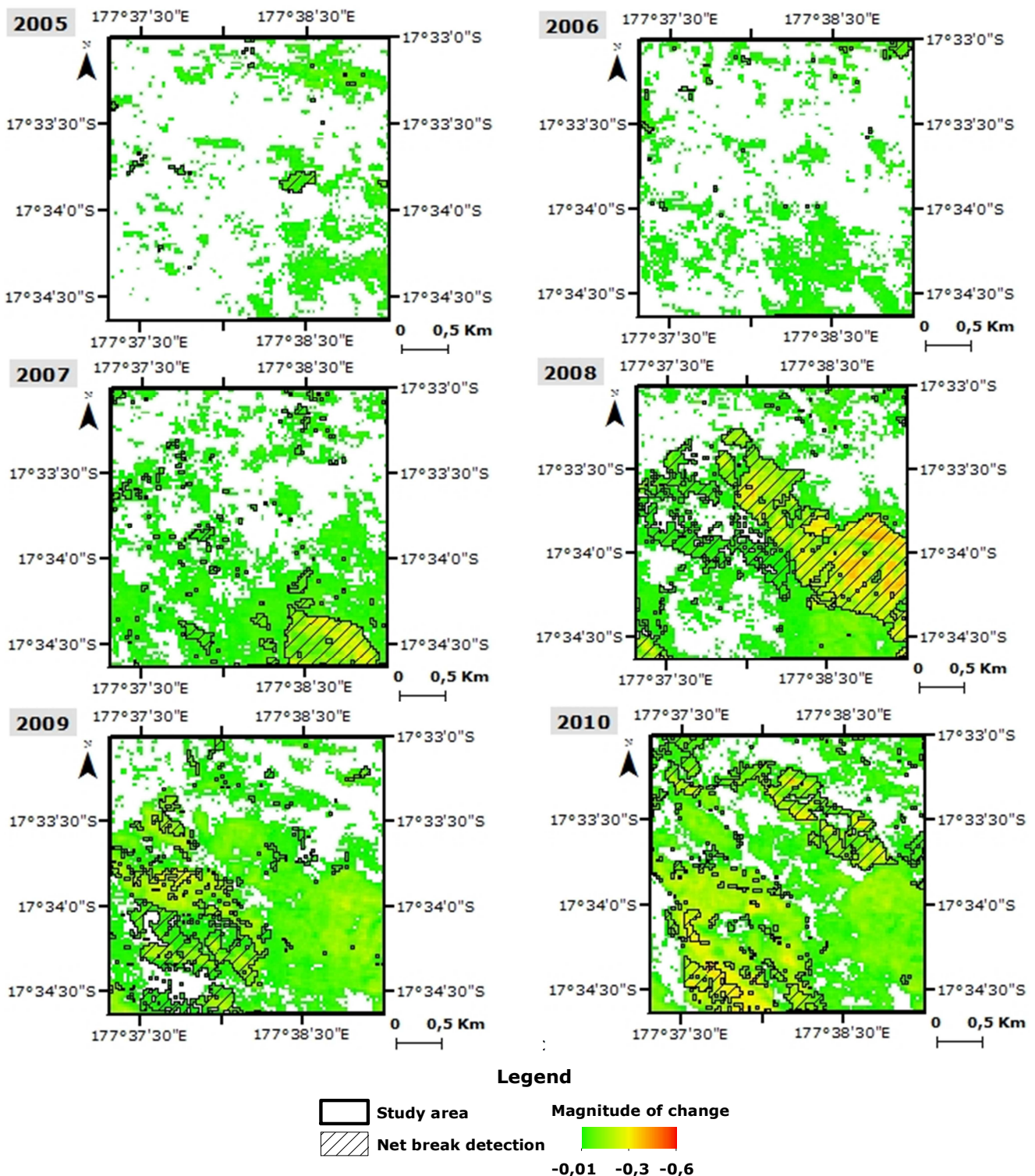
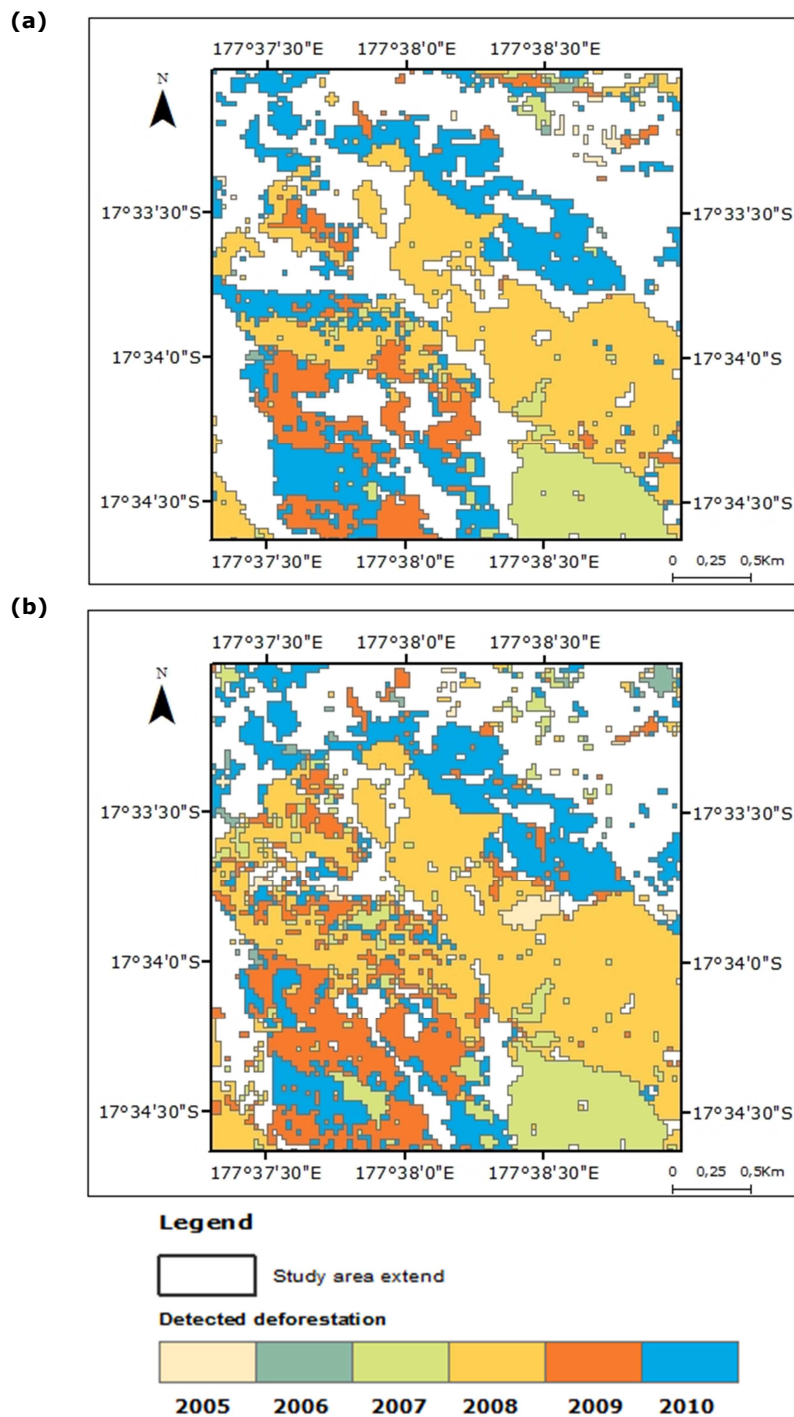


Figure 14. Spatial distribution of land cover changes with negative magnitude and detected breaks by BFASTmonitor analysis in NDFI time series for the monitoring periods 2005 - 2010.

In general, BFASTmonitor break detection in NDFI time series was depicted similar spatial patterns as in NDVI. Though, in NDFI time series the detected breaks were demonstrated generally lower magnitude.

Figure 15, synthesizes the spatiotemporal patterns of the detected breaks by BFASTmonitor analysis for NDVI and NDFI time series over the monitoring years 2005 – 2010.



**Figure 15. Map illustrating the spatial distribution of net break detection by BFASTmonitor analysis in (a) NDVI and (b) NDFI time series for the monitoring years 2005 – 2010.**

BFASTmonitor analysis in NDVI and NDFI time series was illustrated similar spatial patterns for the major land cover changes. High relevance was observed between NDVI and NDFI results for 2007 and 2010. Though, we observed spatial differences in break detection for 2008 and 2009. For 2008 and 2009, BFASTmonitor analysis in NDFI time series was depicted higher rates of breaks relative to NDVI results.

### 6.2.2 Accuracy assessment (static magnitude threshold)

We compared the estimated breaks by BFASTmonitor time series analysis with the generated reference dataset, to assess the prediction accuracy of the monitoring years 2007 – 2010 and stable pine. Initially, we included all the detected breaks with negative magnitude of change ( $m < 0.01$ ).

The overall accuracy of break-time estimation was 61% and 64% for NDVI and NDFI, respectively. The mapping accuracy (MA) was lower for both indices time series (mean MA 45% for both indices). Figure 16, shows the mapping accuracy of predicted breaks in NDVI and NDFI time series for each monitoring year and stable pine.

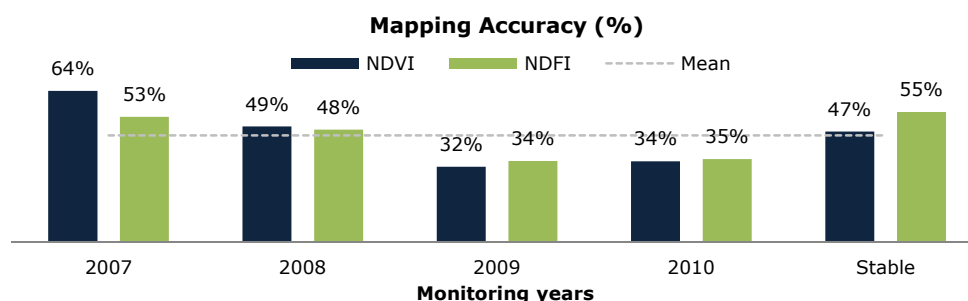


**Figure 16. Mapping accuracy (%) for the individual monitoring years (2007 – 2010, stable pine) and mean mapping accuracy of breaks by BFASTmonitor analysis in NDVI and NDFI time series.**

The mean omission error was 36% for NDVI and 32% for NDFI. Figure 17, shows the omission error of break-time estimation per monitoring year in NDVI and NDFI time series.

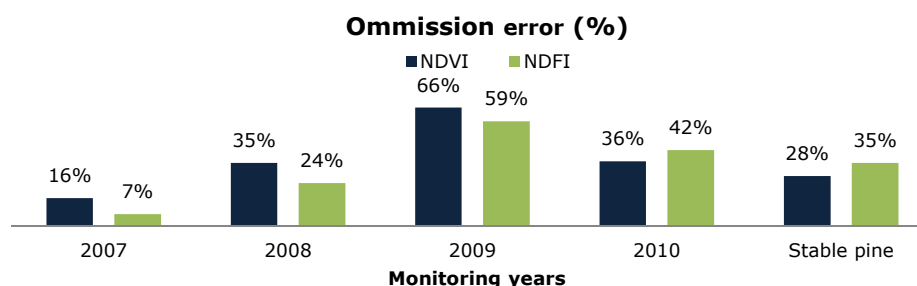


**Figure 17. Error of omission (%) in NDVI and NDFI time series based on the generated reference dataset for detected breaks during 2007 – 2010 and stable pine.**

For 2007 both indices were depicted the lowest rates of omission error, while breaks of 2009 were illustrated the highest values. Mean commission error was 35% and 40% for NDVI and NDFI, respectively. Figure 18, shows the commission error of break-time estimation for NDVI and NDFI time series. In general commission error was higher compared to omission error. For 2010 we observed the highest commission error for NDVI (58%) and NDFI (53%).

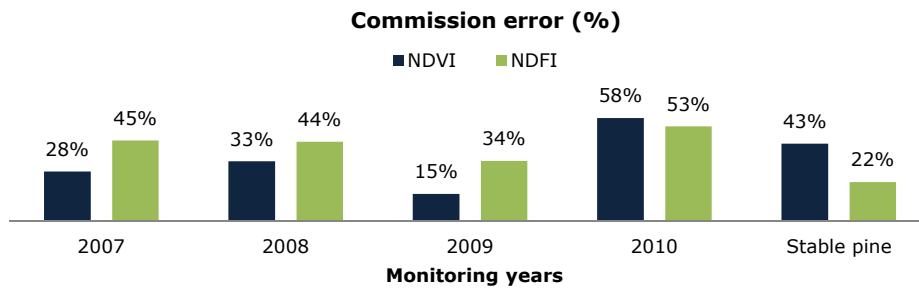


**Figure 18. Error of commission (%) in NDVI and NDFI time series based on the generated reference data for detected changes during 2007 – 2010 and stable pine.**

In previous results, we applied a static threshold for the magnitude of change in the detected breaks ( $m < 0.01$ ). Thus, breaks with low magnitude of change were included to the analysis. However, breaks with low negative magnitude most likely were associated with seasonal indices fluctuations rather than actual forest cover changes. We implemented magnitude thresholds to eliminate the occurrence of breaks unrelated to actual forest cover changes. The accuracy of BFASTmonitor break-time predictions was re-estimated for each threshold.

### 6.2.3 Accuracy assessment over varying magnitude thresholds

Figure 19, depicts the overall accuracy of BFASTmonitor break-time detection for NDVI and NDFI time series over the implemented magnitude thresholds. A systematic raise of break-time estimation overall accuracy was observed for both indices by increasing the magnitude threshold.

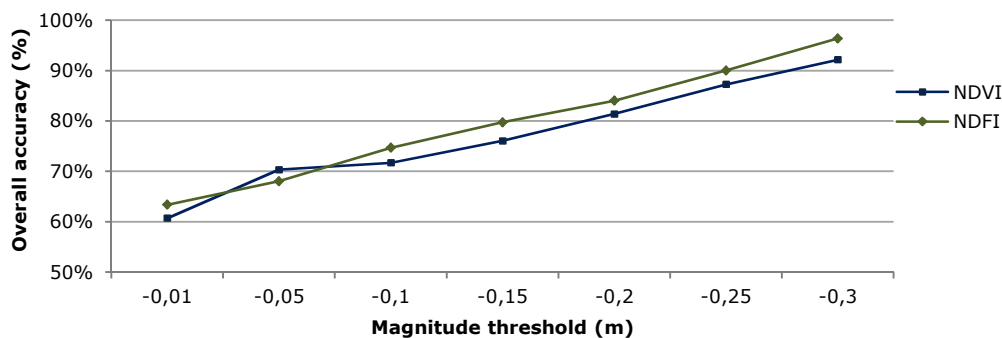


**Figure 19. Overall accuracy (%) of BFASTmonitor break-time detection in NDVI and NDFI over varying magnitude thresholds.**

Generally, NDFI was demonstrated higher rates of overall accuracy compared to the obtained results for NDVI. Both indices were illustrated high rates of overall accuracy (above 80%) when changes with low magnitude were excluded and only breaks with higher magnitude of change ( $m < -0.2$ ) were considered as actual forest cover changes.

Furthermore, we evaluated the break-time estimation accuracy of BFASTmonitor for the individual monitoring years over the implemented magnitude thresholds for NDVI (Appendix VI) and NDFI (Appendix VII) time series. Figure 20, illustrates the mapping

accuracy of detected breaks for each monitoring year by BFASTmonitor analysis in NDVI time series.

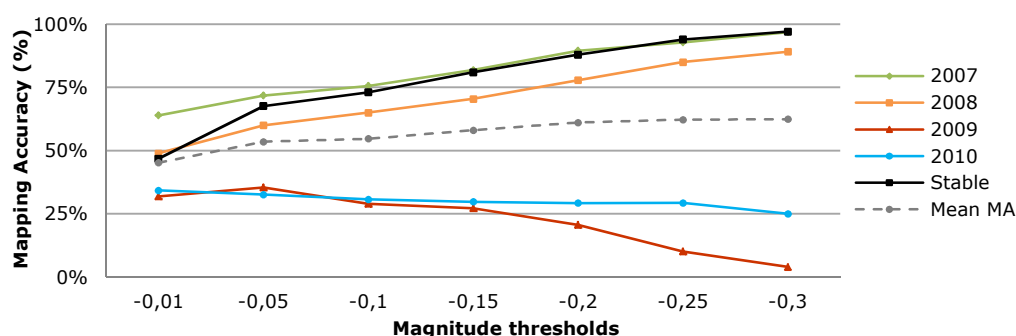


**Figure 20. Mapping accuracy (%) for the individual monitoring years (2007 – 2010, stable pine) and mean mapping accuracy (mean MA) of breaks by BFASTmonitor analysis in NDVI time series over the implemented magnitude thresholds.**

For NDVI time series, break estimation for 2007, 2008 and stable pine was demonstrated high mapping accuracy (above 50%) and an increasing trend by increasing the magnitude threshold. The mapping accuracy of break prediction for 2009 and 2010 was considerably lower than the previous monitoring years over all the implemented magnitude thresholds. Especially for 2009, we observed a negative trend in mapping accuracy by applying higher magnitude threshold. Figure 21, illustrates the omission error of break-time estimation by BFASTmonitor analysis in NDVI time series.

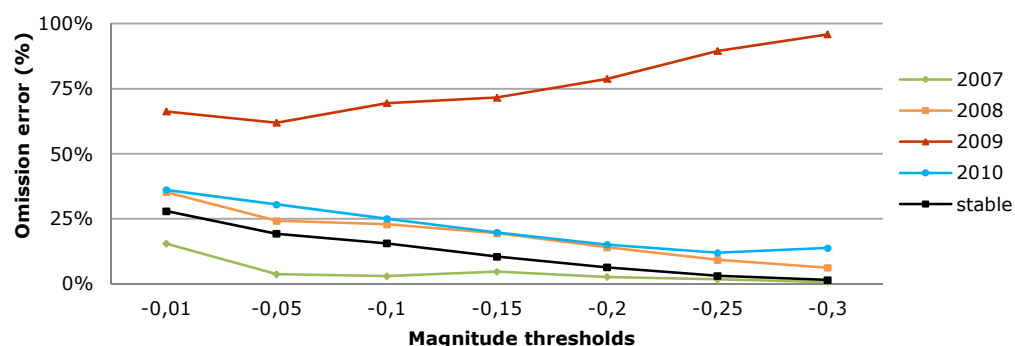


**Figure 21. Omission error (%) of estimated break-time by BFASTmonitor analysis in NDVI time series over the varying magnitude thresholds.**

Error of omission (i.e. break-time incorrectly classified in other than the actual year) was general low for 2007, 2008, 2010 and stable pine. Further, a decreasing trend was depicted for the abovementioned years. Unlike, 2009 was demonstrated significant higher values and an increasing trend of omission error compared to previous monitoring years.

Figure 22, shows the commission error of break-time estimation by BFASTmonitor analysis in NDVI time series over the varying magnitude thresholds.

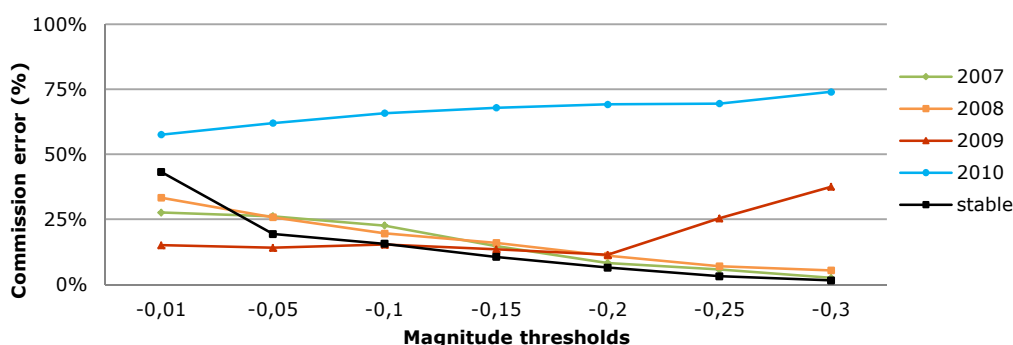


**Figure 22. Commission error (%) of estimated break-time by BFASTmonitor analysis in NDVI time series over the varying magnitude thresholds.**

In general, a negative trend in commission error was observed by increasing the magnitude threshold. The results for 2010 were deviated from the general pattern. High rates of commission error (above 50%) and an increasing trend were depicted for 2010 over all the implemented thresholds.

Unlike the mapping accuracy, where in general a positive trend was observed by increasing the magnitude threshold, the true-positive predictions (i.e. spatial agreement with the reference) were illustrated a negative trend by increasing the magnitude threshold. Figure 23, shows the true-positive predictions and overall accuracy of BFASTmonitor in NDVI time series, over the monitoring years 2007 – 2010 and stable pine.

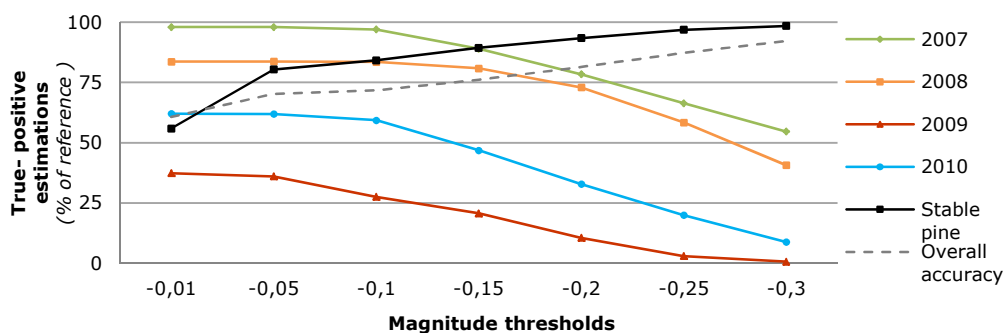
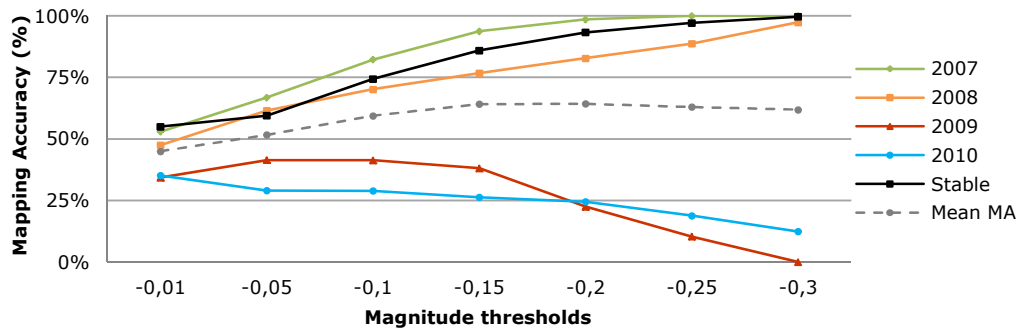


**Figure 23. True-positive predictions and overall accuracy of BFASTmonitor analysis in NDVI time series (as % of total breaks recorded in reference dataset for each monitoring year and stable pine) over varying magnitude thresholds.**

True-positive break-time predictions for 2007 and 2008 have shown high rates of agreement (above 80%) with the referenced change area for low (-0,05) and medium (-0,1) magnitude thresholds. As the magnitude threshold was increasing ( $m < -0,15$ ), a negative trend was depicted for 2007 and 2008. True-positive prediction agreement with the reference dataset was low for 2009 (below 30%), demonstrating a negative trend as the magnitude threshold was increased. For 2010, the correspondence to the reference dataset was above 50% for low (-0,05) and medium (-0,1) magnitude thresholds and was

decreased for higher magnitude of change, but in general did not reach rates higher than 62% of the corresponded reference area. Finally, stable pine was illustrated high rates of agreement (above 50%) and an increasing trend as the magnitude thresholds was raised.

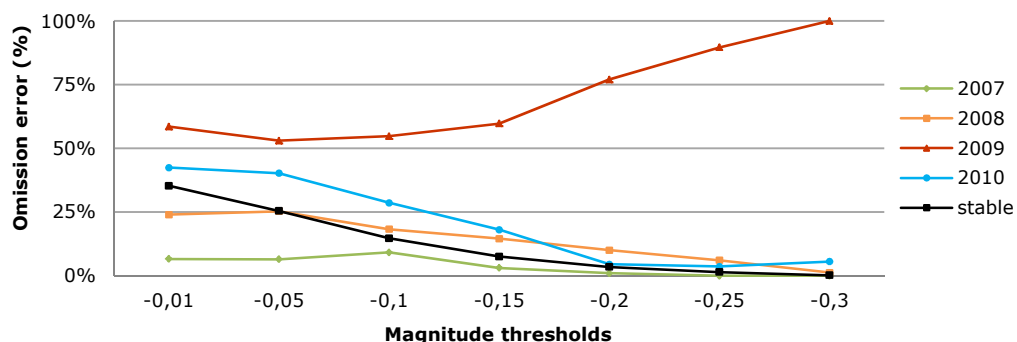
Additionally, we performed accuracy assessment of break-time estimations by BFASTmonitor in NDFI time series. Figure 24, shows the mapping accuracy of break detection for 2007 – 2010 and stable pine in NDFI time series for the applied thresholds.



**Figure 24. Mapping accuracy (%) for the individual monitoring years (2007 – 2010, stable pine) and mean mapping accuracy (mean MA) of breaks by BFASTmonitor analysis in NDFI time series over the implemented magnitude thresholds.**

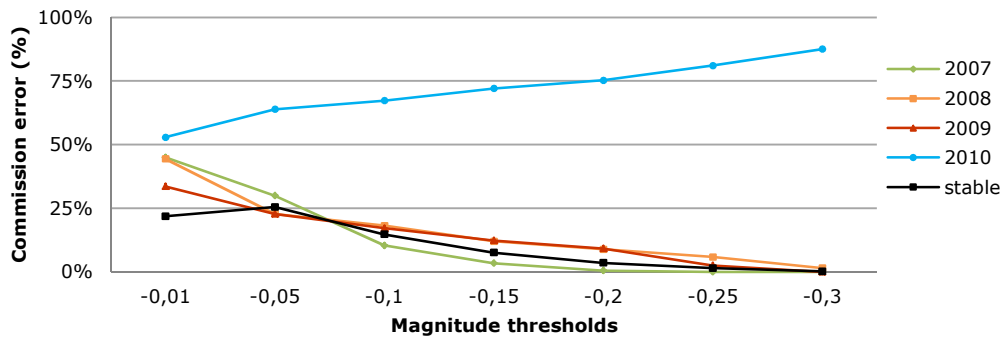
Mapping accuracy of break detection for NDFI time series was demonstrated similar trends and values as NDVI. High mapping accuracy and an increasing pattern was observed for 2007, 2008 and stable pine by increasing the magnitude threshold. Break detection for 2009 and 2010 was illustrated again lower rates and a negative trend for higher magnitude thresholds.

High similarity was depicted between the omission error patterns of NDFI and NDVI. Figure 25, shows the omission error of break-time estimation by BFASTmonitor in NDFI time series for the monitoring years 2007 – 2010 and stable pine, over the implemented magnitude thresholds. By increasing the magnitude threshold, we observed a negative trend of omission error for break-time estimation of 2007, 2008, 2010 and stable pine. Alike NDVI, NDFI results for 2009 were differed from the general trend.



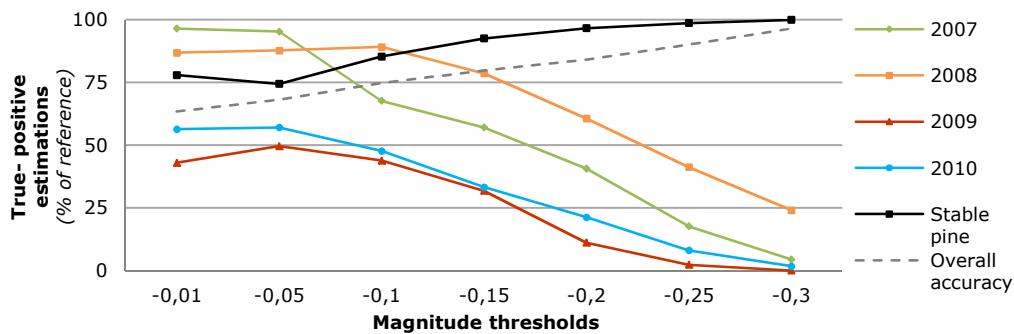
**Figure 25. Omission error (%) of estimated break-time by BFASTmonitor analysis in NDFI time series over the varying magnitude thresholds.**

Figure 26, shows the commission error of break-time estimation in NDFI time series over the varying thresholds, for the monitoring years 2007 – 2010 and stable pine. Commission error in NDFI time series was reached lower values relative to NDVI, by increasing the magnitude threshold. Though, breaks detected at 2010 were revealed higher rates of commission error in relation to NDVI. Likewise NDVI, BFASTmonitor analysis in NDFI time series was depicted lower rates of correct break-time classification for 2010.



**Figure 26. Commission error (%) of estimated break-time by BFASTmonitor analysis in NDFI time series over the varying magnitude thresholds**

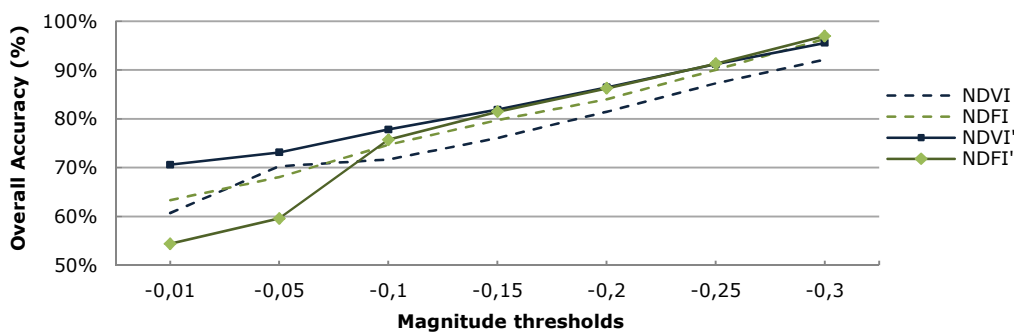
The negative tendency of true-positive predictions by increasing the magnitude threshold was also present to NDFI results. Figure 27, shows the true-positive predictions and overall accuracy by BFASTmonitor analysis in NDFI time series, over the monitoring years 2007 – 2010 and stable pine. Prediction agreement for 2009 was again significant lower than the previous year. However, for low (-0.05) and medium (-0.1) magnitude thresholds NDFI was revealed higher values compared to NDVI. For 2010, the true-positive predictions were higher relative to NDVI for low to medium magnitude thresholds (maximum rates 57%).



**Figure 27. True-positive predictions and overall accuracy of BFASTmonitor analysis in NDFI time series (as % of total breaks recorded in reference dataset for each monitoring year and stable pine) over varying magnitude thresholds.**

### 6.2.4 Improving the accuracy

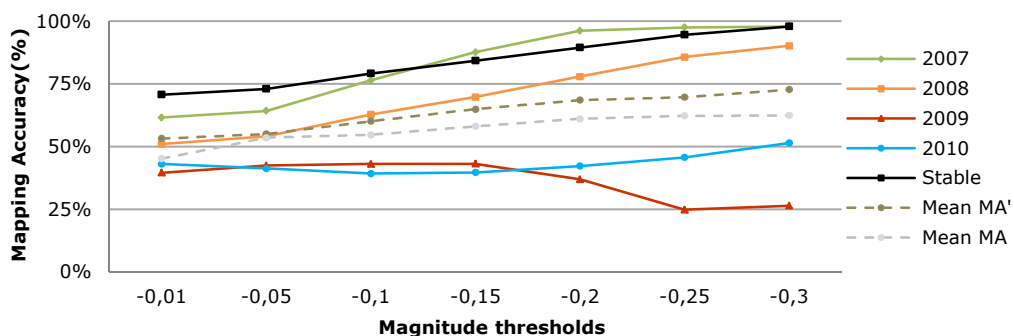
We re-assessed the accuracy of break-time detection in NDVI (Appendix IX) and NDFI (Appendix X) time series after the removal of cloud contaminated scenes. In general, the overall accuracy of BFASTmonitor break-time estimation was increased after the removal of cloud contaminated scenes. Figure 28, illustrates the overall accuracy of break-time estimation by BFASTmonitor in NDVI and NDFI time series before and after the image removal.



**Figure 28. Overall accuracy (%) of break-time detection by BFAST monitor analysis in NDVI and NDFI before (NDVI, NDFI) and after (NDVI', NDFI') the removal of cloud contaminated scenes over the implemented magnitude thresholds.**

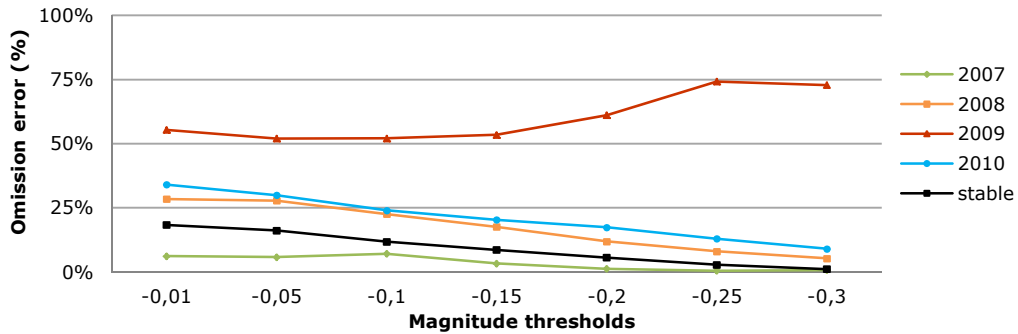
Break detection in NDVI time series was demonstrated higher rates of improvement compared to NDFI. However, break-time estimation by BFASTmonitor in NDFI time series was indicated slightly higher overall accuracy related to NDVI results while considering as breaks, changes with magnitude higher than -0.20.

In addition, improvement was observed in mapping accuracy of breaks in NDVI time series relative to the initial results. Figure 29, shows the mapping accuracy and the mean mapping accuracy for break detection in NDVI time series after the removal of cloud contaminated scenes.



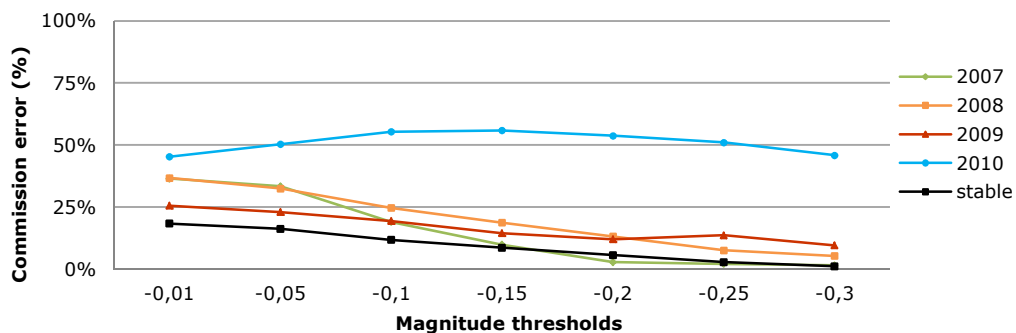
**Figure 29. Mapping accuracy (%) for the individual monitoring years (2007 – 2010, stable pine) and mean mapping accuracy (after the removal: mean MA' and before: mean MA) of breaks by BFASTmonitor analysis in NDVI time series over the implemented magnitude thresholds after the scene removal.**

Omission error for NDVI after the scene removal was demonstrated high similarity relative to the primary results. However, lower rates were observed for 2009 compared to the initial results for high magnitude thresholds. Figure 30, shows the re-computed omission error in NDVI time series after the scene removal.



**Figure 30. Omission error (%) of estimated break-time by BFASTmonitor analysis in NDVI time series over the varying magnitude thresholds after the removal of cloud contaminated Landsat scenes.**

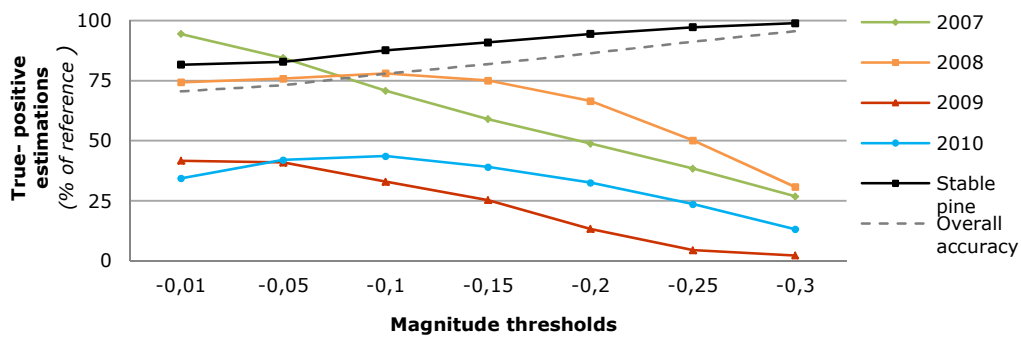
Error of commission for NDVI was illustrated lower rates relatively to the results before the scene removal (Figure 31).



**Figure 31. Commission error (%) of estimated break-time by BFASTmonitor analysis in NDVI time series over the varying magnitude thresholds after the removal of cloud contaminated Landsat scenes.**

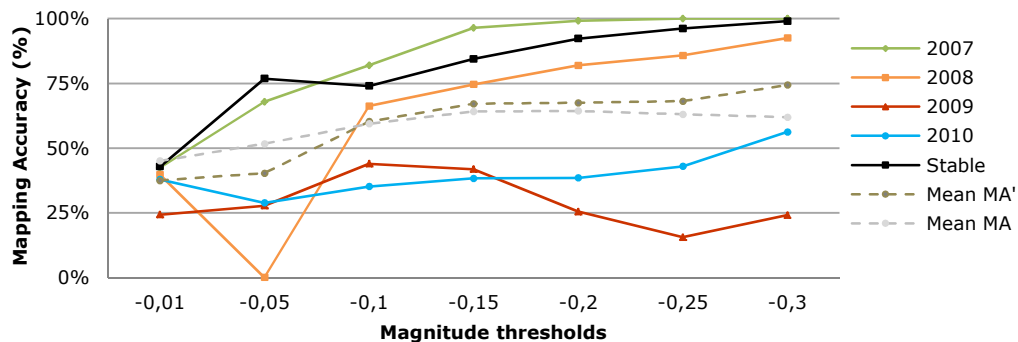
Especially, for 2009 we observed a decrease of commission error for magnitude higher than -0.2. For 2010, commission error was high compared to previous monitoring years, but a small decrease was depicted relative to the primary results.

BFASTmonitor ability to depict the change area of the reference dataset did not indicate major enhancement in NDVI time series (Figure 32). Improvement was observed for stable pine, while no alterations were depicted for 2008 and 2009. Further, the results for 2007 and 2010 were indicated a minor drop.



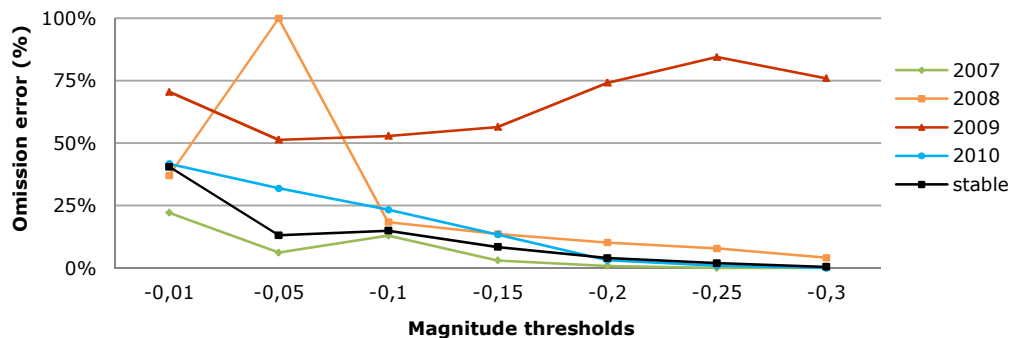
**Figure 32. True-positive predictions and overall accuracy of BFASTmonitor analysis in NDVI time series (as % of total breaks recorded in reference dataset for each monitoring year and stable pine) over varying magnitude thresholds after scene removal.**

Furthermore, accuracy assessment of the detected breaks was performed in NDFI time series after the removal of cloud contaminated scenes. Mapping accuracy for break detection in NDFI time series was slightly improved compared to the initial results for magnitude thresholds higher than -0.15 (Figure 33). For 2009 and 2010, the results remained low regarding other monitoring years; however we observed a small improvement. In addition, significant differences were not depicted between NDVI and NDFI.



**Figure 33. Mapping accuracy (%) for the individual monitoring years (2007 – 2010, stable pine) and mean mapping accuracy (after the removal: mean MA' and before: mean MA) of breaks by BFASTmonitor analysis in NDFI time series over the implemented magnitude thresholds after the scene removal.**

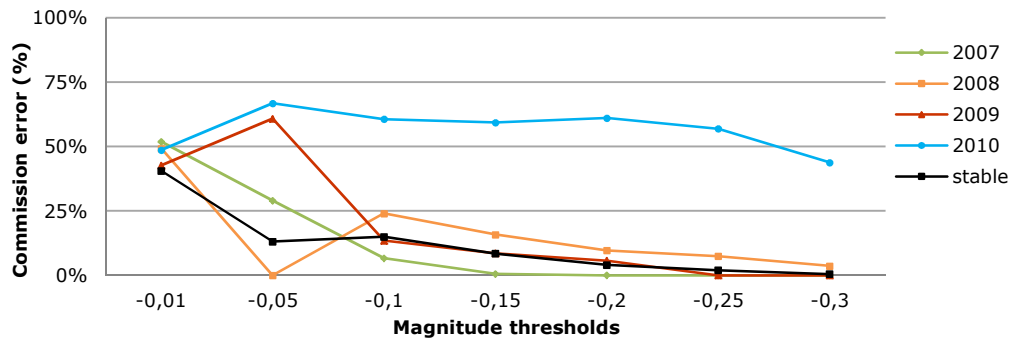
Figure 34, illustrates the re-calculated omission error of break-time estimation by BFASTmonitor over varying magnitude thresholds in NDFI time series.



**Figure 34. Omission error (%) of estimated break-time by BFASTmonitor analysis in NDFI time series over the varying magnitude thresholds after the removal of cloud contaminated Landsat scenes.**

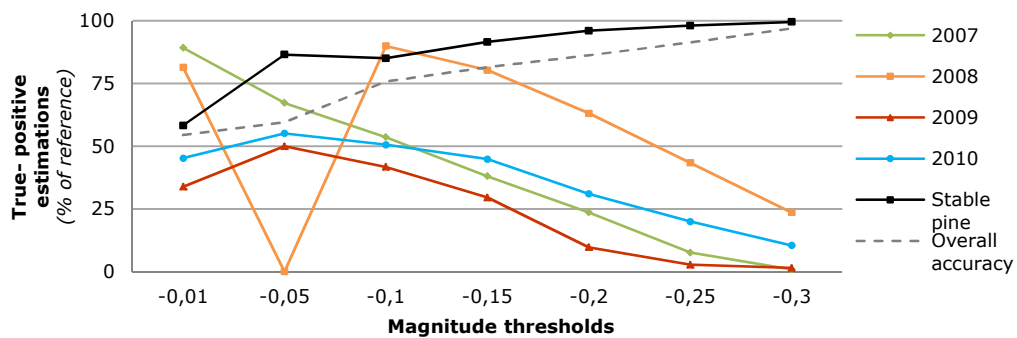
Omission error in NDFI did not indicate significant improvement compared to the primary results. For 2007 and 2008 omission error in general was revealed the same values, while for 2009, 2010 and stable we observed a small reduction.

Figure 35, shows the re-computed commission error in NDFI time series. The general trend was illustrated same rates of commission error, however small improvement was depicted for all monitoring years over high magnitude thresholds ( $m < -0.20$ ).



**Figure 35. Commission error (%) of estimated break-time by BFASTmonitor analysis in NDFI time series over the varying magnitude thresholds after the removal of cloud contaminated Landsat scenes.**

Finally, the true-positive predictions of BFASTmonitor analysis in NDFI time series did not demonstrate significant alterations. Figure 36, shows the true-positive predictions and overall accuracy of BFASTmonitor analysis for NDFI time series over the implemented magnitude thresholds after the removal of cloud contaminated scenes.



**Figure 36. True-positive predictions and overall accuracy of BFASTmonitor analysis in NDFI time series (as % of total breaks recorded in reference dataset for each monitoring year and stable pine) over varying magnitude thresholds after scene removal.**

For 2008, 2009, 2010 and stable pine true-positive predictions were illustrated high values for low magnitude thresholds and negative trend as the magnitude threshold was increased. For 2007 the results were indicated a decrease compared to the initial performance for low to medium magnitude thresholds.

## 7. DISCUSSION

### 7.1 Pixel – level analysis

#### 7.1.1 Spectral indices sensitivity differences towards seasonal variations

We analysed three land-cover classes, mangrove forest, stable hardwood forest and sugarcane plantations, to retrieve the sensitivity differences towards seasonal variations in pixel-level for NDVI, NDFI and DI time series. For mangrove and stable hardwood forest the indices were performed similarly. High rates of biomass and absence of changes (typical characteristics of mangrove and intact hardwood forest), were depicted by high indices values in time series. Further, Landsat time series captured low rates of standard deviation and insignificant seasonal variations.

Higher rates of standard deviation and sensitivity differences were observed between the indices time series for sugarcane pixel-level analysis. The life cycle of sugarcanes was characterised by high seasonal fluctuations. At the growth stages of the plant, the continuing increase of biomass was depicted by gradual raise of indices values. Subsequently, the harvest of sugarcanes was gradually decreased the biomass rates, exposing further the soil properties. A gradual decrease of indices rates was observed at the harvest phase of the plants. NDFI results were demonstrated higher rates of standard deviation in comparison with those for NDVI and DI. Further, higher drop in NDFI values was depicted during the harvest phase relative to NDVI and DI. The spectral properties of NDFI signal could explain this difference. NDFI combines image fractions, such as Green Vegetation (GV), non-photosynthetic vegetation (NPV) and Soil (Souza et al., 2005a). Unlike the simple visible-infrared ratio indices (e.g. NDVI) that are computed only based on the photosynthetic capacity, NDFI considers further factors and characteristics of change (such as the soil exposure). Thus, NDFI has the potential to be more sensitive while depicting biomass loss and soil exposure that constituted the spatial signature of harvest operations.

Further, we performed BFAST algorithm analysis for sugarcane pixel time-series. Within the seasonal component ( $S_t$ ) of the time series were captured the seasonal variations of sugarcanes. We observed a repeated pattern of peaks and valleys in the seasonal component, illustrating the biomass loss and plant regrowth after the harvest. The algorithm was likely able to capture the seasonal fluctuation without misclassifying these variations as breaks. BFAST algorithm integrates the decomposition of time series into seasonal ( $S_t$ ), trend ( $T_t$ ) and remainder ( $e_t$ ) components with methods for detecting changes in time series (Verbesselt et al., 2010b). The decomposition of the time series has the potential to enhance the ability of the method to identify correctly breaks and seasonal variations.

### **7.1.2 Temporal dynamics of Fiji pine**

We performed pixel-level analysis on pine forest to retrieve the temporal dynamics of undisturbed, deforested and reforested Fiji pine. For intact pines, high biomass rates and absence of disturbances were depicted by high values for all the examined indices time series. The temporal resolution of Landsat time series (16 days) was illustrated low ability to depict the seasonality of pines, which is present in other satellite sources with higher temporal resolution (e.g. MODIS data, temporal resolution 1-2 days). However, we observed slightly lower detection sensitivity of pine seasonality, in NDFI and DI time series compared to the corresponding in NDVI.

Further we analysed *P.caribea* pixel time series with documented harvest operations and a visible regrowth. Based on the obtained results, we defined the main phases (pre-harvesting period, breakpoint and regrowth phase) of pine cycle. BFASTmonitor and BFAST algorithms were likely able to detect and characterise changes in time series related to harvest operations. Additionally, the algorithms were appeared capable to depict the regrowth period of the *P.caribea* plantation. The main difference between the indices performance was the depicted length of pine regrowth. In general, NDFI was illustrated more gradual increase of values compared to NDVI and DI, during the recovery phase. Hence, the spatial signature of the harvest operation could be probably detected for longer period of time in NDFI time series.

The obtained results were suggested that the spectral properties of NDFI signal (see section 7.1.1) have the potential to track forest canopy changes of pines for longer period of time. This is of particular importance for monitoring purposes, especially in tropical regions where satellite image acquisition can be challenging due to persistent cloud.

## **7.2 Area analysis**

### **7.2.1 Detection and characteristics of land cover changes**

We implemented BFASTmonitor algorithm to analyse NDVI and NDFI time series (2000 – 2012) for a study area. The selected study area was a small part of a pine plantation, where harvest operations have altered the forest cover. We validated the break detection ability of BFASTmonitor and further we assessed the potentials of NDVI and NDFI time series as temporal change indicators. For the purposes of the present study, the results of BFASTmonitor analysis were limited to breaks with negative magnitude. Initially, we applied a static threshold for the magnitude ( $m$ ) of change. Hence, we analysed all the breaks with negative magnitude ( $m < -0.01$ ).

In general, BFASTmonitor analysis for NDVI and NDFI time series was captured similar spatiotemporal patterns for the major breaks in the study area. The breaks were appeared mainly in clusters where changes were observed with magnitude between  $-0.15$  and  $-0.20$ . Though, breaks were also depicted in areas with lower magnitude of change. Both indices time series were illustrated the major forest cover changes (breaks) between 2007 and 2010. Difference between the indices performance was appeared for changes with low magnitude unrelated to actual forest cover changes (breaks). NDVI time series were illustrated higher rates of areas where changes with low magnitude ( $m < -0.05$ ) were depicted compared to NDFI. The higher sensitivity of NDVI to changes with low magnitude was visible for all the monitoring years but was appeared more dominant for 2005 and 2006.

Figure 37, highlights the sensitivity differences to changes with low magnitude between NDVI and NDFI time series for 2005 and 2006.

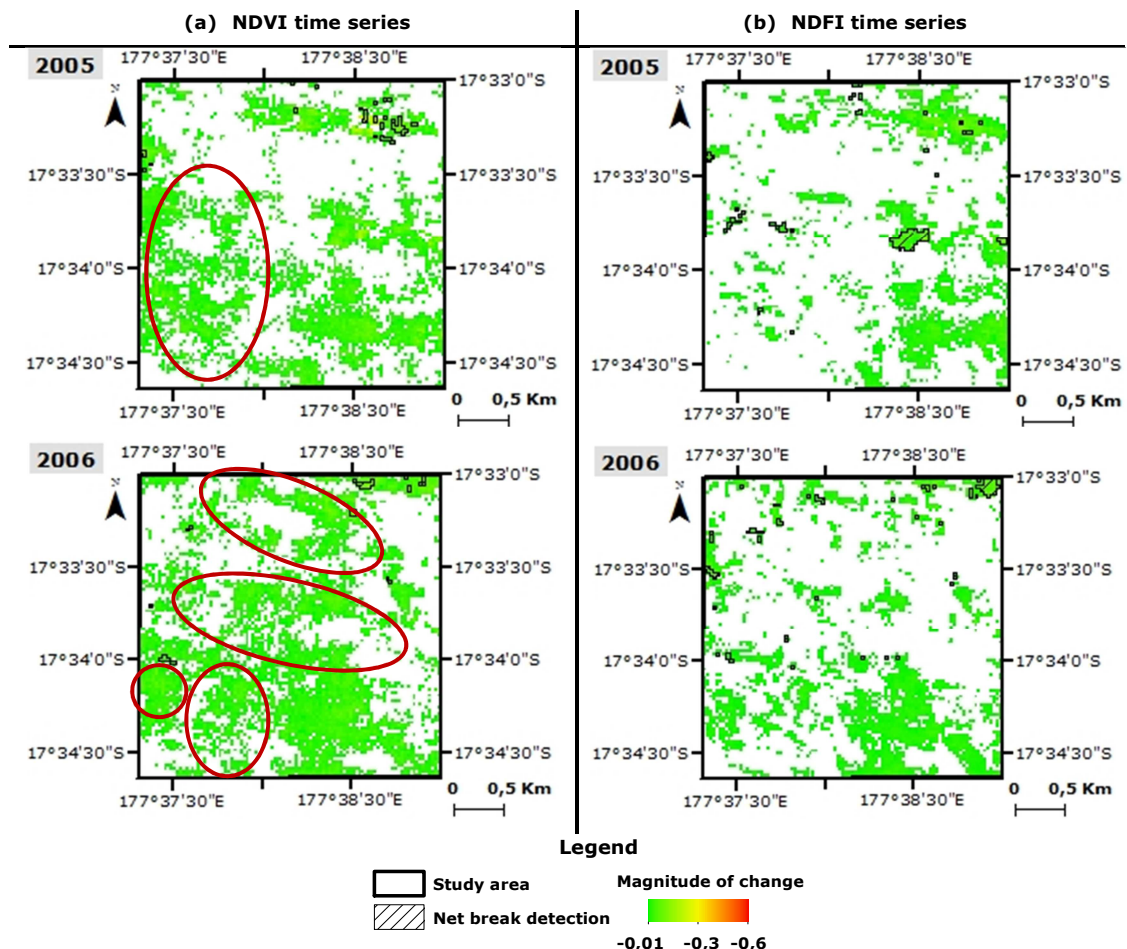


**Figure 37. Sensitivity differences to changes with low magnitude between (a) NDVI time series and (b) NDFI time series for the monitoring years 2005 and 2006.**

Low magnitude changes were probably associated with seasonal variations of pine forest rather than deforestation or cloud contamination (deforestation and clouds would significantly decrease the indices values). NDVI is strongly associated with the chlorophyll content and the photosynthetic capacity of the tree (Rouse et al., 1974). Thus probably

NDVI was appeared more sensitive compared to NDFI, detecting biomass fluctuations related to seasonal variations.

In contrast, our results were indicated slightly higher amount of breaks in NDFI time series compared to NDVI for all the monitoring years. Particularly for 2008 and 2009, breaks in NDFI time series were occupied 45% and 19% of the study area, respectively while in NDVI were 33% and 10%, respectively. Figure 38, shows the spatial difference of the detected breaks for 2008 and 2009 by BFASTmonitor analysis on NDVI and NDFI time series.

As already mentioned the spectral properties of NDFI signal, were likely more sensitive depicting the spatial characteristics (biomass loss and soil exposure) of harvest operations. Therefore, NDFI has the potential to enhance the detection of deforestation caused by logging operations (Souza et al., 2005).

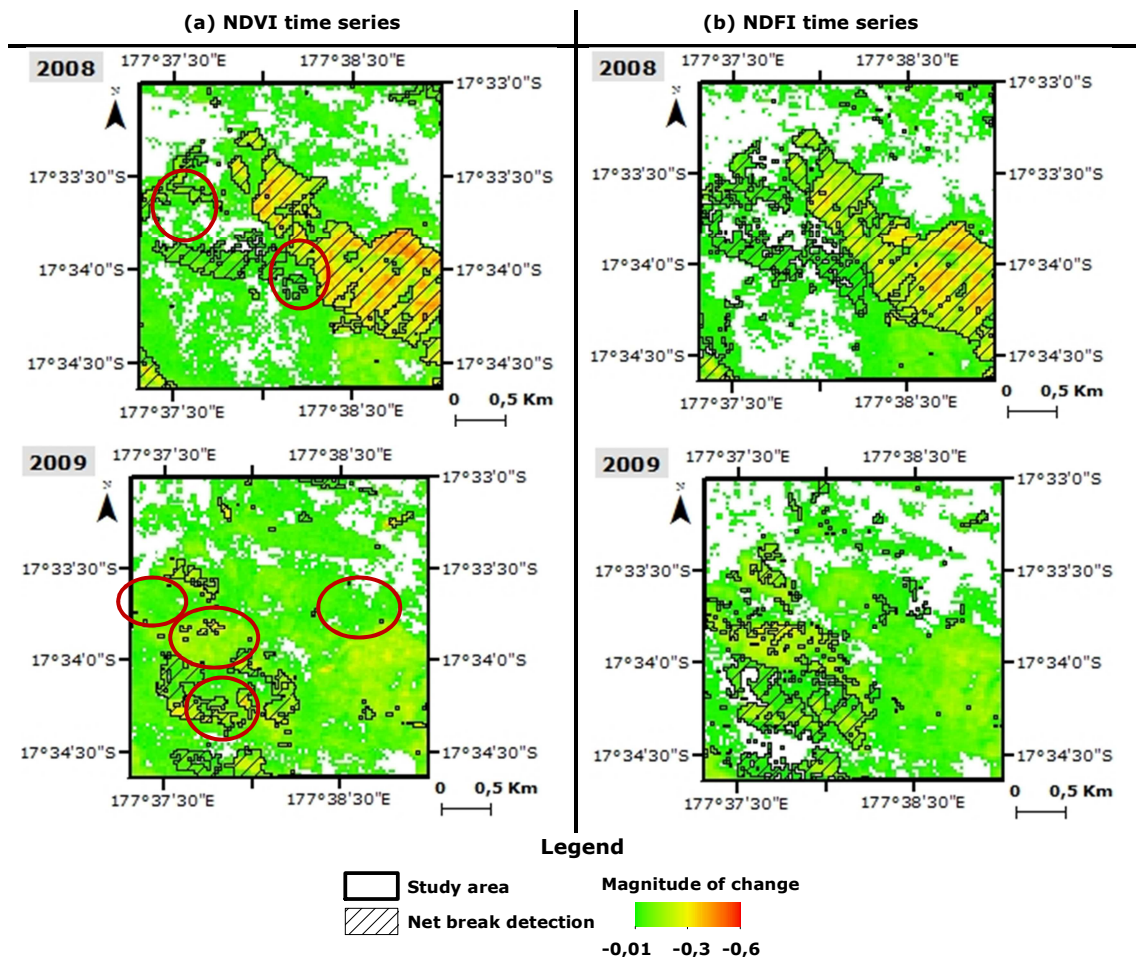


**Figure 38. Detected breaks for 2008 and 2009 by BFASTmonitor analysis in (a) NDVI time series and (b) NDFI time series.**

Furthermore, the results were suggested that in NDFI time series the signature of the harvest operation (break) was visible for longer period of time. Figure 39, shows the breaks and the areas where changes of 2007 and 2010 were detected by BFASTmonitor on NDVI and NDFI time series.

For NDVI time series, the area where breaks were detected at 2007, three years after the break did not show change. Unlike, for NDFI time series, the same area was still appeared as area where changes with negative magnitude occurred in 2010. Hence, NDFI has the potential to track the spatial signature of forest canopy changes for longer. These results are in accordance with the obtained results of the exploratory pixel level analysis on deforestation patterns of pines (see section 7.1.2).

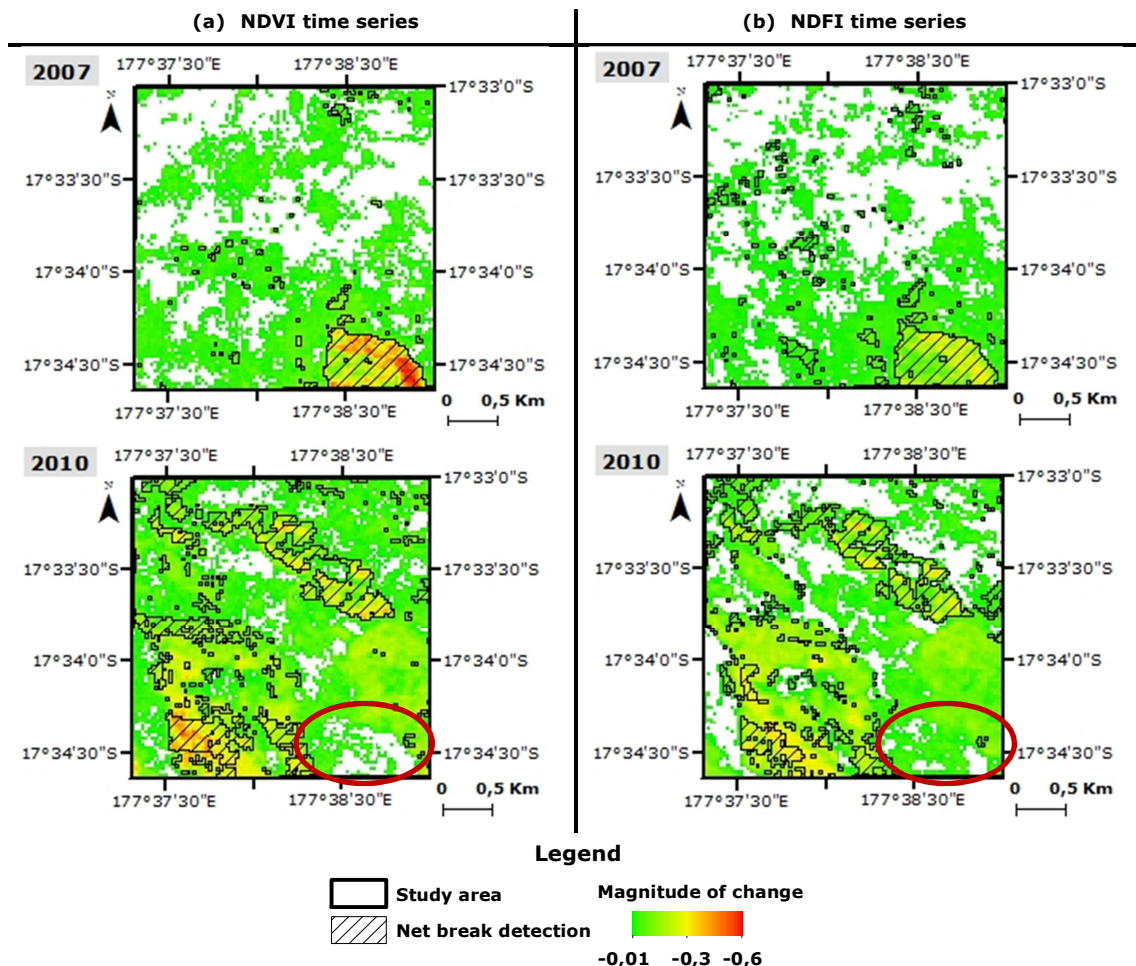


Figure 39. Areas where breaks and changes were detected for 2007 and 2010 by BFASTmonitor analysis in (a) NDVI time series and (b) NDFI time series.

### 7.2.2 Accuracy assessment based on reference data

We validated the accuracy of break detection by BFASTmonitor based on comparison with a generated reference map for the study area. Initially, we applied a static magnitude threshold ( $m < -0.01$ ), including all the detected breaks with negative magnitude to the accuracy assessment.

The overall accuracy of break detection was 61% and 64%, for NDVI and NDFI time series, respectively. In general, BFASTmonitor was able to depict with higher mapping accuracy in both time series breaks of 2007, 2008 and also the stable pine area (mapping accuracy

above 47%), while lower rates were observed for 2009 and 2010 (mapping accuracy below 35%). False break detection and consequently low rates of estimation accuracy were mainly induced by (i) remaining clouds in the time series after the image pre-processing and (ii) the magnitude of change in detected breaks.

High rates of commission error were strongly related to cloud contamination of the time series. Clouds were produced a significant drop of indices values. Hence, BFASTmonitor was misclassified these drops with breaks. Thus, within the results of a certain year remaining clouds were falsely produced breaks. Cloud contamination of time series was mainly associated with lower rates of mapping accuracy that we observed for 2009 and 2010. Clouds within the images of 2010 were produced false breaks (mainly as breaks of 2009), increasing the commission error for 2010. Figure 40, shows the true-positive and false predictions of 2010 by BFASTmonitor for NDVI time series and examples of pixel-level analysis on false prediction, which confirms the presence of clouds.

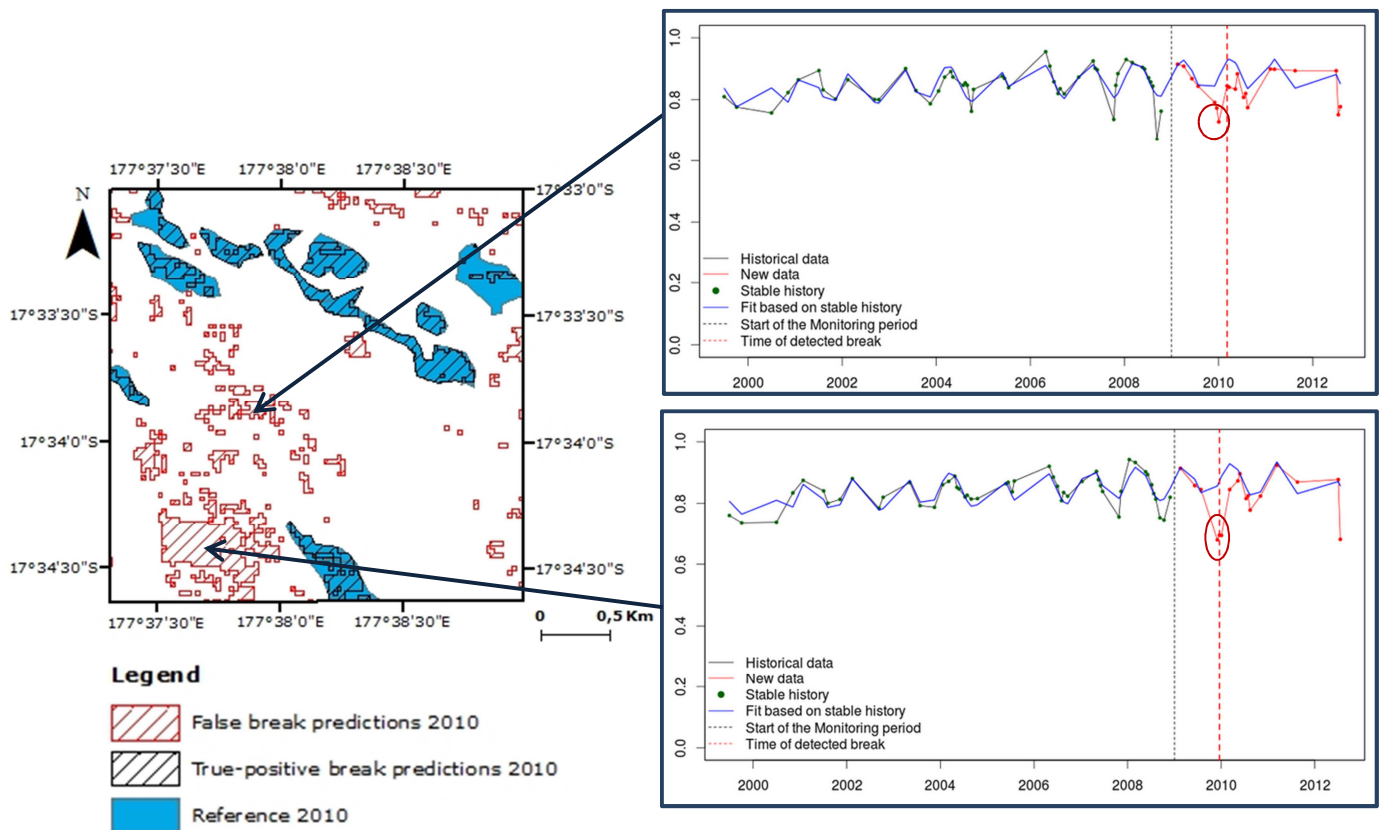


**Figure 40. True-positive and false predictions of 2010 by BFASTmonitor for NDVI time series and pixel-level analysis.**

In addition, the magnitude of change in the detected breaks has influenced the break detection accuracy. Initially, we included all the detected breaks with negative magnitude. However, breaks with insignificant magnitude ( $m > -0.1$ ) were probably related to seasonal variations of pine trees rather than actual changes in forest cover. Thus, by

including breaks associated with seasonal variations, break overestimation was observed within a monitoring year.

Breaks with low magnitude were detected in both indices time series for all the monitoring years. Though, NDVI was demonstrated higher sensitivity compared to NDFI, depicting seasonal variations of pines and hence, higher rates of break overestimation were observed within NDVI results. Thus, NDVI was illustrated lower rates of accuracy relative to NDFI.

### **7.2.3 Improving break-time estimation accuracy**

In order to improve the accuracy of BFASTmonitor break detection for NDVI and NDFI time series, we estimated the magnitude of change that was corresponded to an actual harvest event and further, we removed cloud contaminated images from the time series.

#### ***Applying magnitude thresholds***

We applied seven magnitude thresholds (-0.01, -0.05, -0.1, -0.15, -0.20, -0.25 and 0.30), to define the minimum reduction on indices values that was triggered by an actual forest cover change in the study area. The maximum tested threshold was -0.30 due to limited occurrence of breaks with higher magnitude of change. The accuracy assessment was repeated over the implemented magnitude thresholds.

A systematic increase of overall accuracy was depicted for both indices by increasing the magnitude threshold. Sufficient spatial agreement (overall accuracy above 80%) with the generated reference dataset rates was observed in both time series when low magnitude changes were excluded. Hence, actual forest cover changes due to harvest operations were probably related to breaks with magnitude higher than -0.15. BFASTmonitor break detection in NDFI was illustrated slightly higher ability to classify correctly breaks compared to NDVI. The highest overall accuracy (96%) was observed for break detection in NDFI time series when we applied the maximum magnitude threshold ( $m < -0.30$ ). Additionally, NDFI was depicted slightly better mapping accuracy of breaks for the individual monitoring years relative to NDVI.

In general, BFASTmonitor was able to classify correctly in NDVI and NDFI time series, breaks of 2007, 2008 and further did not detect false breaks within the stable area. However, for 2009 and 2010 the algorithm was demonstrated lower ability to classify properly breaks in both indices time series over all the magnitude thresholds. Considerably higher values of commission error compared to other monitoring years were depicted for 2010 in both indices over all the implemented magnitude thresholds. This observation was

verified the presence of clouds within the time series (especially within the acquired images for 2010) and consequently the false break detection. False break detection due to cloud contamination could not have been prevented even for high magnitude thresholds ( $m < -0.30$ ), since clouds were decreased significantly the indices values.

Despite the general improvement of mapping accuracy by increasing the magnitude threshold, considerable reduction of the true-positive estimations was depicted for BFASTmonitor break predictions for NDVI and NDFI time series. The spatial agreement (true-positive) of break estimations with the actual disturbed area (reference dataset) was decreased by increasing the magnitude threshold. Hence, the break detection ability of BFASTmonitor was downgraded over high magnitude thresholds ( $m < -0.25$ ).

### ***Removal of cloud contaminated scenes from the time series***

In general, the results after the removal of cloud contaminated images were illustrated slight increase of break-time estimation overall accuracy for both NDVI and NDFI time series. Omission and commission errors were decreased, increasing subsequently the mapping accuracy for all the monitoring years in both indices time series. Hence, we observed an improvement in mapping accuracy for both indices after the scene removal.

BFASTmonitor was likely able to classify correctly breaks of 2007, 2008 and further did not detect false breaks within the stable area. But, for 2009 and 2010 the algorithm was demonstrated lower ability of correct break-time classification. Commission error for 2010 and omission error for 2009 were remained high compared to other monitoring years, though improvement was depicted after the scene removal relative to the primary results. For 2010 intensive cloud contamination was observed for all the acquired images after the image pre-processing, resulting in high commission error rates for 2010. Although we removed a large number (more than 50%) of acquired images, cloud contaminated scenes remain, in order to have sufficient number of observation for 2010. Thus, remaining clouds were probably affected the break detection ability of BFASTmonitor for 2010. This is in accordance with Verbesselt et al., 2011, where the signal-to-noise ratio of the time series was influenced the detection ability of BFASTmonitor algorithm.

Additionally, potentially the length of the historical period that was implemented for 2010 has affected the break estimation ability of BFASTmonitor for 2010. The algorithm based on modelling of a historical period (which is considering as stable) is able to detect breaks within newly acquired data (Verbesselt et al., 2011). For 2010, breaks occurred in previous years (between 2007 and 2009), were considered as normal (stable) index behaviour. Hence, break detection ability of BFASTmonitor within the monitoring period of 2010 was probably decreased.

Finally, similar trends as in the primary results were observed after the image removal for the true-positive break estimations. Although, BFASTmonitor accuracy was increasing, the ability to depict the spatial extent of the referenced breaks was likely decreased over higher magnitude thresholds.

The proposed methodology was intended to provide spatial information for REDD+ monitoring purposes, by indicating the spatial extend of forest cover changes. Considering the above, by applying a magnitude threshold of about -0.15 to -0.20 within the BFASTmonitor break estimations for NDVI and NDFI time series, we could extract spatiotemporal information of potential forest cover changes of pines with sufficient accuracy (above 80%).

#### **7.2.4 Methodological considerations**

##### ***Reference data generation***

The assessment of BFASTmonitor break-time estimation accuracy was performed by generating reference data from Landsat image time series depicting the major forest cover changes of the study area. Additional actions were implemented (e.g. single-pixel analysis) to eliminate as possible the human bias, generally contained in visual interpretation of disturbances within time series (Souza et al., 2005a). Due to Landsat spatial resolution (30m) the delineation of forest cover changes was limited to major changes. Changes with smaller spatial extend (less than 5 pixels) were entailed high risk of commission error, thus were excluded from the delineation. Though, we think that this had a minor impact in the analysis.

Further, we acknowledge that the accuracy assessment was performed based on the same satellite product, since the reference data and the break detection were derived from Landsat time series. However, this was the only available satellite data source. It would be ideal to be able to generate reference data from high-resolution dense time series and reliable field observations for the study area.

##### ***BFASTmonitor parameters***

BFASTmonitor is a multi-purpose change detection algorithm for near real-time disturbance detection within time series (Verbesselt et al., 2011). The algorithm is modelling the normal behaviour and data variation of the time series within a certain period (historical period) based upon breaks can be detected within newly acquired data (monitoring period). BFASTmonitor performance is strongly related to the defined historic period. In the present study the varying length of the stable history between the monitoring years was possibly influenced the accuracy of the estimations. Particularly for

2010, where within the implemented historic period breaks occurred in previous years, BFASTmonitor ability to correctly classify breaks was appeared lower than in previous years.

#### ***Cloud-contaminated scene removal***

Removing scenes from the time series entails the risk of reducing the ability of change detection algorithms to successfully capture disturbances of a certain year. Excluding images potentially could remove the image containing the disturbance event. Further, scene removal from the time series could result in early or delay detection phenomena. The low accuracy results in capturing forest cover changes of 2010, among other influencing factors was further opposed the sufficiency of image acquisition density for 2010.

#### ***Effect of remaining topography***

The selected pine plantation area show moderate morphological variations, thus topographic parameters that could possibly influence the indices time series and further the results of BFASTmonitor did not consider in the present study. Further analysis should be performed to evaluate the influence of topography in the time series in order to eliminate the remaining effects of terrain properties from the results.

## 8. CONCLUSIONS

In this research we assessed the change detection ability of BFASTmonitor algorithm and we evaluated the break-time estimation accuracy in Landsat derived NDVI and NDFI time series in Fiji. Further, we estimated the signifying drop in indices values associated with forest cover changes due to harvest operations for a *P.caribea* plantation.

Our results showed that, forest cover changes in the study area, were depicted similarly by BFASTmonitor analysis in NDVI and NDFI time series. The overall accuracy of break-time estimation was 61% and 64% for NDVI and NDFI, respectively and the mean mapping accuracy was 45% for both indices over the monitoring years 2007 – 2010. However, BFASTmonitor ability to classify correctly the time of change varied among the monitoring years. For 2007 and 2008, the results were depicted high rates of accuracy (mean mapping accuracy above 52%, 24% and 36%, mean commission and omission error, respectively), while significant lower rates were observed for 2009 and 2010 (mean mapping accuracy about 35%, 60% and 55% omission and commission error for 2009 and 2010, respectively).

In addition, we assessed the magnitude of change associated with an actual forest cover change. High rates of agreement between the estimated breaks and the generated reference dataset (above 80% and 60%, overall and mean mapping accuracy, respectively for both indices) were obtained by applying a magnitude threshold between -0.15 and -0.20. We suggested that for a *P.caribea* plantation, a drop on NDVI and NDFI values with magnitude between -0.15 to -0.20 would be probably able to characterise a deforestation event. BFASTmonitor analysis in NDFI time series was demonstrated slightly better ability to correctly estimate the time of actual forest cover changes compared to NDVI (overall accuracy 78% and 82%, for NDVI and NDFI, respectively). Moreover, cloud contamination in time series was strongly affected the performance of BFASTmonitor algorithm. High rates of commission and omission error for 2010 and 2009, respectively, were mainly induced by remaining clouds. Our results indicate enhancement of BFASTmonitor break-estimation ability after the removal of cloud contaminated scenes.

According to Verbesselt et al. (2011) BFASTmonitor algorithm enables a rapid response by detecting disturbances in near real-time within new available satellite data. Our results were proposed that BFASTmonitor is probably able to detect spatiotemporal patterns of forest cover changes and further the algorithm under specific pre-conditions (i.e. magnitude of change, low rates of remaining cloud-contamination) has the potential to estimate the break-time with sufficient accuracy (overall accuracy above 80%) for NDVI and NDFI time series.

Monitoring forest cover changes is crucial for any initiative to reduce deforestation in tropical regions. A monitoring system that fits the objectives of REDD+ to calculate

greenhouse gas emissions requires two inputs: activity data and emissions factors (IPCC, 2006). BFASTmonitor analysis can potentially contribute in monitoring deforestation in two ways; as a rapid response to forest canopy changes within newly acquired satellite data and in addition by providing activity data related to deforestation, since has the potential to estimate with sufficient accuracy the spatial extent of forest canopy changes. Further investigation of forest degradation and reforestation patterns in the time series could be performed based on the obtained results from BFASTmonitor analysis. Combing deforestation, forest degradation and regrowth information for an area, is necessary for the establishment of a complete forest carbon inventory. Hence, the method could potentially contribute in the achievement of the eventual goal of forest carbon assessment under REDD+ of policy which according to Baker et al. (2010) is to conduct continuous annual national assessments that form a global REDD+ monitoring system.

## 9. RECOMMENDATIONS

The following recommendations are intended to increase the effectiveness of relevant studies for monitoring forest cover changes in tropical regions.

### ***BFASTmonitor performance***

The ability of BFASTmonitor to detect disturbances is strongly related to the defined stable history and monitoring period. Two main factors are likely influencing BFASTmonitor results; remaining clouds in the time series after image pre-processing and the inclusion of disturbance events within the stable history. Concerning the first influencing factor the implementation of combined methods for cloud and cloud-shadows masking should be considered to eliminate as possible false break detection. Additionally, identification and removal of remaining clouds could be performed by BFASTmonitor analysis in a pixel-level approach. Since clouds are producing a significant drop in indices values, detected breaks related to cloud-contamination with high magnitude of change ( $m < -0.35$ ) could be removed. Furthermore, in case of remaining clouds, masking and removal of the specific area should be preferred rather than scene exclusion, as in this way is preserved the decontaminated remote sensed information.

The presence of disturbances within successive years in the end of historic period is probably influencing the ability of BFASTmonitor to detect disturbances within newly acquired data. Finally, assessment of the remaining effect of topography in the time series would likely contribute to improve BFASTmonitor performance.

### ***Suggested magnitude thresholds***

In the present study we suggested a magnitude threshold possibly describing the drop on indices values related to deforestation events and potentially improving the break estimation accuracy of BFASTmonitor. Specific influencing factors were considered, such as the selected spectral indices time series, the change detection algorithm and the conditions of the study area (e.g. vegetation cover, morphology etc.). Selection of magnitude threshold representing deforestation is challenging as many parameters should be considered for the specific case. Generalisation and use of the specified magnitude threshold for deforestation in varying environments is not suggested. Moreover, future work could estimate the magnitude of change related to forest degradation and regrowth of *P. caribea* trees.

### ***Higher spatial resolution time series analysis***

In the present study BFASTmonitor algorithm was analysed moderate resolution Landsat image time series. The use of satellite sources with higher spatial resolution will possibly better represent the fine-scale heterogeneity found in most disturbed areas (Hurt et al., 2003), particularly concerning small scale deforestation and selective logging activities.

Further, incorporation and evaluation of different data sources could potentially refined remotely sensed measures of forest cover changes. De Sy et al. (2012) were suggested synergies of multiple remote sensing data source for REDD+ monitoring purposes.

### ***Validation based on other satellite sources***

Higher spatial resolution images should be additionally incorporated for validation purposes in conjunction with reliable field data. Such validation would provide more confident accuracy quantification of the obtained results.

### ***Exploring further potentials of BFASTmonitor algorithm***

Future work should be focussed on BFASTmonitor ability in determining and assessing forest degradation and reforestation patterns (changes in forest cover with positive magnitude). Information about deforestation, forest degradation and recovery will contribute to perform further a full forest carbon inventory.

### ***Automation of the procedure***

The proposed methodology could be further fully automated using R and/or Python scripts constituting a fast and cost-effective disturbance monitoring approach within larger spatial and temporal extend. The automation of the implemented methodology would further enable the effectiveness evaluation of additional spectral indices time series for monitoring forest canopy changes.

## REFERENCES

- Achard, F., Eva, H., Stibig, H.-J., Mayaux, P., Gallego, J., Richards, T., Malingreau, J.-P., 2002, "Determination of deforestation rates of the world's humid tropical forests". *Science*, Vol. 297, pp. 999–1002.
- Adams, J.B., Smith, M.O., Gillespie, A.R., 1993, "Imaging Spectroscopy: Interpretation based on Spectral Mixture Analysis", In: Pieters, C.M., Englert, P. (Eds.) *Remote Geochemical Analysis: Elemental and Mineralogical Composition*. Topics in Remote Sensing 4, New York: Cambridge University Press, pp.145-166.
- Arcidiacono-Bársony, C., Ciais, P., Viovy, N., Vuichard, N., 2011, "REDD Mitigation", *Procedia Environmental Sciences*, Vol. 6, pp. 50-59.
- Asner, G. P., 2001, "Cloud cover in Landsat observations of the Brazilian Amazon", *International Journal of Remote Sensing*, Vol. 22, pp. 3855–3862.
- Asner, G.P., Rudel, T.K., Aide, T.M., Defries, R., Emerson, R., 2009, "A contemporary assessment of change in humid tropical forests", *Conservation Biology*, Vol. 23, pp. 1386-1395.
- Baker, D.J., Richards, G., Grainger, A., Gonzalez, P., Brown, S., DeFries, R., Held, A., Kelldorfer, J., Ndunda, P., Ojima, D., Skrovseth, P.E., Souza, C., Stolle, F., 2010, "Achieving forest carbon information with higher certainty: a five-part plan", *Environmental Science and Policy*, Vol. 13, pp. 249–260.
- Bonan, G. B., 2008, "Forests and Climate Change: Forcings, Feedbacks, and the Climate Benefits of Forests", *Science*, Vol. 320, pp. 1444.
- Broich, M., Hansen, M.C., Potapov, P., Adusei, B., Lindquist, E., Stehman, S.V., 2011, "Time-series analysis of multi-resolution optical imagery for quantifying forest cover loss in Sumatra and Kalimantan, Indonesia", *International Journal of Applied Earth Observation and Geoinformation*, Vol. 13, pp. 277–291.
- Change, Vol. 2, pp. 177–189.
- Cohen, W.B. and Goward, S.N., 2004, "Landsat's role in ecological applications of remote sensing", *Bioscience*, Vol. 54, pp. 535 – 545.
- Congalton, R.G., 1991, "A Review of Assessing the Accuracy of Classifications of Remotely Sensed Data", *Remote Sensing of Envi*, Vol. 37, pp. 35-46.
- Coppin, P., Lambin, E., Jonckheere, I., Nackaerts, K., Muys, B., 2004, "Digital change detection methods in ecosystem monitoring: A review", *International Journal of Remote Sensing*, Vol. 25, pp. 1565–1596.
- de Beurs, K. M., & Henebry, G. M., 2005, "A statistical framework for the analysis of long image time series", *International Journal of Remote Sensing*, Vol. 26, pp. 1551–1573.
- de Jong, R., Verbesselt, J., Schaepman, M.E., de Bruin, S., 2012, "Trend changes in global greening and browning: Contribution of short-term trends to longer-term change", *Global Change Biology*, Vol. 18, pp. 642-655.
- DeFries, R., Achard, F., Brown, S. L., Herold, M., Murdiyarto, D., Schlamadinger, B., 2007, "Earth observations for estimating greenhouse gas emissions from deforestation in developing countries", *Environmental Science & Policy*, Vol. 10, pp. 385–394.
- DeFries, R., Houghton, R.A., Hansen, M., Field, C., Skole, D.L., Townshend, J., 2002, "Carbon emissions from tropical deforestation and regrowth based on satellite observations for the 1980s and 90s", *Proceedings of the National Academy of Sciences of the United States of America*, Vol. 99, pp. 14256–14261.
- Eckert, S., Ratsimba, H.R., Rakotondrasoa, L.O., Rajoelison, L.G., Ehrensperger, A., 2011, "Deforestation and forest degradation monitoring and assessment of biomass and carbon stock of lowland rainforest in the Analanjirofo region, Madagascar", *Forest Ecology and Management*, Vol. 262, pp. 1996–2007.
- FAO (Food and Agriculture Organization), 2006, *Forest Resources Assessment*. Rome: FAO.
- Fiji REDD+ policy, 2011, *Fiji REDD-Plus Policy: Reducing emissions from deforestation and forest degradation in Fiji*, Compiled by the Fiji Forestry Department Secretariat of the Pacific Community Suva, Fiji Islands.
- Fijian Department of Environment, 2010, "Fiji's Fourth National Report to the United Nations Convention on Biological Diversity".
- Foley, J.A., DeFries, R., Asner, G.P., Barford, C., Bonan, G., Carpenter, S.R., Chapin, F.S., Coe, M.T., Daily, G.C., Gibbs, H.K., Helkowski, J.H., Holloway, T., Howard, E.A., Kucharik, C.J., Monfreda,

- C., Patz, J.A., Prentice, I.C., Ramankutty, N., Snyder, P.K., 2005, "Global consequences of land use", *Science*, Vol. 309, pp. 570-574.
- Gasparri, N.I., Parmuchi, M.G., Bono, J., Karszenbaum, H., Montenegro, C.L., 2010, "Assessing multi-temporal Landsat 7 ETM+ images for estimating above-ground biomass in subtropical dry forests of Argentina", *Journal of Arid Environments*, Vol. 74, pp. 1262-1270.
- Gitelson, A.A., 2004, "Wide dynamic range vegetation index for remote quantification of biophysical characteristics of vegetation", *Journal of Plant Physiology*, Vol. 161, pp. 165 -173.
- Glenn, E.P., Huete, A.R., Nagler, P.L., Nelson, S.G., 2008, Review "Relationship Between Remotely-sensed Vegetation Indices, Canopy Attributes and Plant Physiological Processes: What Vegetation Indices Can and Cannot Tell Us About the Landscape" , , *Sensors*, Vol. 8, pp. 2136 - 2160.
- Gómez, C., White, J.C., Wulder, M.A., 2011, "Characterizing the state and processes of change in a dynamic forest environment using hierarchical spatio-temporal segmentation", *Remote Sensing of Environment*, Vol. 115, pp. 1665-1679.
- Govaerts, Y. M., Verstraete, M. M., 1999, Designing optimal spectral indices: a feasibility and proof of concept study , *International Journal of Remote Sensing*, Vol. 20, pp. 1853 - 1873.
- Hansen, M., Stehman, S., Potapov, P.V., Loveland, T.R., Townshend, J.R.G., DeFries, R.S., Pittman, K.W., Arunarwati, B., Stolle, F., Steining, M.K., Carroll, M., DiMiceli, C., 2008, "Humid tropical forest clearing from 2000 to 2005 quantified by using multitemporal and multiresolution remotely sensed data", *Proceedings of the National Academy of Sciences of the United States of America*, Vol. 105, pp. 9439-9444.
- Hayes, D.J. and S.A. Sader, 2001, "Change detection techniques for monitoring forest clearing and regrowth in a tropical moist forest", *Photogrammetric Engineering and Remote Sensing*, Vol. 67, pp. 1067 - 1075.
- Healey, S.P., Cohen, W.B., Zhiqiang, Y., Krankina, O. N., 2005, "Comparison of Tasseled Cap-based Landsat data structures for use in forest disturbance detection", *Remote Sensing of Environment*, Vol. 97, pp. 301 - 310.
- Hirsch, A. I., Little, W. S., Houghton, R. A., Scott, N. A., & White, J. D., 2004, "The net carbon flux due to deforestation and forest re-growth in the Brazilian Amazon: Analysis using a process-based model", *Global Change Biology*, Vol. 10, pp. 908-924.
- Houghton, J. T., Ding, Y., Griggs, D. J., Noguer, M., van der Linden, P. J., Dai, X., Maskell, K., Johnson, C. A. (Eds.), 2001, "Climate Change 2001: The Scientific Basis". Contribution of Working Group I to the Third, Assessment Report of the Intergovernmental Panel on Climate Change, Cambridge, U.K.: Cambridge University Press.
- Huang, C., Goward, S.N., Masek, J.G., Thomas, N., Zhu, Z., Vogelmann, J.E., 2010, "An automated approach for reconstructing recent forest disturbance history using dense Landsat time series stacks", *Remote Sensing of Environment*, Vol. 114, pp. 183-198.
- Huang, C.; Yang, W. L., Collin, H., Zylstra, G., 2002, Derivation of a tasseled cap transformation based on Landsat 7 at-satellite reflectance , *International Journal of Remote Sensing*, Vol. 23, pp. 1741 - 1748.
- Huete A.R, Liua, H.Q., Batchilya, K., van Leeuwena, W., 1997, "A comparison of Vegetation Indices over a global set of TM Images for EOS-MODIS", *Remote Sensing of Environment*, Vol. 59, pp. 440-451.
- Huete, A., Didan, K., Miura, T., Rodrguez, E.P., Gao, X., Ferreira, L.G., 2002, "Overview of the radiometric and biophysical performance of the MODIS vegetation indices", *Remote Sensing of Environment*, Vol. 83, pp. 195-213.
- Hurt, G., Xiao, X., Keller, M., Palace, M., Asner, G.P., Braswell, R., Brondizio, E.S., Cardoso, M., Carvalho, C.J.R., Fearon, M.G., Guild, L., Hagen, S., Hetrick, S., Moore, B., Nobre, C., Read, J.M., Sá, T., Schloss, A., Vourlitis, G., Wickel, A.J., 2003, "IKONOS imagery for the Large Scale Biosphere-Atmosphere Experiment in Amazonia (LBA)", *Remote Sensing of Environment*, Vol. 88, pp. 111-127.
- IPCC, Intergovernmental Panel on Climate Change, 2000, "Land use, land-use change, and forestry", IPCC.
- IPCC, Intergovernmental Panel on Climate Change, 2007, "Climate Change 2007 - The Physical Science Basis: Contribution of Working Group I to the Fourth Assessment Report", IPCC.
- Jin, S. M., & Sader, S. A., 2005, "MODIS time-series imagery for forest disturbance detection and quantification of patch size effects" *Remote Sensing of Environment*, Vol. 99, pp. 462-470.
- Killeen, T. J., Calderon, V., Soria, L., Quezada, B., Steining, M. K., Harper, G., Solorzano, L. A., & Tucker, C. J., 2007, "Thirty years of land-cover change in Bolivia", *Ambio*, Vol. 36, pp. 600-606.
- Kohavi, R. and Provost, F., 1998, "Glossary of terms", *Machine learning*, Vol. 30, pp. 271-274.

- Lambert, J., Jacquin, A., Denux, J.-P., Chéret, V., 2011, "Comparison of two remote sensing time series analysis methods for monitoring forest decline" (Conference Paper), 6th International Workshop on the Analysis of Multi-Temporal Remote Sensing Images, Multi-Temp 2011 – Proceedings, Article number 6005056, pp. 93-96.
- Law, B. E., Van Tuyl, S., Ritts, W. D., Cohen, W. B., Turner, D., Campbell, J., & Sun, O. J., 2004, "Disturbance and climate effects on carbon stocks and fluxes across Western Oregon USA", *Global Change Biology*, Vol. 10, pp. 1429–1444.
- Lu, D., 2005, "Aboveground biomass estimation using Landsat TM data in the Brazilian Amazon", *International Journal of Remote Sensing*, Vol. 26, pp. 2509–2525.
- Lu, D., Mausel, P., Brondizio, E., & Moran, E., 2004, "Change detection techniques", *International Journal of Remote Sensing*, Vol. 25, pp. 2365–2407.
- NASA, 2011, *Landsat 7 Science Data Users Handbook* In NASA (Ed.), Greenbelt, Maryland
- Parker, C., Mitchell, A., Trivedi, M., Mardas, N., Sosis, K, 2009, *The Little REDD+ Book*.
- Pesaran, M.H. and Timmermann A., 2002, "Market timing and return prediction under model instability", *Journal of Empirical Finance*, Vol. 9, pp. 495–510.
- Peterken, G. F., 2001, "Structural dynamics of forest stands and natural processes", In J. Evans (Ed.), *The forest handbook*, Vol. 1. (pp. 83–104)Malden, MA: Blackwell Science.
- Potter, C., Tan, P. N., Steinbach, M., Klooster, S., Kumar, V., Myneni, R., 2003, "Major disturbance events in terrestrial ecosystems detected using global satellite data sets", *Global Change Biology*, Vol. 9, pp. 1005–1021.
- Rouse, J.W., Haas, R.H., Schell, J. A., Deering, D.W., Harlan, J. C., 1974, "Monitoring the vernal advancement of retrogradation of natural vegetation", NASA/GSFC, Greenbelt.
- Roy, D. P., Borak, J. S., Devadiga, S., Wolfe, R. E., Zheng, M., Desloires, J., 2002, "The MODIS Land product quality assessment approach", *Remote Sensing of Environment*, Vol. 83, pp. 62–76.
- Siren, A.H. and Brondizio, E.S., 2009, "Detecting subtle land use change in tropical forests", *Applied Geography*, Vol. 29, pp. 201–211.
- Souza Jr., C., Firestone, L., Silva, M. L., & Roberts, D. A., 2003, "Mapping forest degradation in the Eastern Amazon from SPOT 4 through spectral mixture models", *Remote Sensing of Environment*, Vol. 87, pp. 494–506.
- Souza Jr., C.M., Roberts, D.A., Cochranes, M.A., 2005a, "Combining spectral and spatial information to map canopy damage from selective logging and forest fires", *Remote Sensing of Environment*, Vol. 98, pp. 329 – 343.
- Souza Jr., C.M., Roberts, D.A., Monteiro, A., 2005b, "Multi-temporal analysis of degraded forests in the Southern Brazilian Amazon", *Earth Interactions*, Vol. 9, pp. 1-25.
- Steininger, M. K., 2000, "Satellite estimation of tropical secondary forest above-ground biomass: Data from Brazil and Bolivia. *International Journal of Remote Sensing*, Vol. 21, pp. 1139–1157.
- Stone, T. A., and Lefebvre, P., 1998, "Using multi-temporal satellite data to evaluate selective logging in Para, Brazil", *International Journal of Remote Sensing*, Vol. 19, pp. 2517–2517.
- Story, M., and Congalton, R., 1986, "Accuracy assessment: a user's perspective", *Photogrammetric engineering and remote sensing*, Vol. 52, pp. 397 – 399.
- Tanago-Meñaca, J.G., 2012, "Towards an innovative remote sensing tool for tropical forest change monitoring by integrating spatial segments and time series analysis. The Case of Tra-Bui, Central Vietnam", Thesis code number: GRS-80436, Wageningen University and Research Centre, Laboratory of Geo-Information Science and Remote Sensing, Wageningen, The Netherlands.
- Tucker, C.J., 1979, "Red and photographic infrared linear combinations for monitoring vegetation", *Remote Sensing of Environment*, Vol. 8, pp. 127–150.
- Turner, M. G., 2010, "Disturbance and landscape dynamics in a changing world", *Ecology*, Vol. 91, pp. 2833–2849.
- UNFCCC, United Nations Framework Convention on Climate Change, 2005, "Reducing Emissions from Deforestation in Developing Countries: Approaches to Stimulate Action", Draft Conclusions Proposed by the President, Bonn: UNFCCC Secretariat.
- UNFCCC, United Nations Framework Convention on Climate Change, 2009, "Methodological guidance for activities relating to reducing emissions from deforestation and forest degradation and the role of conservation, sustainable management of forests and enhancement of forest carbon stocks in developing countries", Decision COP 15/4. Report of the Conference of the Parties on its fifteenth session, held in Copenhagen from 7 to 19 December 2009, Part Two: Action taken by the Conference of the Parties at its fifteenth session, In UNFCC (Ed.) (p. 43), Copenhagen: UNFCC
- UNFCCC, United Nations Framework Convention on Climate Change, 2010, "Outcome of the work of the Ad Hoc Working Group on long-term Cooperative Action under the Convention" – C. Policy

- approaches and positive incentives on issues relating to reducing emissions from deforestation and forest degradation in developing countries; and the role of conservation, sustainable management of forests and enhancement of forest carbon stocks in developing countries, UNFCCC COP 16, Cancun: UNFCC.
- Verbesselt, J., Herold, M., Hyndman, R., Zeileis, A., Culvenor, D., 2011, "A robust approach for phenological change detection within satellite image time series" (Conference paper), 6th International Workshop on the Analysis of Multi-Temporal Remote Sensing Images, Multi-Temp 2011 – Proceedings 2011, Article number 6005042, pp. 41-44.
- Verbesselt, J., Hyndman, R., Newnham, G., Culvenor, D., 2010a, "Detecting trend and seasonal changes in satellite image time series", *Remote Sensing of Environment*, Vol. 114, pp. 106–115.
- Verbesselt, J., Hyndman, R., Zeileis, A., Culvenor, D., 2010b, "Phenological change detection while accounting for abrupt and gradual trends in satellite image time series", *Remote Sensing of Environment*, Vol. 114, pp.2970- 2980.
- Verstraete, M.M., Pinty, B., Myneni, R.B.,1996, "Potential and limitations of information extraction on the terrestrial biosphere from satellite remote sensing", *Remote Sensing of Environment*, Vol. 58, pp. 201–214.
- Viña, A., Gitelson, A.,A., Nguy-Robertson, A.L., Peng,Y., 2011, "Comparison of different vegetation indices for the remote assessment of green leaf area index of crops", *Remote Sensing of Environment*, Vol. 115, pp. 3468 – 3478.
- Weaver, S., Herold, M., Payton, I., 2009, "Fiji REDD Policy & Scoping Consultation, 24 August – 04 September 2009, Suva, Fiji, Final Report", Report prepared for Deutsche Gesellschaft für Technische Zusammenarbeit/ Secretariat of the Pacific Community (GTZ/SPC) by Carbon Partnership Ltd.
- Williams, D.L., Goward, S., Arvidson, T., 2006, "Landsat: Yesterday, today, and tomorrow", *Photogrammetric Engineering and Remote Sensing*, Vol. 72, pp. 1171-1178.
- Zhu, Z. and Woodcock, C. E., 2012b,"Object-based cloud and cloud shadow detection in Landsat imagery", *Remote Sensing of Environment*, Vol. 118, pp. 83 – 94 .
- Zhu, Z., Woodcock, C.E., Olofsson, P., 2012," Continuous monitoring of forest disturbance using all available Landsat imagery", *Remote Sensing of Environment*, Vol. 122, pp. 75 – 91.

## APPENDIXES

### I. Appendix – Available Landsat scenes.

No.	Landsat Scene Identifier (ID)	Date acquired (YYYY-MM-DD)	Landsat Product	Cloud Cover (%)
1	LE70750722000136EDC00	2000-05-15	ETM+ L1T	6
2	LE70750722000184EDC00	2000-07-02	ETM+ L1T	73
3	LE70750722000216EDC00	2000-08-03	ETM+ L1T	13
4	LE70750722000264EDC00	2000-09-20	ETM+ L1T	69
5	LE70750722000312EDC00	2000-11-07	ETM+ L1T	9
6	LE70750722001026EDC00	2001-01-26	ETM+ L1T	31
7	LE70750722001042EDC00	2001-02-11	ETM+ L1T	28
8	LE70750722001138EDC00	2001-05-18	ETM+ L1T	36
9	LE70750722001186EDC00	2001-07-05	ETM+ L1T	15
10	LE70750722001218EDC00	2001-08-06	ETM+ L1T	21
11	LE70750722001266EDC00	2001-09-23	ETM+ L1T	33
12	LE70750722001314EDC00	2001-11-10	ETM+ L1T	4
13	LE70750722002045EDC00	2002-02-14	ETM+ L1T	10
14	LE70750722002125EDC00	2002-05-05	ETM+ L1T	54
15	LE70750722002141EDC00	2002-05-21	ETM+ L1T	34
16	LE70750722002253EDC00	2002-09-10	ETM+ L1T	60
17	E70750722002285EDC00	2002-10-12	ETM+ L1T	7
18	LE70750722002333EDC00	2002-11-29	ETM+ L1T	46
19	LE70750722003128EDC00	2003-05-08	ETM+ L1T	10
20	LE70750722003208EDC01	2003-07-27	ETM+ L1T	35
21	LE70750722003240EDC01	2003-08-28	ETM+ L1T	32
22	LE70750722003272EDC01	2003-09-29	ETM+ L1T	9
23	LE70750722003320EDC02	2003-11-16	ETM+ L1T	16
24	LE70750722004019EDC01	2004-01-19	ETM+ L1T	3
25	LE70750722004035EDC01	2004-02-04	ETM+ L1T	25
26	LE70750722004067EDC02	2004-03-07	ETM+ L1T	18
27	LE70750722004115EDC01	2004-04-24	ETM+ L1T	5
28	LE70750722004131EDC01	2004-05-10	ETM+ L1T	0
29	LE70750722004147EDC01	2004-05-26	ETM+ L1T	8
30	LE70750722004179EDC01	2004-06-27	ETM+ L1T	53
31	LE70750722004195EDC01	2004-07-13	ETM+ L1T	1
32	LE70750722004211EDC02	2004-07-29	ETM+ L1T	24
33	LE70750722004227EDC02	2004-08-14	ETM+ L1T	6
34	LE70750722004243EDC02	2004-08-30	ETM+ L1T	15
35	LE70750722004275EDC02	2004-10-01	ETM+ L1T	13
36	LE70750722004291EDC01	2004-10-17	ETM+ L1T	51
37	LE70750722004323EDC00	2004-11-18	ETM+ L1T	17
38	LE70750722004355EDC00	2004-12-20	ETM+ L1T	46
39	LE70750722005021EDC00	2005-01-21	ETM+ L1T	27
40	LE70750722005037EDC00	2005-02-06	ETM+ L1T	6
41	LE70750722005053EDC00	2005-02-22	ETM+ L1T	43
42	LE70750722005133EDC00	2005-05-13	ETM+ L1T	52
43	LE70750722005149EDC00	2005-05-29	ETM+ L1T	4
44	LE70750722005165EDC00	2005-06-14	ETM+ L1T	7
45	LE70750722005197EDC00	2005-07-16	ETM+ L1T	0
46	LE70750722005213EDC00	2005-08-01	ETM+ L1T	11
47	LE70750722005245EDC00	2005-09-02	ETM+ L1T	46
48	LE70750722005261EDC00	2005-09-18	ETM+ L1T	11
49	LE70750722005293EDC00	2005-10-20	ETM+ L1T	18
50	LE70750722005309EDC00	2005-11-05	ETM+ L1T	89

*(Table continued)*

<b>No.</b>	<b>Landsat Scene Identifier (ID)</b>	<b>Date acquired (YYYY-MM-DD)</b>	<b>Landsat Product</b>	<b>Cloud Cover (%)</b>
50	LE70750722006056EDC00	2006-02-25	ETM+ L1T	53
51	LE70750722006072EDC00	2006-03-13	ETM+ L1T	41
52	LE70750722006088EDC00	2006-03-29	ETM+ L1T	7
53	LE70750722006104EDC00	2006-04-14	ETM+ L1T	11
54	LE70750722006120EDC00	2006-04-30	ETM+ L1T	13
55	LE70750722006136EDC00	2006-05-16	ETM+ L1T	90
56	LE70750722006152EDC00	2006-06-01	ETM+ L1T	10
57	LE70750722006168EDC00	2006-06-17	ETM+ L1T	71
58	LE70750722006168EDC00	2006-08-20	ETM+ L1T	6
59	LE70750722006248EDC00	2006-09-05	ETM+ L1T	44
60	LE70750722006264EDC00	2006-09-21	ETM+ L1T	7
61	LE70750722006360EDC00	2006-12-26	ETM+ L1T	40
62	LE70750722007011EDC01	2007-01-11	ETM+ L1T	9
63	LE70750722007027EDC00	2007-01-27	ETM+ L1T	13
64	LE70750722007123EDC00	2007-05-03	ETM+ L1T	15
65	LE70750722007139EDC00	2007-05-19	ETM+ L1T	14
66	LE70750722007155EDC00	2007-06-04	ETM+ L1T	18
67	LE70750722007171EDC00	2007-06-20	ETM+ L1T	2
68	LE70750722007187EDC00	2007-07-06	ETM+ L1T	3
69	LE70750722007203EDC00	2007-07-22	ETM+ L1T	15
70	LE70750722007283EDC00	2007-10-10	ETM+ L1T	9
71	LE70750722007299EDC00	2007-10-26	ETM+ L1T	6
72	LE70750722007315EDC00	2007-11-11	ETM+ L1T	11
73	LE70750722007331EDC00	2007-11-27	ETM+ L1T	43
74	LE70750722007347EDC00	2007-12-13	ETM+ L1T	25
75	LE70750722008014EDC00	2008-01-14	ETM+ L1T	36
76	LE70750722008046EDC00	2008-02-15	ETM+ L1T	9
77	LE70750722008062EDC02	2008-03-02	ETM+ L1T	3
78	LE70750722008142EDC00	2008-05-21	ETM+ L1T	29
79	LE70750722008158EDC00	2008-06-06	ETM+ L1T	19
80	LE70750722008174EDC00	2008-06-22	ETM+ L1T	21
81	LE70750722008190EDC00	2008-07-08	ETM+ L1T	4
82	LE70750722008206EDC00	2008-07-24	ETM+ L1T	3
83	LE70750722008222EDC00	2008-08-09	ETM+ L1T	3
84	LE70750722008238EDC01	2008-08-25	ETM+ L1T	13
85	LE70750722008254EDC01	2008-09-10	ETM+ L1T	3
86	LE70750722008270EDC00	2008-09-26	ETM+ L1T	37
87	LE70750722008286EDC00	2008-10-12	ETM+ L1T	4
88	LE70750722008318EDC00	2008-11-13	ETM+ L1T	21
89	LE70750722008334EDC00	2008-11-29	ETM+ L1T	10
90	LE70750722008350EDC00	2008-12-15	ETM+ L1T	13
91	LE70750722009048EDC02	2009-02-17	ETM+ L1T	4
92	LE70750722009064EDC00	2009-03-05	ETM+ L1T	32
93	LE70750722009096EDC00	2009-04-06	ETM+ L1T	46
94	LE70750722009112EDC00	2009-04-22	ETM+ L1T	71
95	LE70750722009160EDC00	2009-06-09	ETM+ L1T	6
96	LE70750722009176EDC00	2009-06-25	ETM+ L1T	69
97	LE70750722009192EDC01	2009-07-11	ETM+ L1T	98
98	LE70750722009208EDC00	2009-07-27	ETM+ L1T	5
99	LE70750722009224EDC01	2009-08-12	ETM+ L1T	97
100	LE70750722009240EDC00	2009-08-28	ETM+ L1T	36
101	LE70750722009288EDC00	2009-10-15	ETM+ L1T	48
102	LE70750722009320EDC00	2009-11-16	ETM+ L1T	41

*(Table continued)*

<b>No.</b>	<b>Landsat Scene Identifier (ID)</b>	<b>Date acquired (YYYY-MM-DD)</b>	<b>Landsat Product</b>	<b>Cloud Cover (%)</b>
103	LE70750722009336EDC00	2009-12-02	ETM+ L1T	11
104	LE70750722009352EDC01	2009-12-18	ETM+ L1T	18
105	LE70750722010003EDC00	2010-01-03	ETM+ L1T	16
106	LE70750722010019EDC00	2010-01-19	ETM+ L1T	8
107	LE70750722010035EDC00	2010-02-04	ETM+ L1T	16
108	LE70750722010067EDC00	2010-03-08	ETM+ L1T	4
109	LE70750722010083EDC00	2010-03-24	ETM+ L1T	22
110	LE70750722010099EDC00	2010-04-09	ETM+ L1T	9
111	LE70750722010131EDC00	2010-05-11	ETM+ L1T	5
112	LE70750722010147EDC00	2010-05-27	ETM+ L1T	0
113	LE70750722010195EDC00	2010-07-14	ETM+ L1T	8
114	LE70750722010211EDC00	2010-07-30	ETM+ L1T	17
115	LE70750722010227EDC00	2010-08-15	ETM+ L1T	7
116	LE70750722010307EDC00	2010-11-03	ETM+ L1T	6
117	LE70750722010355EDC00	2010-12-21	ETM+ L1T	82
118	LE70750722011038EDC00	2011-02-07	ETM+ L1T	9
119	LE70750722011054EDC00	2011-02-23	ETM+ L1T	14
120	LE70750722011070EDC00	2011-03-11	ETM+ L1T	4
121	LE70750722011230EDC00	2011-08-18	ETM+ L1T	19
122	LE70750722011246EDC00	2011-12-08	ETM+ L1T	83
123	LE70750722011342EDC00	2012-01-09	ETM+ L1T	5
124	LE70750722012025EDC00	2012-01-25	ETM+ L1T	47
125	LE70750722012073EDC00	2012-03-13	ETM+ L1T	67
126	LE70750722012185EDC00	2012-07-03	ETM+ L1T	6
127	LE70750722012201EDC00	2012-07-19	ETM+ L1T	9
128	LE70750722012217EDC00	2012-08-04	ETM+ L1T	71
129	LE70750722012265EDC00	2012-09-21	ETM+ L1T	59
130	LE70750722012313ASN00	2012-11-08	ETM+ L1T	21

## II. Appendix - Location of selected pixels for pixel-level analysis.

### a. Mangrove forest pixels

X	Y	Mean			Standard Deviation (SD)		
		NDVI	NDFI	DI	NDVI	NDFI	DI
519	1874	0,945	0,764	0,898	0,023	0,008	0,026
521	1926	0,942	0,761	0,897	0,024	0,017	0,026
582	1796	0,940	0,767	0,911	0,023	0,009	0,026
1522	629	0,937	0,765	0,917	0,026	0,006	0,027
1522	628	0,946	0,766	0,920	0,028	0,008	0,029
1543	628	0,905	0,758	0,904	0,027	0,010	0,025
1545	622	0,916	0,760	0,907	0,026	0,011	0,021
1547	620	0,912	0,759	0,900	0,026	0,012	0,023
1548	657	0,939	0,765	0,917	0,023	0,009	0,021
1549	628	0,910	0,760	0,908	0,024	0,010	0,024
1549	632	0,925	0,763	0,909	0,023	0,006	0,020
1560	630	0,954	0,766	0,923	0,024	0,009	0,023
1563	632	0,941	0,764	0,916	0,020	0,007	0,019
1563	635	0,916	0,761	0,905	0,025	0,009	0,019
1566	617	0,928	0,764	0,919	0,025	0,009	0,020
1659	640	0,860	0,734	0,896	0,030	0,026	0,026
1664	610	0,907	0,759	0,907	0,029	0,015	0,027
1712	670	0,929	0,762	0,910	0,029	0,013	0,028
1722	661	0,916	0,761	0,910	0,027	0,010	0,024
1928	521	0,944	0,764	0,901	0,024	0,015	0,025
1928	523	0,945	0,764	0,907	0,026	0,015	0,026
1948	524	0,946	0,766	0,906	0,019	0,007	0,025
1948	523	0,938	0,763	0,888	0,021	0,011	0,028
2256	438	0,881	0,748	0,895	0,030	0,019	0,022
2265	442	0,914	0,764	0,908	0,022	0,005	0,020
2266	440	0,922	0,765	0,911	0,020	0,004	0,017
2269	440	0,924	0,764	0,910	0,019	0,004	0,017
2269	442	0,929	0,765	0,913	0,019	0,004	0,018
2271	442	0,902	0,761	0,905	0,022	0,009	0,021
2274	442	0,876	0,752	0,900	0,022	0,017	0,019
2276	442	0,898	0,760	0,903	0,021	0,011	0,018
2276	444	0,898	0,761	0,905	0,024	0,010	0,020
2276	449	0,916	0,763	0,907	0,024	0,008	0,020
2278	441	0,906	0,763	0,904	0,020	0,007	0,017
2278	442	0,907	0,762	0,903	0,018	0,008	0,018
2278	444	0,906	0,762	0,902	0,021	0,008	0,020
2278	448	0,892	0,759	0,902	0,026	0,012	0,021
2278	449	0,885	0,754	0,897	0,029	0,016	0,024
2704	423	0,907	0,761	0,905	0,021	0,008	0,017
2739	427	0,893	0,758	0,902	0,028	0,012	0,019

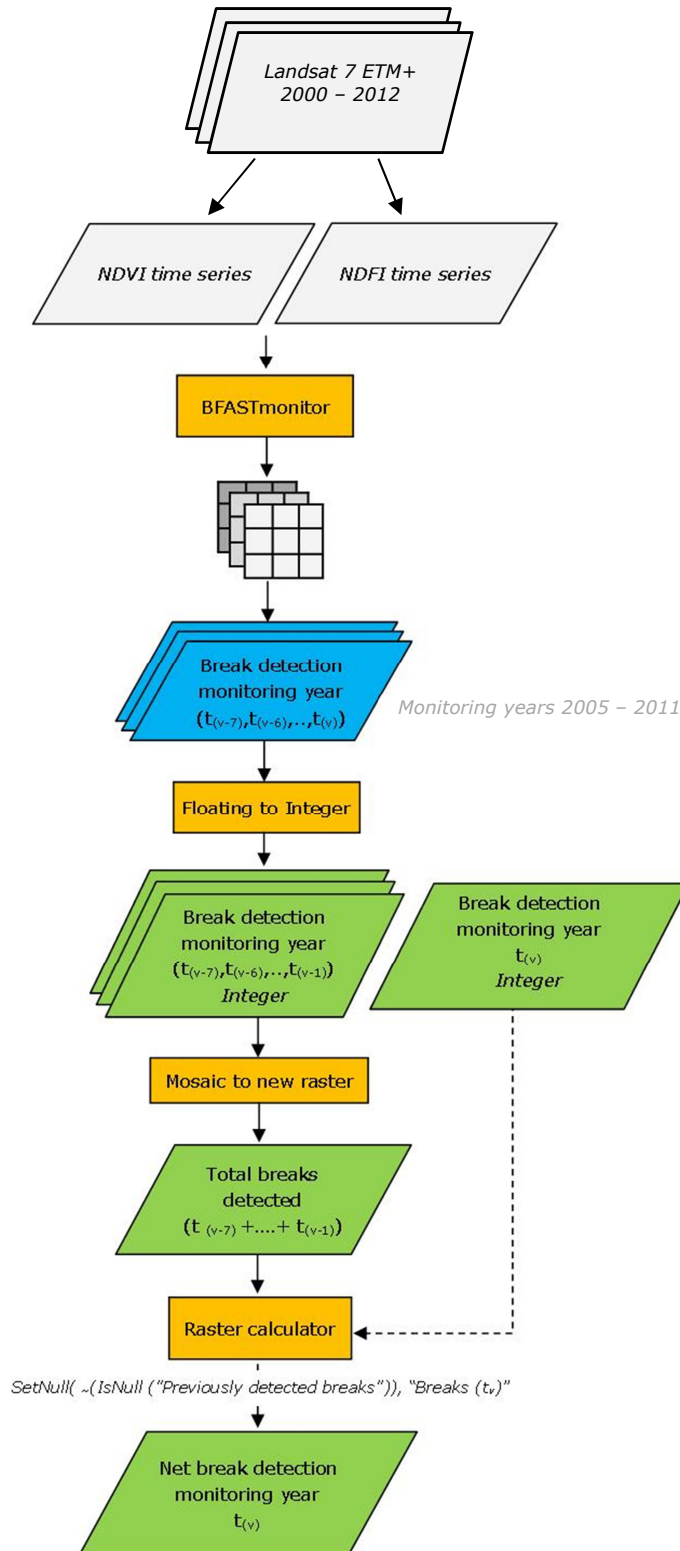
**b. Intact hardwood forest pixels**

X	Y	Mean			Standard Deviation (SD)		
		NDVI	NDFI	DI	NDVI	NDFI	DI
1917	3084	0,931	0,708	0,842	0,018	0,015	0,027
1918	3084	0,937	0,712	0,842	0,017	0,016	0,028
1919	3084	0,938	0,716	0,850	0,019	0,016	0,029
2769	1110	0,940	0,742	0,864	0,019	0,019	0,028
2770	1123	0,932	0,754	0,878	0,021	0,017	0,025
2772	1124	0,937	0,745	0,844	0,013	0,016	0,018
2772	1123	0,937	0,744	0,838	0,013	0,015	0,018
2772	1121	0,938	0,746	0,843	0,013	0,013	0,022
2772	1122	0,939	0,745	0,841	0,012	0,015	0,022
2773	1116	0,949	0,755	0,864	0,009	0,011	0,018
2773	1115	0,947	0,742	0,840	0,009	0,013	0,019
2773	1122	0,937	0,741	0,838	0,012	0,015	0,019
2773	1121	0,938	0,737	0,834	0,013	0,013	0,022
2773	1114	0,948	0,737	0,835	0,010	0,015	0,022
2773	1120	0,938	0,731	0,833	0,014	0,017	0,024
2774	1114	0,946	0,736	0,844	0,010	0,016	0,022
2774	1113	0,942	0,747	0,876	0,012	0,015	0,025
2774	1099	0,938	0,748	0,849	0,016	0,015	0,028
2774	1110	0,934	0,749	0,892	0,021	0,016	0,028
2775	1122	0,936	0,733	0,854	0,013	0,014	0,019
2775	1114	0,944	0,747	0,870	0,010	0,018	0,022
2775	1123	0,933	0,730	0,841	0,014	0,018	0,022
2775	1116	0,943	0,732	0,833	0,012	0,016	0,022
2775	1115	0,943	0,735	0,839	0,014	0,018	0,023
2775	1121	0,936	0,748	0,878	0,017	0,018	0,025
2775	1117	0,940	0,727	0,829	0,013	0,017	0,025
2775	1120	0,939	0,764	0,901	0,017	0,015	0,026
2775	1098	0,941	0,759	0,863	0,016	0,012	0,028
2776	1119	0,943	0,749	0,854	0,012	0,014	0,020
2776	1118	0,942	0,738	0,841	0,010	0,015	0,024
2776	1120	0,943	0,757	0,879	0,014	0,017	0,026
2776	1121	0,937	0,761	0,895	0,016	0,014	0,028
2776	1123	0,936	0,752	0,879	0,020	0,019	0,028
2777	1117	0,940	0,748	0,857	0,010	0,012	0,020
2777	1116	0,940	0,740	0,855	0,010	0,016	0,020
2777	1118	0,943	0,746	0,850	0,012	0,013	0,022
2777	1120	0,945	0,751	0,856	0,014	0,016	0,025
2777	1121	0,944	0,758	0,872	0,014	0,015	0,025
2777	1115	0,937	0,742	0,873	0,017	0,019	0,029
2777	1123	0,941	0,761	0,888	0,018	0,015	0,030

**c. Sugarcane pixels**

X	Y	Mean			Standard Deviation (SD)		
		NDVI	NDFI	DI	NDVI	NDFI	DI
851	1788	0,830	0,660	0,718	0,083	0,166	0,088
852	1789	0,827	0,569	0,717	0,084	0,126	0,087
855	1791	0,842	0,595	0,729	0,079	0,107	0,079
856	1782	0,839	0,607	0,751	0,073	0,090	0,068
1678	998	0,833	0,599	0,746	0,077	0,098	0,096
1678	994	0,830	0,588	0,736	0,092	0,134	0,122
1678	982	0,832	0,574	0,717	0,082	0,124	0,120
1678	979	0,832	0,590	0,728	0,088	0,125	0,127
1682	990	0,821	0,589	0,741	0,089	0,115	0,105
1682	994	0,817	0,602	0,759	0,082	0,097	0,083
1682	996	0,830	0,592	0,741	0,080	0,098	0,098
1697	986	0,849	0,609	0,737	0,087	0,108	0,096
1697	993	0,845	0,604	0,738	0,082	0,100	0,088
1697	990	0,847	0,619	0,753	0,082	0,094	0,079
1704	820	0,836	0,582	0,732	0,080	0,114	0,079
1716	983	0,836	0,599	0,731	0,077	0,088	0,091
1719	818	0,801	0,560	0,730	0,076	0,110	0,075
1725	851	0,821	0,591	0,752	0,060	0,084	0,077
1725	856	0,834	0,587	0,731	0,083	0,124	0,108
1725	858	0,785	0,495	0,645	0,067	0,114	0,098
1730	849	0,802	0,552	0,714	0,084	0,138	0,119
1730	857	0,830	0,577	0,723	0,082	0,118	0,090
1730	859	0,840	0,563	0,702	0,076	0,138	0,122
1733	995	0,829	0,594	0,745	0,088	0,121	0,104
1736	851	0,838	0,583	0,731	0,081	0,135	0,115
1736	937	0,844	0,618	0,771	0,082	0,105	0,070
1740	869	0,828	0,566	0,739	0,081	0,112	0,062
1744	871	0,840	0,597	0,760	0,074	0,107	0,072
1745	870	0,846	0,609	0,767	0,078	0,113	0,071
1746	869	0,838	0,606	0,768	0,083	0,114	0,073
1746	871	0,848	0,615	0,771	0,074	0,104	0,070
1758	861	0,833	0,562	0,724	0,068	0,089	0,054
1758	863	0,819	0,535	0,710	0,067	0,095	0,054
1758	868	0,845	0,548	0,708	0,063	0,095	0,057
1767	867	0,829	0,567	0,567	0,071	0,099	0,099
1785	803	0,815	0,534	0,676	0,088	0,156	0,147
1804	770	0,840	0,597	0,745	0,082	0,115	0,099
1805	769	0,842	0,605	0,758	0,076	0,108	0,085
1816	746	0,814	0,556	0,719	0,091	0,155	0,122
1825	775	0,823	0,566	0,726	0,079	0,125	0,102

### III. Appendix – Net break calculation flow chart.



Appendix Figure 1. Net break detection calculation flowchart in NDVI and NDFI time series.

## IV. Appendix –Reference dataset generation.

Year	Landsat image	Pixel (Path/row)	BFASTmonitor single-pixel time series analysis
2007	<p>ID: LE70750722007187EDC00</p>	1483/1040	
2007		1481/1044	<p>Break detected at: 2007(315)</p>
2007		1468/1038	<p>Break detected at: 2007(315)</p>

(Table continued)

Year	Landsat image	Pixel (Path/row)	BFASTmonitor single-pixel time series analysis
	<i>ID:LE70750722008190EDC00</i>		
2008	<p>177°37'30"E 177°38'30"E 17°33'0"S 17°33'30"S 17°33'30"S 17°33'30"S 17°34'0"S 17°34'0"S 17°34'0"S 17°34'0"S 17°34'30"S 17°34'30"S 17°34'30"S 17°34'30"S 177°37'30"E 177°38'30"E</p>	1445/985	<p>Break detected at: 2008(253)</p> <p>Historical data New data Stable history Fit based on stable history Start of the Monitoring period Time of detected break</p>
2008	<p>177°37'30"E 177°38'30"E 17°33'0"S 17°33'30"S 17°33'30"S 17°33'30"S 17°34'0"S 17°34'0"S 17°34'0"S 17°34'0"S 17°34'30"S 17°34'30"S 17°34'30"S 17°34'30"S 177°37'30"E 177°38'30"E</p>	1463/1010	<p>Break detected at: 2008(189)</p> <p>Historical data New data Stable history Fit based on stable history Start of the Monitoring period Time of detected break</p>
2008	<p>177°37'30"E 177°38'30"E 17°33'0"S 17°33'30"S 17°33'30"S 17°33'30"S 17°34'0"S 17°34'0"S 17°34'0"S 17°34'0"S 17°34'30"S 17°34'30"S 17°34'30"S 17°34'30"S 177°37'30"E 177°38'30"E</p>	1479/1016	<p>Break detected at: 2008(205)</p> <p>Historical data New data Stable history Fit based on stable history Start of the Monitoring period Time of detected break</p>
2008	<p>177°37'30"E 177°38'30"E 17°33'0"S 17°33'30"S 17°33'30"S 17°33'30"S 17°34'0"S 17°34'0"S 17°34'0"S 17°34'0"S 17°34'30"S 17°34'30"S 17°34'30"S 17°34'30"S 177°37'30"E 177°38'30"E</p>	1490/1032	<p>Break detected at: 2008(285)</p> <p>Historical data New data Stable history Fit based on stable history Start of the Monitoring period Time of detected break</p>

(Table continued)

Year	Landsat image	Pixel (Path/row)	BFASTmonitor single-pixel time series analysis
2008		1488/1001	<p>Break detected at: 2008(285)</p>
ID: LE70750722009208EDC00			
2009		1420/984	<p>Break detected at: 2009(96)</p>
2009		1419/1007	<p>Break detected at: 2009(48)</p>
2009		1411/1017	<p>Break detected at: 2009(352)</p>

(Table continued)

Year	Landsat image	Pixel (Path/row)	BFASTmonitor single-pixel time series analysis
2009	<p>177°37'30"E 177°38'30"E 17°33'0"S 17°33'30"S 17°34'0"S 17°34'30"S</p>	1423/1042	<p>Break detected at: 2009(352)</p> <p>Historical data New data Stable history Fit based on stable history Start of the Monitoring period Time of detected break</p>
2009	<p>177°37'30"E 177°38'30"E 17°33'0"S 17°33'30"S 17°34'0"S 17°34'30"S</p>	1452/1021	<p>Break detected at: 2009(48)</p> <p>Historical data New data Stable history Fit based on stable history Start of the Monitoring period Time of detected break</p>
ID: LE70750722010099EDC00			
2010	<p>177°37'30"E 177°38'30"E 17°33'0"S 17°33'30"S 17°34'0"S 17°34'30"S</p>	1411/958	<p>Break detected at: 2010(3)</p> <p>Historical data New data Stable history Fit based on stable history Start of the Monitoring period Time of detected break</p>
2010	<p>177°37'30"E 177°38'30"E 17°33'0"S 17°33'30"S 17°34'0"S 17°34'30"S</p>	1415/969	<p>Break detected at: 2010(99)</p> <p>Historical data New data Stable history Fit based on stable history Start of the Monitoring period Time of detected break</p>

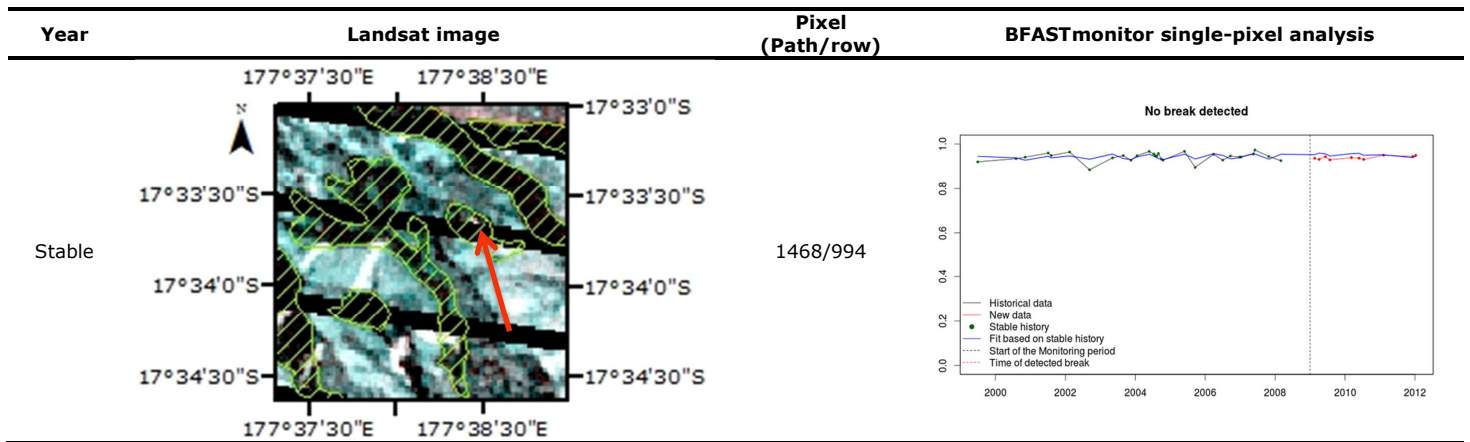
(Table continued)

Year	Landsat image	Pixel (Path/row)	BFASTmonitor single-pixel analysis
2010		1441/961	
2010		1455/967	
2010		1492/973	
ID: LE70750722012185EDC00			
Stable		1408/1031	

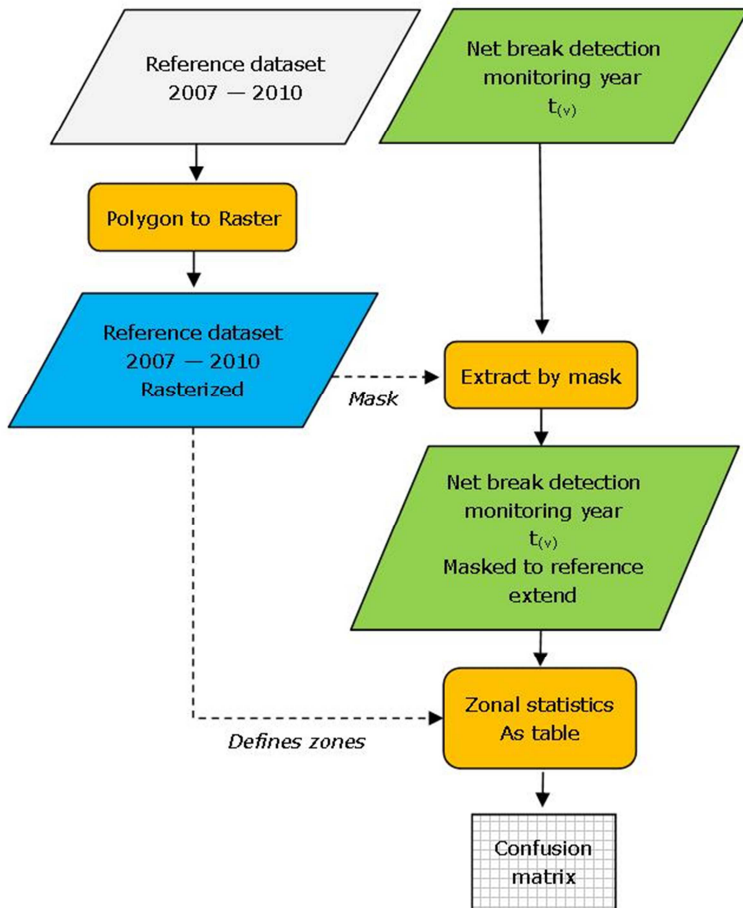
(Table continued)

Year	Landsat image	Pixel (Path/row)	BFASTmonitor single-pixel analysis
Stable	<p>177°37'30"E 177°38'30"E 17°33'0"S 17°33'30"S 17°34'0"S 17°34'30"S</p>	1431/1020	<p>No break detected</p>
Stable	<p>177°37'30"E 177°38'30"E 17°33'0"S 17°33'30"S 17°34'0"S 17°34'30"S</p>	1436/986	<p>No break detected</p>
Stable	<p>177°37'30"E 177°38'30"E 17°33'0"S 17°33'30"S 17°34'0"S 17°34'30"S</p>	1476/974	<p>No break detected</p>
Stable	<p>177°37'30"E 177°38'30"E 17°33'0"S 17°33'30"S 17°34'0"S 17°34'30"S</p>	1492/959	<p>No break detected</p>

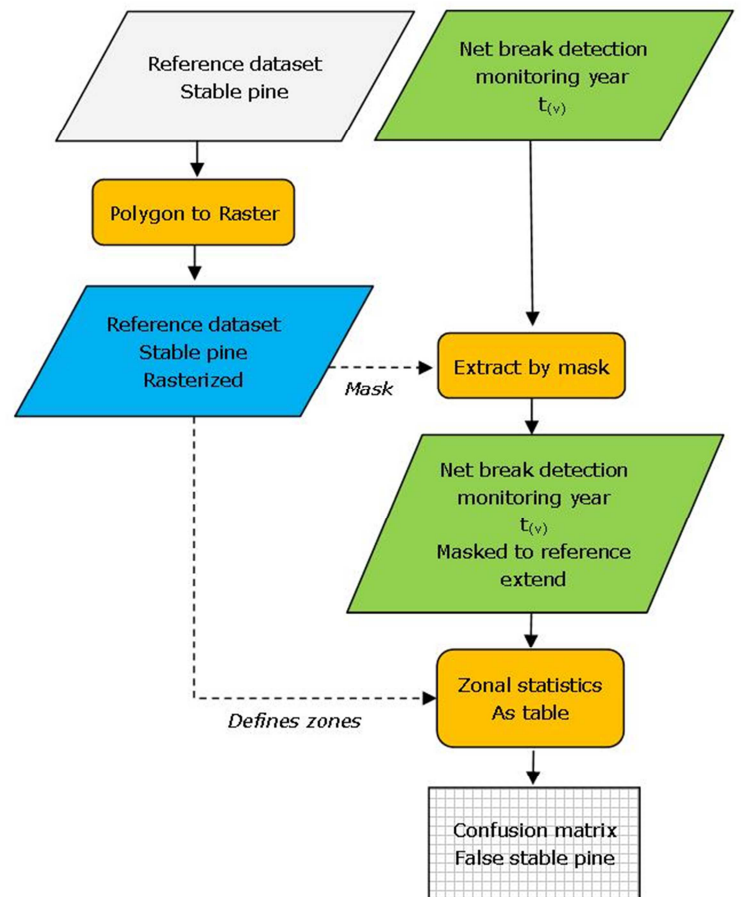
(Table continued)



## V. Appendix - Accuracy assessment flow chart for monitoring years 2007 - 2010 and stable pine forest.



Appendix Figure 2. Accuracy assessment flowchart for monitoring years 2007 - 2010



Appendix Figure 3. Accuracy assessment flowchart for stable pine

## VI. Appendix – Confusion matrices and error matrix metrics for NDVI time series.

<b>Magnitude threshold <math>m &lt; -0.01</math></b>										
	<i>Actual year of change (Reference dataset)</i>									
	2007	2008	2009	2010	Stable	Total predicted	Commission error	Omission error	Producer's accuracy	User's accuracy
	<i>(No. of pixels)</i>									
Predicted year of change (BFASTmonitor)										
2007	490	89	54	16	28	677	28%	16%	84%	72%
2008	1	1410	337	40	325	2113	33%	35%	65%	67%
2009	0	28	638	16	69	751	15%	66%	34%	85%
2010	0	34	573	616	229	1452	58%	36%	64%	42%
Stable Pine	89	619	287	276	1689	2973	43%	28%	72%	57%
<b>Magnitude threshold <math>m &lt; -0.05</math></b>										
	<i>Actual year of change (Reference dataset)</i>									
	2007	2008	2009	2010	Stable	Total predicted	Commission error	Omission error	Producer's accuracy	User's accuracy
	<i>(No. of pixels)</i>									
Predicted year of change (BFASTmonitor)										
2007	490	88	52	16	18	664	26%	4%	96%	74%
2008	1	1411	152	32	303	1899	26%	24%	76%	74%
2009	0	27	615	18	56	716	14%	62%	38%	86%
2010	0	35	762	615	205	1617	62%	31%	69%	38%
Stable Pine	18	303	56	205	2428	3010	19%	19%	81%	81%
<b>Magnitude threshold <math>m &lt; -0.10</math></b>										
	<i>Actual year of change (Reference dataset)</i>									
	2007	2008	2009	2010	Stable	Total predicted	Commission error	Omission error	Producer's accuracy	User's accuracy
	<i>(No. of pixels)</i>									
Predicted year of change (BFASTmonitor)										
2007	485	81	32	16	13	627	23%	3%	97%	77%
2008	2	1407	48	16	274	1747	20%	23%	77%	81%
2009	0	23	470	22	40	555	15%	69%	31%	85%
2010	0	41	949	589	143	1722	66%	25%	75%	34%
Stable Pine	13	274	40	143	2544	3014	16%	16%	84%	84%
<b>Magnitude threshold <math>m &lt; -0.15</math></b>										
	<i>Actual year of change (Reference dataset)</i>									
	2007	2008	2009	2010	Stable	Total predicted	Commission error	Omission error	Producer's accuracy	User's accuracy
	<i>(No. of pixels)</i>									
Predicted year of change (BFASTmonitor)										
2007	445	53	9	6	9	522	15%	5%	95%	85%
2008	13	1362	13	6	211	1605	16%	20%	80%	85%
2009	0	18	353	21	16	408	13%	72%	28%	87%
2010	0	48	854	465	82	1449	68%	20%	80%	32%
Stable Pine	9	211	16	82	2699	3017	11%	11%	89%	89%
<b>Magnitude threshold <math>m &lt; -0.20</math></b>										
	<i>Actual year of change (Reference dataset)</i>									
	2007	2008	2009	2010	Stable	Total predicted	Commission error	Omission error	Producer's accuracy	User's accuracy
	<i>(No. of pixels)</i>									
Predicted year of change (BFASTmonitor)										
2007	392	24	2	2	7	427	8%	3%	97%	92%
2008	4	1229	2	2	140	1377	11%	14%	86%	89%
2009	0	10	179	10	3	202	11%	79%	21%	89%
2010	0	28	659	326	44	1057	69%	15%	85%	31%
Stable Pine	7	140	3	44	2823	3017	6%	6%	94%	94%

(Table Continued)

<b>Magnitude threshold <math>m &lt; -0.25</math></b>										
<i>Actual year of change (Reference dataset)</i>										
	2007	2008	2009	2010	Stable	Total predicted	Commission error	Omission error	Producer's accuracy	User's accuracy
	<i>(No. of pixels)</i>									
Predicted year of change (BFASTmonitor)										
2007	332	13	0	2	5	352	6%	2%	98%	94%
2008	1	984	0	1	71	1057	7%	9%	91%	93%
2009	0	12	50	5	0	67	25%	90%	10%	75%
2010	0	5	427	198	19	649	69%	12%	88%	31%
Stable Pine	5	71	0	19	2926	3021	3%	3%	97%	97%
<b>Magnitude threshold <math>m &lt; -0.30</math></b>										
<i>Actual year of change (Reference dataset)</i>										
	2007	2008	2009	2010	Stable	Total predicted	Commission error	Omission error	Producer's accuracy	User's accuracy
	<i>(No. of pixels)</i>									
Predicted year of change (BFASTmonitor)										
2007	273	6	0	0	1	280	3%	1%	99%	98%
2008	1	685	0	1	36	723	5%	6%	94%	95%
2009	0	2	10	4	0	16	38%	96%	4%	63%
2010	0	2	236	87	9	334	74%	14%	86%	26%
Stable Pine	1	36	0	9	2975	3021	2%	2%	98%	98%

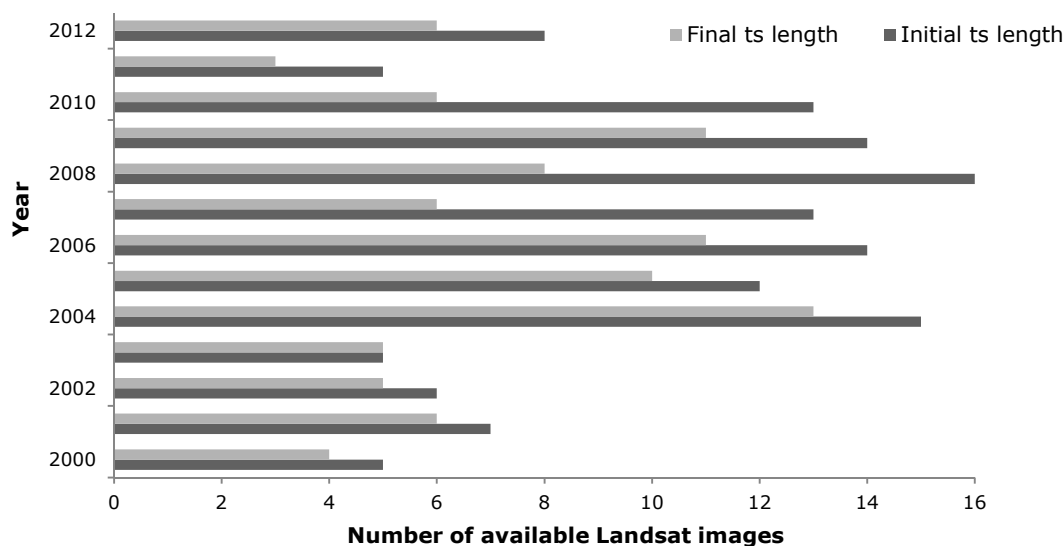
## VII. Appendix – Confusion matrices and error matrix metrics for NDFI time series.

<b>Magnitude threshold <math>m &lt; -0.01</math></b>										
<i>Actual year of change (Reference dataset)</i>										
	2007	2008	2009	2010	Stable	Total predicted	Commission error	Omission error	Producer's accuracy	User's accuracy
<i>(No. of pixels)</i>										
Predicted year of change (BFASTmonitor)										
2007	482	113	159	33	89	876	45%	7%	93%	55%
2008	6	1462	463	67	619	2617	44%	24%	76%	56%
2009	0	8	732	75	287	1102	34%	59%	41%	66%
2010	0	13	338	559	276	1186	53%	42%	58%	47%
Stable Pine	28	325	69	229	2351	3007	22%	35%	65%	78%
<b>Magnitude threshold <math>m &lt; -0.05</math></b>										
<i>Actual year of change (Reference dataset)</i>										
	2007	2008	2009	2010	Stable	Total predicted	Commission error	Omission error	Producer's accuracy	User's accuracy
<i>(No. of pixels)</i>										
Predicted year of change (BFASTmonitor)										
2007	476	98	54	28	23	679	30%	6%	94%	70%
2008	10	1477	30	20	362	1899	23%	25%	75%	78%
2009	0	23	846	84	134	1087	22%	53%	47%	78%
2010	0	18	737	566	247	1568	64%	40%	60%	36%
Stable Pine	23	362	134	247	2246	3012	25%	25%	75%	75%
<b>Magnitude threshold <math>m &lt; -0.10</math></b>										
<i>Actual year of change (Reference dataset)</i>										
	2007	2008	2009	2010	Stable	Total predicted	Commission error	Omission error	Producer's accuracy	User's accuracy
<i>(No. of pixels)</i>										
Predicted year of change (BFASTmonitor)										
2007	338	25	2	3	9	377	10%	9%	91%	90%
2008	25	1501	7	7	263	1803	18%	18%	82%	83%
2009	0	19	748	72	64	903	17%	55%	45%	83%
2010	0	29	834	473	108	1444	67%	29%	71%	33%
Stable Pine	9	263	64	108	2576	3020	15%	15%	85%	85%
<b>Magnitude threshold <math>m &lt; -0.15</math></b>										
<i>Actual year of change (Reference dataset)</i>										
	2007	2008	2009	2010	Stable	Total predicted	Commission error	Omission error	Producer's accuracy	User's accuracy
<i>(No. of pixels)</i>										
Predicted year of change (BFASTmonitor)										
2007	285	5	0	1	4	295	3%	3%	97%	97%
2008	5	1323	1	2	167	1498	12%	15%	85%	88%
2009	0	29	542	30	17	618	12%	60%	40%	88%
2010	0	25	787	330	40	1182	72%	18%	82%	28%
Stable Pine	4	167	17	40	2793	3021	8%	8%	92%	92%
<b>Magnitude threshold <math>m &lt; -0.20</math></b>										
<i>Actual year of change (Reference dataset)</i>										
	2007	2008	2009	2010	Stable	Total predicted	Commission error	Omission error	Producer's accuracy	User's accuracy
<i>(No. of pixels)</i>										
Predicted year of change (BFASTmonitor)										
2007	203	0	0	0	1	204	0%	1%	99%	100%
2008	1	1021	0	1	96	1119	9%	10%	90%	91%
2009	0	12	189	4	3	208	9%	77%	23%	91%
2010	0	6	630	211	5	852	75%	5%	95%	25%
Stable Pine	1	96	3	5	2916	3021	3%	3%	97%	97%

(Table Continued)

<b>Magnitude threshold <math>m &lt; -0.25</math></b>										
<i>Actual year of change (Reference dataset)</i>										
	2007	2008	2009	2010	Stable	Total predicted	Commission error	Omission error	Producer's accuracy	User's accuracy
	<i>(No. of pixels)</i>									
Predicted year of change (BFASTmonitor)										
2007	88	0	0	0	0	88	0%	0%	100%	100%
2008	0	694	0	1	42	737	6%	6%	94%	94%
2009	0	1	39	0	0	40	3%	90%	10%	98%
2010	0	2	338	80	2	422	81%	4%	96%	19%
Stable Pine	0	42	0	2	2977	3021	1%	1%	99%	99%
<b>Magnitude threshold <math>m &lt; -0.30</math></b>										
<i>Actual year of change (Reference dataset)</i>										
	2007	2008	2009	2010	Stable	Total predicted	Commission error	Omission error	Producer's accuracy	User's accuracy
	<i>(No. of pixels)</i>									
Predicted year of change (BFASTmonitor)										
2007	22	0	0	0	0	22	0%	0%	100%	100%
2008	0	405	0	1	5	411	1%	1%	99%	99%
2009	0	0	0	0	0	0	0%	100%	0%	0%
2010	0	0	119	17	0	136	88%	6%	94%	13%
Stable Pine	0	5	0	0	3016	3021	0%	0%	100%	100%

## VIII. Appendix - Length of time series and available Landsat images after the scene removal.



**Appendix Figure 2.** Annual length of Landsat time series (ts) before and after the removal of cloud-contaminated scenes.

### Available Landsat images after the scene removal

No.	Landsat Scene Identifier (ID)	Date acquired (YYYY-MM-DD)	Landsat Product	Cloud Cover (%)
1	LE70750722000136EDC00	2000-05-15	ETM+ L1T	6
2	LE70750722000216EDC00	2000-08-03	ETM+ L1T	13
3	LE70750722000264EDC00	2000-09-20	ETM+ L1T	69
4	LE70750722000312EDC00	2000-11-07	ETM+ L1T	9
5	LE70750722001026EDC00	2001-01-26	ETM+ L1T	31
6	LE70750722001042EDC00	2001-02-11	ETM+ L1T	28
7	LE70750722001138EDC00	2001-05-18	ETM+ L1T	36
8	LE70750722001186EDC00	2001-07-05	ETM+ L1T	15
9	LE70750722001218EDC00	2001-08-06	ETM+ L1T	21
10	LE70750722001266EDC00	2001-09-23	ETM+ L1T	33
11	LE70750722002045EDC00	2002-02-14	ETM+ L1T	10
12	LE70750722002125EDC00	2002-05-05	ETM+ L1T	54
13	LE70750722002253EDC00	2002-09-10	ETM+ L1T	60
14	E70750722002285EDC00	2002-10-12	ETM+ L1T	7
15	LE70750722003128EDC00	2003-05-08	ETM+ L1T	10
16	LE70750722003208EDC01	2003-07-27	ETM+ L1T	35
17	LE70750722003240EDC01	2003-08-28	ETM+ L1T	32
18	LE70750722003272EDC01	2003-09-29	ETM+ L1T	9
19	LE70750722003320EDC02	2003-11-16	ETM+ L1T	16
20	LE70750722004019EDC01	2004-01-19	ETM+ L1T	3
21	LE70750722004035EDC01	2004-02-04	ETM+ L1T	25
22	LE70750722004067EDC02	2004-03-07	ETM+ L1T	18
23	LE70750722004131EDC01	2004-05-10	ETM+ L1T	0
24	LE70750722004147EDC01	2004-05-26	ETM+ L1T	8

*(Table continued)*

<b>No.</b>	<b>Landsat Scene Identifier (ID)</b>	<b>Date acquired (YYYY-MM-DD)</b>	<b>Landsat Product</b>	<b>Cloud Cover (%)</b>
25	LE70750722004179EDC01	2004-06-27	ETM+ L1T	53
26	LE70750722004195EDC01	2004-07-13	ETM+ L1T	1
27	LE70750722004211EDC02	2004-07-29	ETM+ L1T	24
28	LE70750722004227EDC02	2004-08-14	ETM+ L1T	6
29	LE70750722004243EDC02	2004-08-30	ETM+ L1T	15
30	LE70750722004275EDC02	2004-10-01	ETM+ L1T	13
31	LE70750722004291EDC01	2004-10-17	ETM+ L1T	51
32	LE70750722004323EDC00	2004-11-18	ETM+ L1T	17
33	LE70750722004355EDC00	2004-12-20	ETM+ L1T	46
34	LE70750722005037EDC00	2005-02-06	ETM+ L1T	6
35	LE70750722005053EDC00	2005-02-22	ETM+ L1T	43
36	LE70750722005133EDC00	2005-05-13	ETM+ L1T	52
37	LE70750722005149EDC00	2005-05-29	ETM+ L1T	4
38	LE70750722005165EDC00	2005-06-14	ETM+ L1T	7
39	LE70750722005197EDC00	2005-07-16	ETM+ L1T	0
40	LE70750722005213EDC00	2005-08-01	ETM+ L1T	11
41	LE70750722005245EDC00	2005-09-02	ETM+ L1T	46
42	LE70750722005261EDC00	2005-09-18	ETM+ L1T	11
43	LE70750722005293EDC00	2005-10-20	ETM+ L1T	18
44	LE70750722005309EDC00	2005-11-05	ETM+ L1T	89
45	LE70750722006072EDC00	2006-03-13	ETM+ L1T	41
46	LE70750722006088EDC00	2006-03-29	ETM+ L1T	7
47	LE70750722006104EDC00	2006-04-14	ETM+ L1T	11
48	LE70750722006136EDC00	2006-05-16	ETM+ L1T	9
49	LE70750722006152EDC00	2006-06-01	ETM+ L1T	10
50	LE70750722006168EDC00	2006-06-17	ETM+ L1T	71
51	LE70750722006184EDC00	2006-07-03	ETM+ L1T	39
52	LE70750722006216EDC00	2006-08-04	ETM+ L1T	3
53	LE70750722006264EDC00	2006-09-21	ETM+ L1T	7
54	LE70750722006360EDC00	2006-12-26	ETM+ L1T	40
55	LE70750722007011EDC01	2007-01-11	ETM+ L1T	9
56	LE70750722007027EDC00	2007-01-27	ETM+ L1T	13
57	LE70750722007123EDC00	2007-05-03	ETM+ L1T	15
58	LE70750722007139EDC00	2007-05-19	ETM+ L1T	14
59	LE70750722007155EDC00	2007-06-04	ETM+ L1T	18
60	LE70750722007171EDC00	2007-06-20	ETM+ L1T	2
61	LE70750722007187EDC00	2007-07-06	ETM+ L1T	3
62	LE70750722007203EDC00	2007-07-22	ETM+ L1T	15
63	LE70750722007299EDC00	2007-10-26	ETM+ L1T	6
64	LE70750722007315EDC00	2007-11-11	ETM+ L1T	19
65	LE70750722008014EDC00	2008-01-14	ETM+ L1T	36
66	LE70750722008046EDC00	2008-02-15	ETM+ L1T	9
67	LE70750722008062EDC02	2008-03-02	ETM+ L1T	3
68	LE70750722008142EDC00	2008-05-21	ETM+ L1T	29
69	LE70750722008222EDC00	2008-08-09	ETM+ L1T	3
70	LE70750722008238EDC01	2008-08-25	ETM+ L1T	13
71	LE70750722008254EDC01	2008-09-10	ETM+ L1T	3
72	LE70750722008270EDC00	2008-09-26	ETM+ L1T	37
73	LE70750722008286EDC00	2008-10-12	ETM+ L1T	4
74	LE70750722008334EDC00	2008-11-29	ETM+ L1T	10
75	LE70750722008350EDC00	2008-12-15	ETM+ L1T	13
76	LE70750722009048EDC02	2009-02-17	ETM+ L1T	4
77	LE70750722009064EDC00	2009-03-05	ETM+ L1T	32

*(Table continued)*

<b>No.</b>	<b>Landsat Scene Identifier (ID)</b>	<b>Date acquired (YYYY-MM-DD)</b>	<b>Landsat Product</b>	<b>Cloud Cover (%)</b>
78	LE70750722009096EDC00	2009-04-06	ETM+ L1T	46
79	LE70750722009112EDC00	2009-04-22	ETM+ L1T	71
80	LE70750722009160EDC00	2009-06-09	ETM+ L1T	6
80	LE70750722009176EDC00	2009-06-25	ETM+ L1T	69
81	LE70750722009240EDC00	2009-08-28	ETM+ L1T	36
82	LE70750722009288EDC00	2009-10-15	ETM+ L1T	48
83	LE70750722009320EDC00	2009-11-16	ETM+ L1T	41
84	LE70750722009336EDC00	2009-12-02	ETM+ L1T	11
85	LE70750722009352EDC01	2009-12-18	ETM+ L1T	18
86	LE70750722010019EDC00	2010-01-19	ETM+ L1T	8
87	LE70750722010035EDC00	2010-02-04	ETM+ L1T	16
88	LE70750722010147EDC00	2010-05-27	ETM+ L1T	0
89	LE70750722010195EDC00	2010-07-14	ETM+ L1T	8
90	LE70750722010211EDC00	2010-07-30	ETM+ L1T	17
91	LE70750722010227EDC00	2010-08-15	ETM+ L1T	7
92	LE70750722010307EDC00	2010-11-03	ETM+ L1T	6
93	LE70750722010355EDC00	2010-12-21	ETM+ L1T	82
94	LE70750722011038EDC00	2011-02-07	ETM+ L1T	9
95	LE70750722011054EDC00	2011-02-23	ETM+ L1T	14
96	LE70750722011070EDC00	2011-03-11	ETM+ L1T	4
97	LE70750722011246EDC00	2011-12-08	ETM+ L1T	83

## IX. Appendix – Confusion matrices and error matrix metrics for NDVI time series after scene removal.

<b>Magnitude threshold <math>m &lt; -0.01</math></b>										
<i>Actual year of change (Reference dataset)</i>										
	2007	2008	2009	2010	Stable	Total predicted	Commission error	Omission error	Producer's accuracy	User's accuracy
	<i>(No. of pixels)</i>									
Predicted year of change (BFASTmonitor)										
2007	472	113	97	39	22	743	36%	6%	94%	64%
2008	2	1252	409	31	282	1976	37%	28%	72%	63%
2009	0	81	711	27	136	955	26%	55%	45%	74%
2010	0	7	203	341	72	623	45%	34%	66%	55%
Stable Pine	22	282	136	72	2467	3021	18%	18%	82%	82%
<b>Magnitude threshold <math>m &lt; -0.05</math></b>										
<i>Actual year of change (Reference dataset)</i>										
	2007	2008	2009	2010	Stable	Total predicted	Commission error	Omission error	Producer's accuracy	User's accuracy
	<i>(No. of pixels)</i>									
Predicted year of change (BFASTmonitor)										
2007	422	111	63	27	10	633	33%	6%	94%	67%
2008	14	1278	294	18	268	1872	32%	28%	72%	68%
2009	1	81	699	32	91	904	23%	52%	48%	77%
2010	0	31	296	417	95	839	50%	30%	70%	50%
Stable Pine	10	268	91	95	2503	2986	16%	16%	84%	84%
<b>Magnitude threshold <math>m &lt; -0.10</math></b>										
<i>Actual year of change (Reference dataset)</i>										
	2007	2008	2009	2010	Stable	Total predicted	Commission error	Omission error	Producer's accuracy	User's accuracy
	<i>(No. of pixels)</i>									
Predicted year of change (BFASTmonitor)										
2007	354	56	21	4	2	437	19%	7%	93%	81%
2008	23	1315	137	13	226	1714	25%	23%	77%	77%
2009	2	71	563	28	34	698	19%	52%	48%	81%
2010	0	30	418	433	89	970	55%	24%	76%	45%
Stable Pine	2	226	34	89	2647	3000	12%	12%	88%	88%
<b>Magnitude threshold <math>m &lt; -0.15</math></b>										
<i>Actual year of change (Reference dataset)</i>										
	2007	2008	2009	2010	Stable	Total predicted	Commission error	Omission error	Producer's accuracy	User's accuracy
	<i>(No. of pixels)</i>									
Predicted year of change (BFASTmonitor)										
2007	295	25	4	2	1	327	10%	3%	97%	90%
2008	9	1265	93	5	173	1545	19%	18%	82%	82%
2009	0	41	432	20	12	505	14%	53%	47%	86%
2010	0	31	388	388	72	879	56%	20%	80%	44%
Stable Pine	1	173	12	72	2746	3004	9%	9%	91%	91%
<b>Magnitude threshold <math>m &lt; -0.20</math></b>										
<i>Actual year of change (Reference dataset)</i>										
	2007	2008	2009	2010	Stable	Total predicted	Commission error	Omission error	Producer's accuracy	User's accuracy
	<i>(No. of pixels)</i>									
Predicted year of change (BFASTmonitor)										
2007	244	5	0	2	0	251	3%	1%	99%	97%
2008	3	1121	49	2	113	1288	13%	12%	88%	87%
2009	0	15	227	12	4	258	12%	61%	39%	88%
2010	0	19	304	323	52	698	54%	17%	83%	46%
Stable Pine	0	113	4	52	2852	3021	6%	6%	94%	

(Table Continued)

<b>Magnitude threshold <math>m &lt; -0.25</math></b>										
<i>Actual year of change (Reference dataset)</i>										
	2007	2008	2009	2010	Stable	Total predicted	Commission error	Omission error	Producer's accuracy	User's accuracy
	<i>(No. of pixels)</i>									
Predicted year of change (BFASTmonitor)										
2007	192	3	0	1	0	196	2%	1%	99%	98%
2008	1	845	7	1	59	913	8%	8%	92%	93%
2009	0	5	76	7	0	88	14%	74%	26%	86%
2010	0	7	212	235	26	480	51%	13%	87%	49%
Stable Pine	0	59	0	26	2936	3021	3%	3%	97%	97%
<b>Magnitude threshold <math>m &lt; -0.30</math></b>										
<i>Actual year of change (Reference dataset)</i>										
	2007	2008	2009	2010	Stable	Total predicted	Commission error	Omission error	Producer's accuracy	User's accuracy
	<i>(No. of pixels)</i>									
Predicted year of change (BFASTmonitor)										
2007	134	2	0	0	0	136	1%	1%	99%	99%
2008	1	518	1	1	25	546	5%	5%	95%	95%
2009	0	0	38	4	0	42	10%	73%	27%	90%
2010	0	2	101	131	8	242	46%	9%	91%	54%
Stable Pine	0	25	0	8	2988	3021	1%	1%	99%	99%

## X. Appendix – Confusion matrices and error matrix metrics for NDFI time series after scene removal.

<b>Magnitude threshold <math>m &lt; -0.01</math></b>										
<i>Actual year of change (Reference dataset)</i>										
	2007	2008	2009	2010	Stable	Total predicted	Commission error	Omission error	Producer's accuracy	User's accuracy
<i>(No. of pixels)</i>										
Predicted year of change (BFASTmonitor)										
2007	446	156	168	63	93	926	52%	22%	78%	48%
2008	27	1373	555	75	623	2653	49%	37%	63%	52%
2009	6	15	577	62	346	1006	43%	71%	29%	57%
2010	0	10	303	449	112	874	49%	42%	58%	51%
Stable Pine	93	623	346	112	1759	2957	41%	41%	59%	59%
<b>Magnitude threshold <math>m &lt; -0.05</math></b>										
<i>Actual year of change (Reference dataset)</i>										
	2007	2008	2009	2010	Stable	Total predicted	Commission error	Omission error	Producer's accuracy	User's accuracy
<i>(No. of pixels)</i>										
Predicted year of change (BFASTmonitor)										
2007	336	84	32	18	3	473	29%	6%	94%	71%
2008	0	0	0	0	0	0	0%	100%	0%	0%
2009	19	1007	852	70	225	2173	61%	51%	49%	39%
2010	0	288	643	547	166	1644	67%	32%	68%	33%
Stable Pine	3	0	225	166	2614	3008	13%	13%	87%	87%
<b>Magnitude threshold <math>m &lt; -0.10</math></b>										
<i>Actual year of change (Reference dataset)</i>										
	2007	2008	2009	2010	Stable	Total predicted	Commission error	Omission error	Producer's accuracy	User's accuracy
<i>(No. of pixels)</i>										
Predicted year of change (BFASTmonitor)										
2007	268	14	0	2	3	287	7%	13%	87%	93%
2008	37	1516	87	10	297	1947	24%	18%	82%	78%
2009	0	7	712	47	57	823	13%	53%	47%	87%
2010	0	24	655	502	94	1275	61%	23%	77%	39%
Stable Pine	3	297	57	94	2568	3019	15%	15%	85%	85%
<b>Magnitude threshold <math>m &lt; -0.15</math></b>										
<i>Actual year of change (Reference dataset)</i>										
	2007	2008	2009	2010	Stable	Total predicted	Commission error	Omission error	Producer's accuracy	User's accuracy
<i>(No. of pixels)</i>										
Predicted year of change (BFASTmonitor)										
2007	190	1	0	0	0	191	1%	3%	97%	99%
2008	6	1353	51	2	188	1600	16%	14%	86%	85%
2009	0	11	504	18	18	551	9%	56%	44%	91%
2010	0	14	585	445	49	1093	59%	13%	87%	41%
Stable Pine	0	188	18	49	2766	3021	8%	8%	92%	92%
<b>Magnitude threshold <math>m &lt; -0.20</math></b>										
<i>Actual year of change (Reference dataset)</i>										
	2007	2008	2009	2010	Stable	Total predicted	Commission error	Omission error	Producer's accuracy	User's accuracy
<i>(No. of pixels)</i>										
Predicted year of change (BFASTmonitor)										
2007	118	0	0	0	0	118	0%	1%	99%	100%
2008	1	1063	3	1	108	1176	10%	10%	90%	90%
2009	0	4	165	1	5	175	6%	74%	26%	94%
2010	0	9	466	308	8	791	61%	3%	97%	39%
Stable Pine	0	108	5	8	2900	3021	4%	4%	96%	96%

(Table Continued)

<b>Magnitude threshold <math>m &lt; -0.25</math></b>										
<i>Actual year of change (Reference dataset)</i>										
	2007	2008	2009	2010	Stable	Total predicted	Commission error	Omission error	Producer's accuracy	User's accuracy
	<i>(No. of pixels)</i>									
Predicted year of change (BFASTmonitor)										
2007	38	0	0	0	0	38	0%	0%	100%	100%
2008	0	731	0	1	58	790	7%	8%	92%	93%
2009	0	0	47	0	0	47	0%	84%	16%	100%
2010	0	4	256	198	1	459	57%	1%	99%	43%
Stable Pine	0	58	0	1	2962	3021	2%	2%	98%	98%
<b>Magnitude threshold <math>m &lt; -0.30</math></b>										
<i>Actual year of change (Reference dataset)</i>										
	2007	2008	2009	2010	Stable	Total predicted	Commission error	Omission error	Producer's accuracy	User's accuracy
	<i>(No. of pixels)</i>									
Predicted year of change (BFASTmonitor)										
2007	4	0	0	0	0	4	0%	0%	100%	100%
2008	0	398	0	0	15	413	4%	4%	96%	96%
2009	0	0	25	0	0	25	0%	76%	24%	100%
2010	0	2	79	104	0	185	44%	0%	100%	56%
Stable Pine	0	15	0	0	3006	3021	0%	0%	100%	100%

